OPTOMECHANICAL DESIGN OF A SPACE TELESCOPE PRIMARY MIRROR

SAEED UR REHMAN

SpaceLab, Department of Electrical Engineering

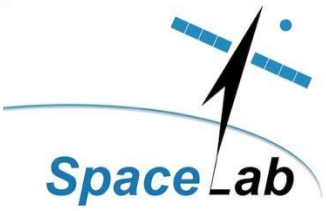

This dissertation is submitted in partial fulfilment of the requirements for the degree of Master of Philosophy in Space Studies

October 2022

SL20-04M

DECLARATION

I know the meaning of plagiarism and declare that all the work in the document, save for that which is properly acknowledged, is my own. It has not been previously submitted, in part or whole, to any university of institution for any degree, diploma, or other qualification. This thesis/dissertation has been submitted to the Turnitin module (or equivalent similarity and originality checking software) and I confirm that my supervisor has seen my report and any concerns revealed by such have been resolved with my supervisor.

Signed Signed by candidate Date: 20th March 2020

SAEED UR REHMAN, M.Phil Space Studies

University of Cape Town

ABSTRACT

The primary mirror is the most critical component of a space-borne telescope. The size of the primary mirror is the main driver for the resolution of the telescope. A high-resolution telescope requires a larger primary mirror with the high-precision requirement of deformation due to space thermal loads, gravity loads in AIT environment and pressure loads during surface polishing. In addition to this, mass is also an important criterion. Telescope mass is also derived from the mass of the primary mirror. So, a lightweight primary mirror with sufficient stiffness to avoid distortion due to gravity and thermal loads is necessary to get the required optical performance from high-resolution telescopes. It will also keep the mirror within its allowable stress limit with a sufficient Margin of Safety in external acceleration and vibrational launch loads so that it can survive during launch. Flexure support is also a very critical component of the primary mirror assembly. The aim of flexure support is to isolate the mirror surface so that it will not distort because of thermal expansion/contraction, gravity loads and mounting stresses. Stiffness of the flexure is a very critical design variable. It should be enough stiff that there will be no plastic deformation due to launch loads and it must be flexible enough that it can isolate the optical surface from the distortion of the optical bench. Researchers have worked on the design solution for large size lightweight primary mirrors and based on the research they have proposed their optimized design for primary mirror and its support. The objective of this research is to propose the optomechanical design solution the primary mirror of a space telescope. It includes designing of the lightweight structure of the primary mirror based on Finite Element Analysis. Open back pocketing will be used to lightweight the primary mirror. The primary mirror support will be designed to a-thermalize and isolate the primary mirror from the external structure. The performance of the primary mirror will be analyzed for deflection due to gravity & thermal loads and stress due to external acceleration and thermal loads based on Finite Element Analysis. Trade off study will be performed for the selection of mirror material and the pocketing shape. The impact of different design variables for pocketing material will be analyzed. On the basis of these analyses a comprehensive workable design solution will be proposed for the Primary Mirror that meet the requirements for surface error and have enough strength to bear launch loads.

ACKNOWLEDGEMENTS

First of all, I am very thankful to almighty ALLAH for all his blessings, because of that I am able to complete this dissertation.

I would like to dedicate my dissertation to my parents and my family, whose support and prayers motivate me to complete it.

I would like to express my sincere gratitude to my advisor Prof. Peter Martinez for his continuous support, time, and help in academics and administrative matters as well as in the writing of the thesis. I cannot imagine the completion of my M.Phil. degree without his support, guidance and help. I am very thankful to Ms. Debbie Singh and Ms. Nicole Moodley for their support to sort out all the administrative matters.

Besides my advisor, I would like to thanks to my technical mentors Mr. Jan Botha and Mr. Christie Engelbrecht from Space Advisory Company for their guidance and support throughout my research.

My sincere thanks to my fellows Mr. Noman Majid for his help to calculate the Zernike polynomials and Mr. Asim Raza for his help to analyze the optical performance of the mirror using Zeemax studio.

Last but not the least, I would like to thanks to all my friends for their constant source of inspiration to complete the dissertation.

CONTENTS

LIST OF FIGURES

LIST OF TABLES

LIST OF ABBREVIATIONS

AIT	Assembly Integration and Testing
CAD	Computer Aided Design
CTE	Coefficient of Thermal Expansion
DLL	Design Limit Load
DV	Design Variable
FE	Finite Element
FEA	Finite Element Analysis
FOSU	Factor of Safety for Ultimate Strength
FOSY	Factor of Safety for Yield Strength
PM	Primary Mirror
PMA	Primary Mirror Assembly
OB	Optical Bench
PoF	Probability of Failure
PV	Peak to Valley
RMS	Root Mean Square
SE	Surface Error

1 INTRODUCTION

1.1 Motivation and Objective

Development in remote sensing technology enables the use of high-resolution space borne telescopes for different commercial and military applications. The main challenge for the development of high-resolution telescopes is to design the largest possible diameter primary mirror with a high surface finishing requirement. The diameter of a primary mirror increases as we move toward higher and higher resolution telescopes. Optical sensitivity of mirrors increases with their diameter. Large diameter mirrors are more sensitive to optical surface errors under temperature fluctuation, gravity loading and mounting constraints. It will make the designing of a large primary mirror more challenging and complex because of a very precise requirement of surface error due to gravity load, polishing pressure, mounting loads and temperature fluctuation. Surface errors of optical elements severely degrade the optical performance of the system during in-orbit operation. On the other hand, strength of the optical element and its mechanics is also a very critical design parameter because it has to withstand severe launch loads without any permanent deformation or cracks. The complexity of the mirror increases for large diameter mirrors as the weight of the mirror increase proportionally with the diameter of the mirror. Heavy mirrors need a stiffer mounting that increases the total weight of the system. In a space telescope, weight is the main deciding factor to estimate the launch cost of the system and must be controlled as it works as one of the design drivers of a space telescope.

Lightweight mirrors are the possible solution for larger primary mirrors. In lightweight design process the mass of the mirror reduces with least compromise on the stiffness of the mirror structure, so that the requirement of surface error can be achieved for gravity loads and polishing loads. Stiffness of the mirror also contribute to the strength of the mirror to withstand the severe a lunch load. Mirror an be called lightweight mirror if it has higher stiffness as compared to the same size solid conventional mirror with equivalent mass. Thermal distortion of the mirror can be controlled by combination of using low CTE material and defining the range of operational temperature for the Primary Mirror so that the mirror itself will least expand and contract. The surface error problem raises again when the low CTE mirror is mounted on mechanics with different CTE value. This problem is addressed by the designing of a kinematic flexure mount that constrains the mirror with the mechanics in least three degrees of freedom. These kinematic flexure mounts is used to isolate the mirror from its mechanics so that mirror surface will not distort due to distortion in the mechanics of the mirror. Support system designing of kinematic flexure mount is more challenging for large diameter mirror because expansion and contraction in large mirrors is more as compared with small mirrors. Designing of a large diameter mirror is more challenging because of high optical surface sensitivity of mirror as well.

The objective of this thesis is to design a 620mm diameter primary mirror for 1m a resolution space born telescope for remote sensing applications. The design should meet all the requirements for the optical surface error under gravity and thermal loads. The mirror design should meet the natural frequency requirement and it must have enough strength to survive the launch loads. The primary objective of this research is to find an effective way to lightweight the primary mirror and a workable design solution for lightweight primary mirror. Although the mounting flexure designing is not the scope of this thesis, some suitable flexure design will be used to evaluate that design to meet the optical performance and strength requirement of the mirror. Manufacturing and testing of the mirror will not covered in the scope of this thesis. Mirror performance will be evaluated on the basis on PV surface error and RMS surface error. It will also evaluate the mirror performance by calculating the Zernike polynomials.

1.2 Introduction to Primary Mirror

This section will present different types of Primary Mirrors that are very common in use for telescope designing. The classification of the mirrors has been performed on the basis of their structure design, mirror materials, mirror mounting and requirement for gravity loading

1.2.1 Structure Design

D Vukobratovich [1] has classified mirrors into three types based on the structure of the mirror. The solid contoured back mirror, sandwich mirror and open back pocketed mirror.

1.2.1.1 Solid Contoured back mirror

Solid contoured back mirrors are the mirrors that are contoured from the back side of the mirror to reduce weight. They are further classified into three types: single arch, double arch and double concave as shown in Figure 1.1. Weight reduction of contoured back mirrors are up to 25% with respect to a solid mirror of 6:1 aspect ratio of diameter to thickness. They have low fabrication cost and are relatively easy to mount. The disadvantages of these types of mirrors are the high surface distortion sensitivity due to temperature change as the thickness of mirror is not constant throughout. These three designs are based on the mounting location of the mirror. The single arch mirror is mounted from the centre of the mirror, the double arch mirror is mounted from the back side of the mirror and the double concave mirror is mounted from the outer diameter of the mirror. Figure 1.1 shows the concept of the solid contoured back mirror.

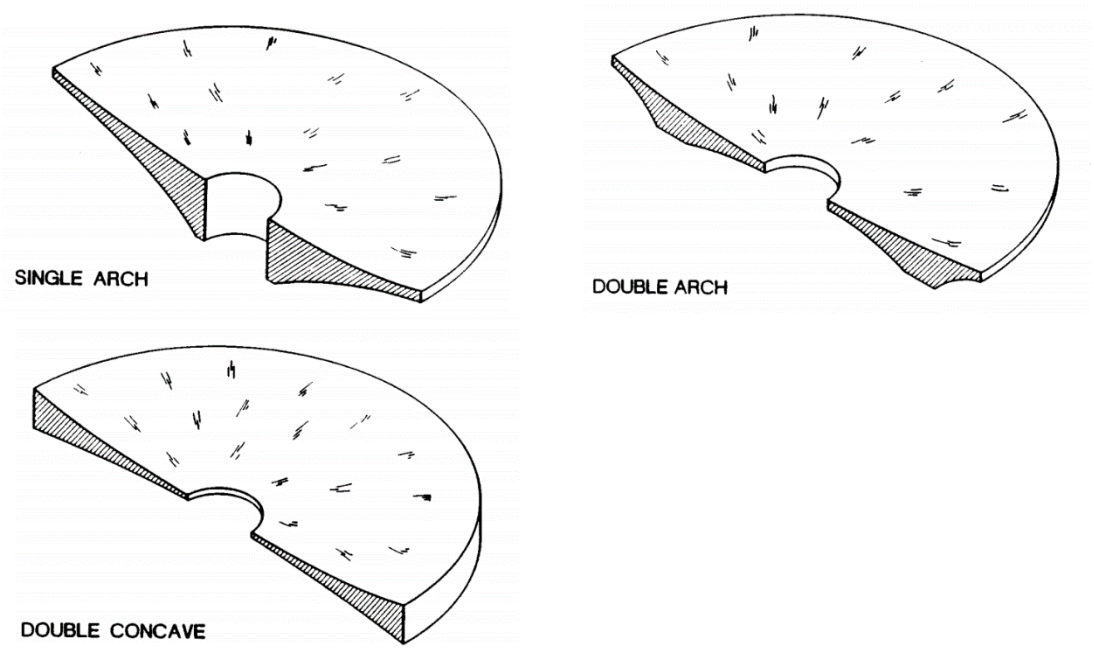

Figure 1.1: Solid Contoured back Mirror. [1]

1.2.1.2 Sandwich Mirrors

Sandwich mirrors have the stiffest mirror structure among the all other types of mirror. They also have the highest stiffness to weight ratio. Weight reduction of sandwich mirrors are 60 to 80% with respect to solid mirrors, although more than 80% can be achievable at high cost and fabrication risk. A sandwich mirror consists of a thin face sheet on front and rear side of the mirror and a pocketed core structure between the face sheets. The core structure can be based on hexagonal, square, triangular and customized shape pocketing. The disadvantages of sandwich mirrors are its controversial thermal response. The other disadvantages of the sandwich mirror are the quilting effect. Quilting is a permanent pattern deformation induced in the mirror surface during polishing because of polishing pressure load. Figure 1.2 shows the concept of a sandwich mirror.

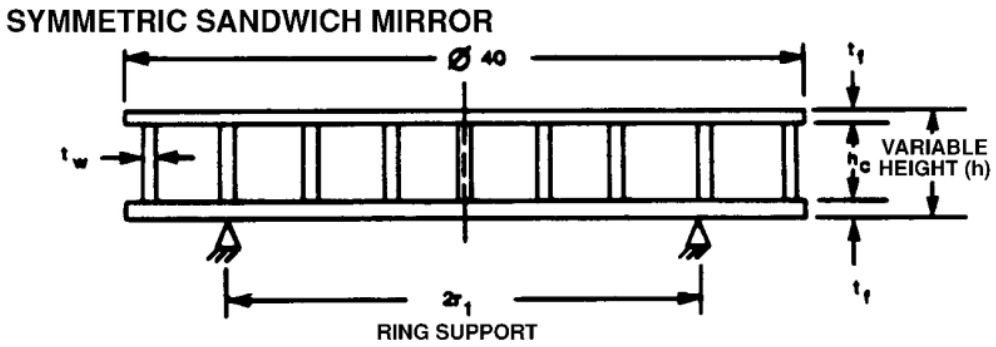

Figure 1.2: Design Concept of the Sandwich Mirror. [1]

1.2.1.3 Open Back Pocketed Mirrors

Open back pocketed mirrors are the most common way of producing a lightweight mirror. It consists of a thin face sheet and pocket structure. Hexagonal, triangular and square pockets are the most common shapes. Customized rib structures also used for mirror pocketing. Weight reduction of open back pocketed mirrors are up to 30 to 40%. Stiffness to weight ratios of open back pocketed mirrors are not good as sandwich and contoured mirrors. Thermal behavior of open back mirrors is very good, and they have lower thermal time constants. Manufacturing costs of open back mirrors are relatively low as compare to sandwich mirrors. They can easily be mounted from centre, back or outside of the mirror based on the mirror design. Figure 1.3 shows the concept of open back pocketed mirror with commonly used pocketed shapes having same inscribed circle diameter define as parameter B.

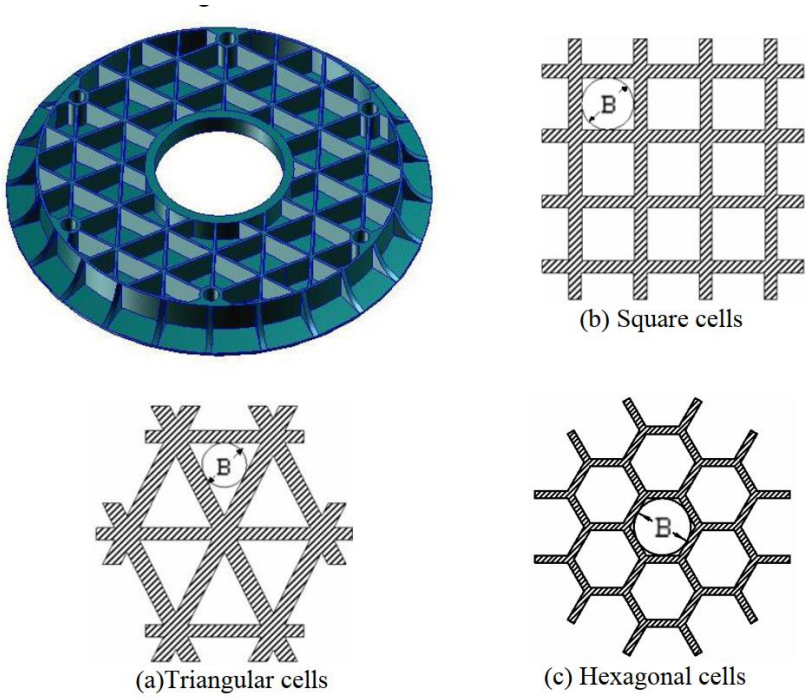

Figure 1.3: Concept of open back pocketed mirror. [2]

Valente and Vukobratovich [1] presented the comparison of all three types of structure of mirror based on the self-weight deflection, efficiency of mirrors and ease of fabrication. Mirror efficiency is defined as a function of self-weight deflection and thickness of mirror. They concluded that the single arch mirrors are worst for self-weight deflection for constant height. While sandwich mirrors perform best, overall if we compare only machine-able mirrors than the solid and open back pocketed mirrors are the best. In comparison of weight to height ratio, the solid mirrors are the worst and the open back mirrors are the best. Overall, in terms of weight to deflection the sandwich mirrors are the best, then double arch and open back mirrors. In terms of manufacturing, the sandwich mirrors have high manufacturing cost due to complexity and risk involved in manufacturing. The manufacturing cost of open back mirrors are lower as they can be manufactured by machining of glass blocks.

1.2.2 Mirror Materials

Paul Yoder [3] classified the mirror in two parts, the reflective surface and rigid structure. Selection of mirror material is based on the combination of different properties that varies subject to application and environment in which mirror will be used. There is a wide range of metallic and non-metallic materials used for the manufacturing of

mirrors. Only most commonly used mirror materials will be discussed. The critical properties of mirror materials are stiffness, density, specific stiffness, CTE and specific heat capacity.

Once manufacturing and polishing of mirror has been done, it is very important that the optical surface should maintain its shape under different types of loading. Some of the loads are the part of its optical operation, like thermal temperature changes. Distortion of the optical surface depends on the CTE of mirror material. In space, optical CTE materials are preferred to use because it will not distort the mirror optical surface due to change in temperature. Low CTE material allows to use the mirror in wide range of temperature. This wide operating temperature range makes the thermal design of system simple and low cost.

There is no gravitational load of the mirror on its support system as it would be the case if the mirror were resting on its support system on the surface of the Earth. This induces errors in optical surfaces. That distortion is due to the self-weight of the mirror. It will make the AIT of the system complex. Surface distortion under gravity load depends on the mirror stiffness and density. Higher density exerts high force and induce more distortion. Low stiffness means less resistance to bending and material will bend on low force. To evaluate the effect these properties a new term of specific stiffness has been introduced. That is the ratio of stiffness and density of a material. High specific stiffness materials help to prevent optical surface error under gravity load. It depends on the AIT plane of the system in which direction gravity will applied. Specific stiffness also helps the material to achieve the mirrors natural frequency requirement and gives it strength to survive he launch loads. High stiffness materials also reduce the surface error due to mirror mounting stresses. There are wide range of materials that can be used for manufacturing of primary mirrors. Table 1.1 presents commonly used materials with their mechanical properties:

Table 1.1: Properties of Primary Mirror Materials.

Materials	CTE m/m °K (10^{-6})	Young Modulus (GPa)	Specific Stiffness (MN-m/kg)	Density (kg/m^3)	Knoop hardness (kg/mm^2)
ULE 7971	0.015	67.6	30.6	2205	460
Zerodur	0±0.05	90.6	35.8	2530	60
Fused Silica 7940	0.58	73	33.1	2205	500
Aluminum 6061-T6	23.6	68.2	25.4	2680	30-95
Beryllium (O-30H)	11.46	289	156.2	1850	80
Silicon carbide	2.4	466	145	3210	2540

Table 1.1 show that ULE, Zerodur and fused silica are the materials with low CTE value while beryllium and silicon carbide are the high specific stiffness materials. Aluminum is readily available and has low manufacturing cost but can only use in limited applications. Beryllium is restricted due to its hazardous nature and is only used in high performance applications having high manufacturing cost.

The most commonly used materials for primary mirror are ULE, Zerodur for its low CTE value and silicon carbide for high specific stiffness and moderate CTE value.

Other important properties for primary mirror materials are specific heat capacity, thermal conductivity, hardness and surface smoothness. These properties are not directly involved in the structure design of a primary mirror.

1.2.3 Mounting Techniques

A mirror should be mounted in a way that it will have least distortion of the optical surface during AIT and operation. The mirror should be mounted from at least three points to fix all six degrees of freedom. Constraining from more than three points will

induce mounting stress due imperfection of surface finish. These mounting stresses generate surface errors which further degrade the optical performance of the system.

When large mirrors are mounted on three points gravity induces distortion in the surface of the mirror. So, the mirror should be designed in a way that its structure has enough stiffness to resist the bending in the optical surface of the mirror. Gravity can be applied parallel or perpendicular to the optical axis of the mirror depending on the AIT planning of the mirror.

There is another important consideration that the mirror mounting should also isolate the mirror from the thermal expansion/contraction of mirror mechanics. The CTE of mirror mechanics are much larger than the CTE of the mirror. The mirror will start bending due to change in temperature if it is mounted rigidly with its mechanics. A good mounting is flexible enough so that gives the provision of mechanics to move freely without transferring any stress on the mirror and it must be enough stiff to meet the natural frequency requirement of the mirror assembly.

Based on the location of the mirror mountings are classified into three types of centrally mounted, back supported and mounted from the outer diameter. Mounting location of the mirror has an influenced the designing of mirror structure.

1.2.4 Design requirements

Mirror surface distortion under a 1g gravity load in the lateral or longitudinal direction must be within desired limits. Optical surface error due to temperature fluctuation of mirror and mechanics should be least value for design operational temperature range. These two are the main design drivers for primary mirror design. Mirror surface error due polishing pressure load is also considerable requirement for designing of primary mirror. Natural Frequency and strength of the mirror is also important requirement for designing of primary mirror to ensure that it can bear the launch load and successfully reach its orbit without any mechanical failure. Lightweight mirror is another important requirement for primary mirror design.

To avoid over constraining the mirror, flexible three points mounts are common to use. This constraint has been imposed by the assembly and integration of the mirror to avoid mounting stresses due to over constraining the mirror. Mounting from more than 3

points will over constrain the mirror and result in the surface error due to mounting stress.

1.3 Outline of this dissertation

This thesis has six chapters. The first chapter presents an overview of the primary mirror designing, and the challenges that need to be addressed to meet the objective of workable design of a primary mirror that will give the required optical performance. The second chapter is a literature review. It highlights that how people provide the lightweight design solution for large diameter primary mirror, what approach they have used and what are the issues they have faced for designing. The third chapter defines the requirements and constraints that will used for designing of the primary mirror. The fourth chapter will present the basic top-level trade off comparison for different mirror materials, structure designs and mounting techniques. On the basis of these tradeoffs one design concept will be selected for further analysis. In this chapter performance of mirror will also be evaluated for different design variables to refine the selected design concept. Chapter five will present the CAD modeling, FE modeling and analysis of the proposed design solution. In this chapter we will be verify that our proposed design solution is meeting the design requirements with imposed design constraints. Chapter six will present the results and conclusion of our research.

All the CAD modeling and first order analysis will be performed using Solid works. FEMAP will be used for Finite Element Analysis of the proposed design.

2 LITERATURE REVIEW

H Kihm et al. [4] presented the design method for a 1 m lightweight mirror in a space optical system. The mirror is made up off Zerodur and mirror design is based on the concept of an open back hexagonal pocketed mirror with an additional face skin on the back side of the mirror. Front face skin of mirror has been pocketed in steps to keep the face skin at optimal thickness. The mirror has been mounted on three extruded bosses at the outer diameter of the mirror. The paper also presented the concept of using flexures to mount the mirror. The design requirement of the mirror is mass of less than 47 kg with areal density of 60 kg/m^2. Gravity is taken into the horizontal direction with the optical axis of the mirror perpendicular to the gravity. This requirement is generated from the AIT setup of the mirror that is considered to be done in horizontal direction. The main design parameter for the mirror is the optical surface distortion due to gravity effect by optimizing the mass at minimal level. The mirror is designed to meet the requirement of <10 nm rms surface error due to gravity in horizontal direction. Design loads are assembly error of 30 micron, quasi-static vibration load 20 g and thermal load of 20 ±10 °C. Design parameters of the mirrors are the minimum front face thickness, minimum back face thickness and height of the mirror and pocket web thickness and depth, height and width of mounting boss. Several design parameters have been define for flexure as well. Gravity distortion analysis results shows the surface error of PV=49.8 nm, RMS=8.6 nm in horizontal and PV=239 9 nm, RMS=461 nm in vertical directions.

Table **2.1** presents the design requirement for the primary mirror and Figure 2.1 shows the design concept presented by author.

Table 2.1: Design requirements for Primary Mirror.

S.NO	Requirements Parameter:	Value
1	Diameter Size	1 m
2	Mirror mass	<47 kg
3	RMS SE	<10 nm
4	Natural Frequency	>120 Hz
5	Mirror's decenter under 1g	<20 µm
6	Mirror's Tip/tilt under 1g	<0.01°
7	Assembly error	30 µm
8	Vibration Load	20 g
9	thermal load	20±10 °C

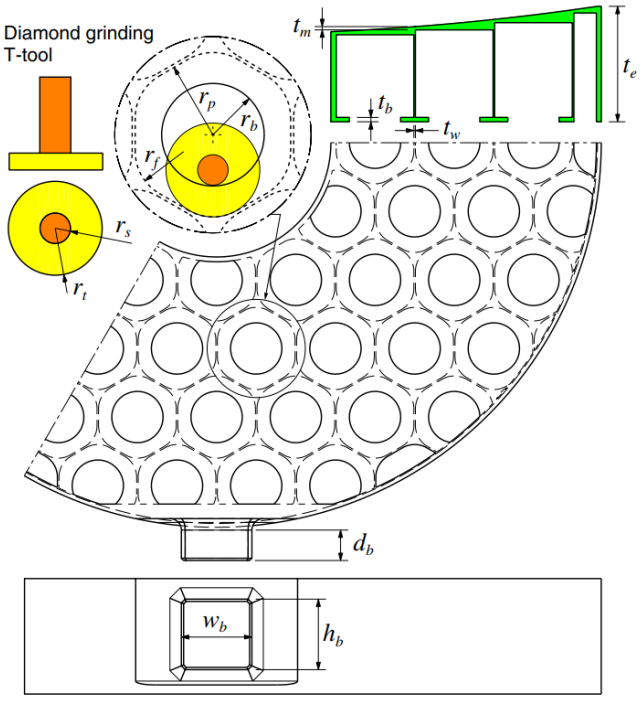

Figure 2.1: 1m Primary Mirror design concept [4]

H. Kihm et al. [5] presented a paper on the mirror mounting technique for a space telescope primary mirror. The mounting technique adds the provision of adjustment by using mechanical shims to reduce the mounting errors while tested in horizontal gravity directions. Astigmatic aberration is minimized by using shims of different thickness. The relation between the astigmatic aberration and shim thickness is investigated in the paper. Papers presented that conventional flexure gravitational stress at adhesive coupling between the mirror and mirror mount is reduced by up to half by splitting the conventional flexure into two flexures. They presented the sensitivity of Zernike coefficient Z5 (Astigmatism) with respect to different design variables of mirror and flexure. Kihm et al also presented the surface error in horizontal gravity to be SE PV = 91.6, 53.8, 119.1 nm and SE RMS = 19.3, 7.5, 19.5 nm and Z5=37.9, 0.07, -38.1 nm respectively for 0.5 mm, 2 mm and 3.5 mm shims. These authors conclude that the Zernike coefficient Z5 has a linear relation with the shim thickness and it could be minimized by using correct shim thickness. Adhesive stresses can be reduced by using the proposed flexure A. Sensitivity of Zernike coefficient Z5 with respect to different design variables is presented in Figure 2.2.

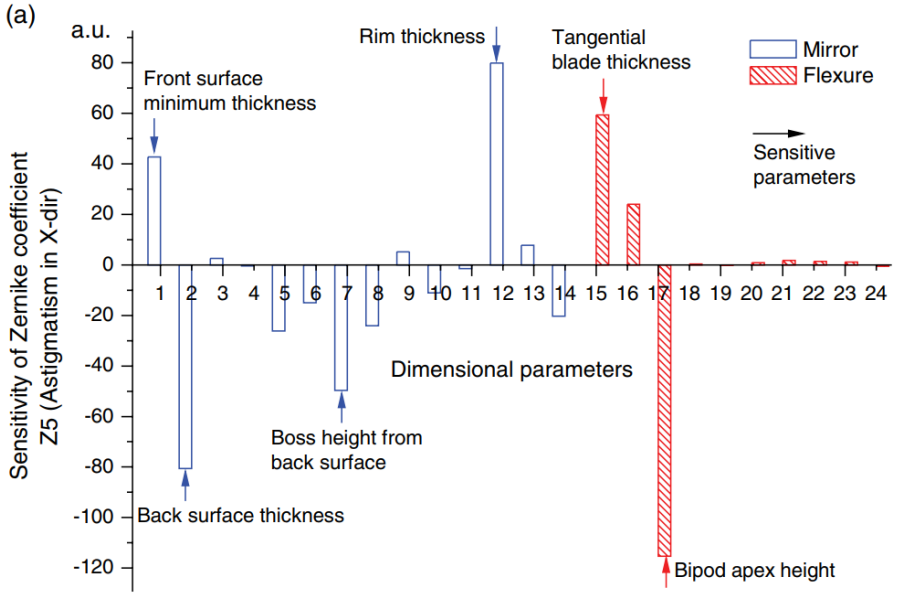

Figure 2.2: Sensitivity of Zernike Coefficient Z5 [5].

Chen et al. [6] presented their work for optimization of lightweight structure of a space mirror. Their mirror design is based on a 566 mm diameter of hexagonal open back pocketed with three-point support at the outer rim of the mirror. The design is based on Schott Zerodur. He introduced radial ribs at outer diameter in his design to lightweight

the mirror at out diameter. Seven design variables have been defined to optimize the mirror structure, they are pocket inscribed circle diameter, diameter for outer ribs and variable pocket depth that define the minimum thickness of face skin. Mirror structure has been designed on the requirement of surface distortion due to polishing pressure of 5 kpa and gravity load in the vertical direction when the mirror is place on flat surface and gravity effect in the horizontal direction when mirror is mounted in three bipod flexures. The natural frequency of mirror should be greater than 800 Hz. Surface error should be ≤63.3 nm in gravity and polishing load. PV ≤21.1 nm for self-weight deformation in horizontal direction. His design has minimum face skin thickness of 7 mm, rib thickness of 3 mm, inscribed circle diameter of 45 mm, central hole diameter of 130 mm, mirror thickness at the outer rim is 70 mm and the mass of mirror is 16.41 kg. Optimization of bipod flexure is also presented in the paper. Invar 36 bosses were bonded with 0.02 mm thick adhesive layer at the periphery of the mirror. Invar 36 bipod flexures were bonded with mounting bosses. Thirteen bipod flexure variables were defined to optimize the design for minimizing the deformation in mirror surface due to gravity in horizontal direction. Optimum bipod flexure design has been achieved for optimal value of the design variables. Results presented that the PV surface error reduced from 228 nm to 61 nm and surface RMS error reduced from 46 nm to 12 nm. Figure 2.3 shows the design of the primary mirror, primary mirror flexure and mounting boss.

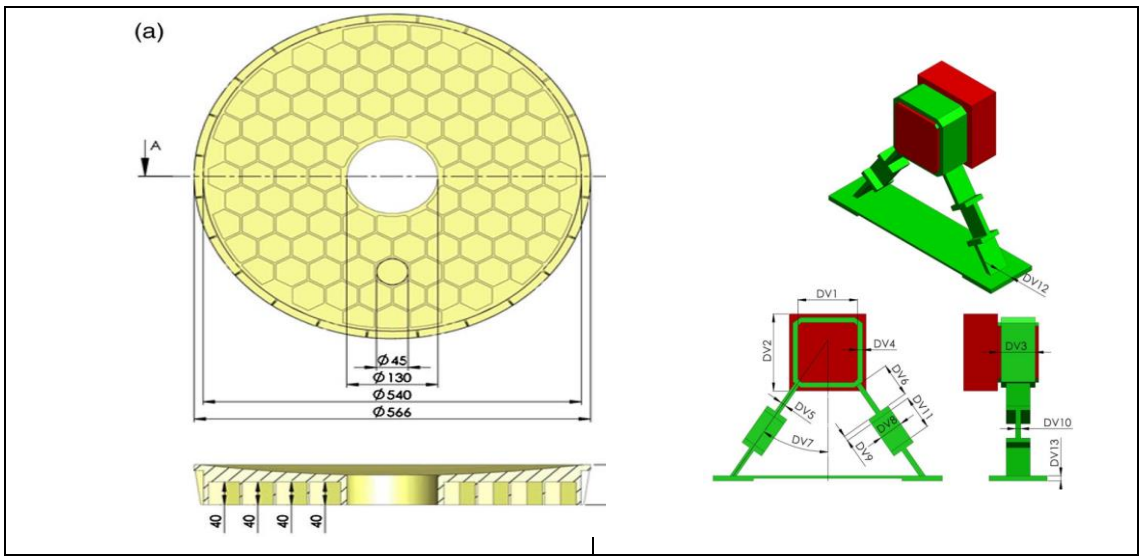

Figure 2.3: Assembly Design Concept for a 566mm diameter Primary Mirror [6]

Yong et al. [2] presented work for designing of a Ø650 mm primary mirror and its support system based on the open back pocketed mirror, supported from back side of the

mirror. The design was evaluated for different materials as well three different pocketing concepts of Hexagonal, Square and Triangular pockets. There are two important properties of mirror material, that is, specific stiffness and thermal diffusivity. Silicon carbide (SiC) has been selected on the bases of these critical properties as the SiC has highest specific stiffness and thermal diffusivity. Surface deformation evaluation criteria were defined as PV $\leq\lambda/10$ and RMS $\leq\lambda/50$. The surface deformation due to polishing pressure mainly depends on the size and shape of pocket cell and face skin thickness. An equation has been presented to calculate the deformation due to polishing pressure for specific cell size shape and mirror. As triangular pocketing has the highest shape factor among all three pocketing shapes it makes triangular pocketing best among three. Comparison has been presented between the hexagonal and triangular pocketing shape as square pocketing is rarely used in circular mirror due to non-symmetric shape. Analysis shows that a triangular pocketed mirror has better design in term of lightweight ratio, max displacement, first natural frequency and stress. The pitch circle diameter of the mirror mounting has been optimized by performing FEA and found optimal radius of 0.681R. Yong et al also presented a concept for a back supported flexure for mirror mounting that stabilized the mirror in a thermal load of 18°C ±4 °C and 1 g gravity load on horizontal axis (Perpendicular to mirror optical axis). P-V face figure error has been observed as 62.8 nm, 60.2 nm and 59.4 nm. The triangular pocketed design of the primary mirror presented by young et al, [2] is shown in Figure 2.4.

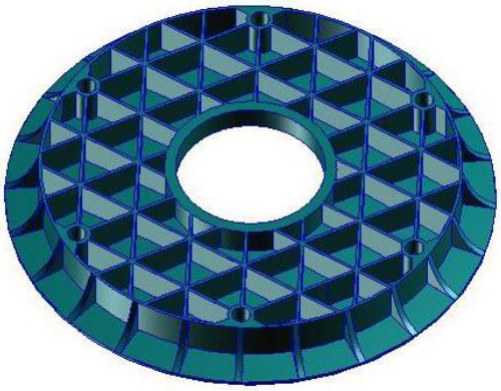

Figure 2.4: 650mm Primary Mirror Design concept [2]

Huang et al. [7] presented the design of mirrors for an off axis Korsch telescope optical system with a Ø550 mm primary mirror of Schott Zerodur. Primary mirror design is based on the open back hexagonal pocketing with flying buttresses at the outer diameter of the mirror. The mirror is designed to be supported at its outer rim with three bi pod

flexures. The design was optimized for lightweight the mass and minimize the P-V surface distortion under horizontal 1 g gravity load and thermal load of ±10 °C. P-V Surface distortion requirement of λ/10 (632.8/10=63.2 nm). Analysis results shows that the optimum design has surface distortion of PV=62 nm and RMS= 7 nm with mass of mirror =10.15 kg and 1st modal frequency of 306 Hz.The design presented by author for primary mirror assembly is shown in Figure 2.5.

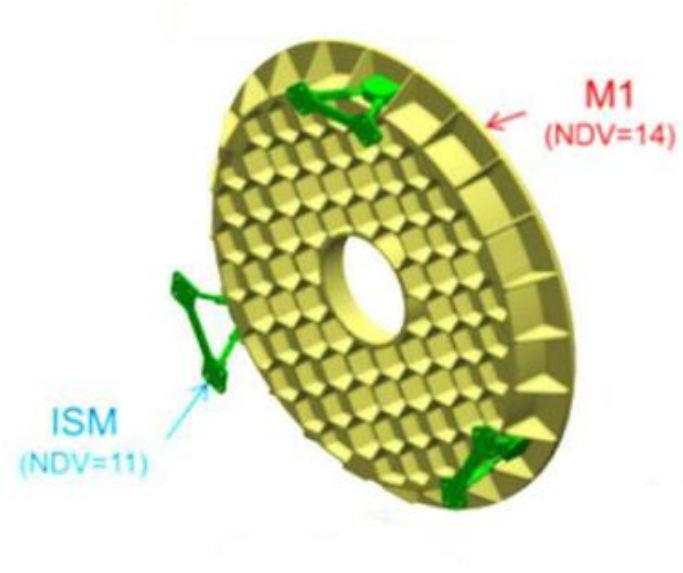

Figure 2.5: Design of 550mm diameter Primary Mirror [7]

Wang et al [8] presented the design of a Ø500 mm primary mirror for surface requirement of PV ≤λ/ 10 and RMS ≤λ/40 (λ=632.8 nm) under 1 g vertical gravity load and 18±4 °C of thermal temperature load. The mirror design also validated the natural frequency requirement of >75 Hz. Design should have enough strength to survive under static acceleration of 10 g and random vibration during launch. The design is based on an open back triangular pocketed mirror. The mirror is supported by three flexures at six points on the back side of the mirror. SiC was used to design mirror because of its high specific stiffness. The low-thermal expansion nickel-iron base invar 4J36 is selected to design the Flexure mounting of the mirror because its CTE matches with the SiC Mounting platform is design with SiC/Al. Face skin of mirror is 5mm and pocketing rib thickness is 4 mm while pitch circle radius is 180mm. The weight of mirror is 7.83 kg and lightweight rate is 60%. Mounting flexure should be design in way that it should be enough flexible, so it will not deform mirror due to thermal expansion/contraction and it should be enough stiff that it can meet the gravity and launch loads requirements. In 1st iteration the mirror design fails to meet the design requirement. So, author has

modified the design of flexure mount and optimization has been performed on the pitch circle radius of mounting and got optimum performance at 170 mm. Optimum design has surface error of PV=37 nm and RMS=10.4 nm under vertical a gravity load and PV=46 nm and RMS=10.5 nm under gravity and thermal load. Furthermore, maximum stress in the mirror support under a 10 g load is within yield limit and 1st natural frequency of 130 Hz. The design of the primary mirror assembly presented by these authors is shown in Figure 2.6

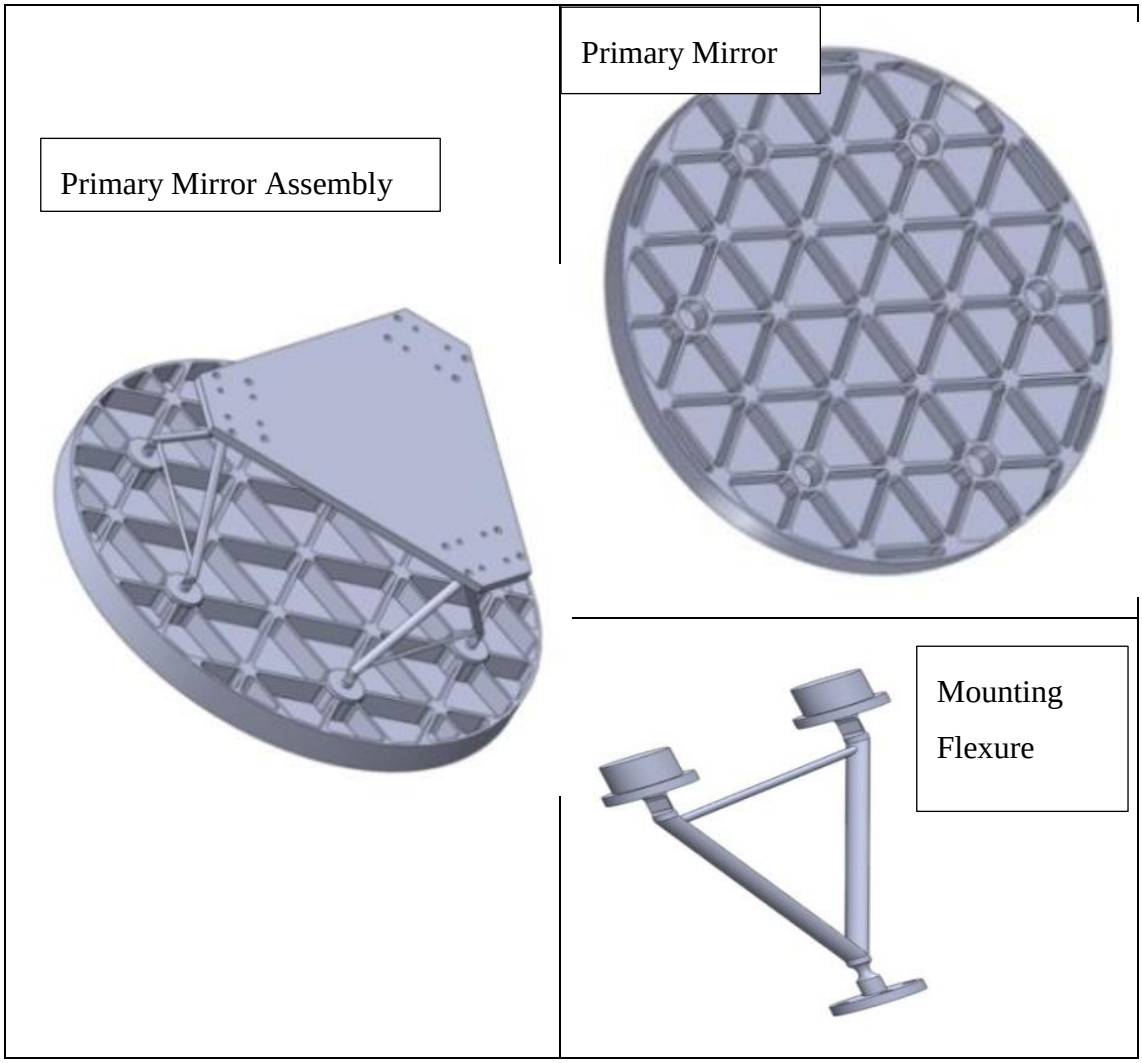

Figure 2.6: Design of 500mm Primary Mirror Assembly [8]

Park et al. [9] presented a primary mirror assembly design by using topology optimization. Their primary mirror having Ø610 mm outer diameter and Ø204.4 mm inner diameter, designed from Zerodur. The design is based on open back pocketed with flexures mounted on the outer diameter. Thickness of the mirror is 65 mm. Optimization was performed for self-weight loading and polishing pressure of 0.2068 KPa. These authors presented the results of optimized design compared to a hexagonal cell mirror.

It has RMS surface error of 134 nm while a hexagonal mirror has 156.6 nm due to gravity parallel to optical axis and polishing pressure. RMS surface error of 10.5 nm and hexagonal has 8.93 nm for gravity perpendicular to the optical axis. Figure 2.7 shows the design of 610 mm primary mirror using topology optimization technique.

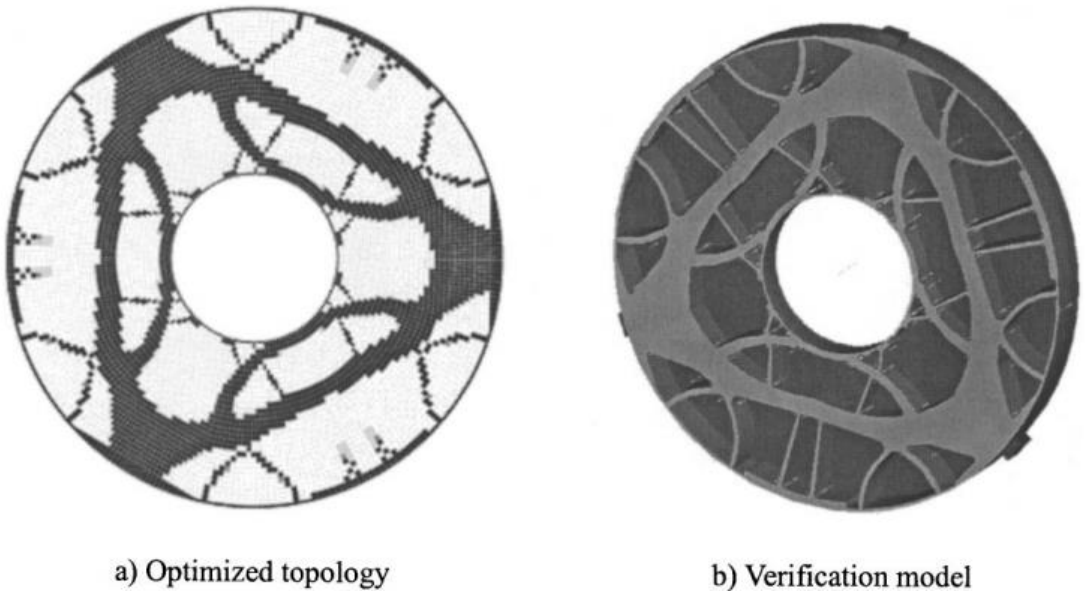

Figure 2.7: Primary Mirror design by Topology Optimization [9]

Z Li et al [10] presented a paper on the design of a 760 mm diameter primary mirror made of Silicon carbide and its mounting flexure. They used the topology optimization technique to design a lightweight mirror that has three points support on the back side of the mirror. The designed mirror structure is much similar to the Triangular pocketing having face skin on pocketed ribs. The mirror has an outer diameter of 760 mm and inner diameter of 240 mm and outer rims of 120 mm thickness. Mass of the mirror is 31.8 kg and lightweight ratio is 73.5%. Mirror height is 120 mm. These authors investigated the sensitivity of trefoil Zernike coefficient with respect to change in the dimension parameters of mirrors and it was reported that the back-plate thickness contributes a lot to the stiffness of the mirror. These authors proposed the flexure concept for back mounting. Their mirror has been designed for 1 g lateral and axial gravity and ΔT of 10 °C. They reported the surface error of 12.3 nm, 48.7 nm and 38.6 nm PV and RMS of 0.9 nm 11.1 nm and 5.8 nm for lateral gravity, axial gravity and thermal load respectively. The natural frequency of mirror is 218 Hz. The mirror design has been validated by optical testing for mirror surface error, modal frequency and quasi static

and random vibration analysis to validate the strength of mirror. Figure 2.10 show the design concept for the mirror and flexure mount. The proposed design of primary mirror and Flexure mount is shown in Figure 2.8, Figure 2.9 and Figure 2.10

Figure 2.8 Primary Mirror design for 760 mm diameter.

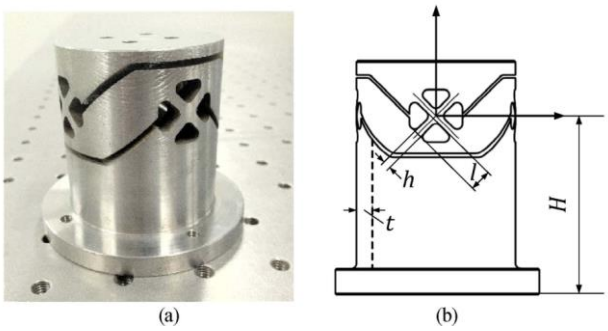

Figure 2.9: Back mounted Flexure design for Primary Mirror.

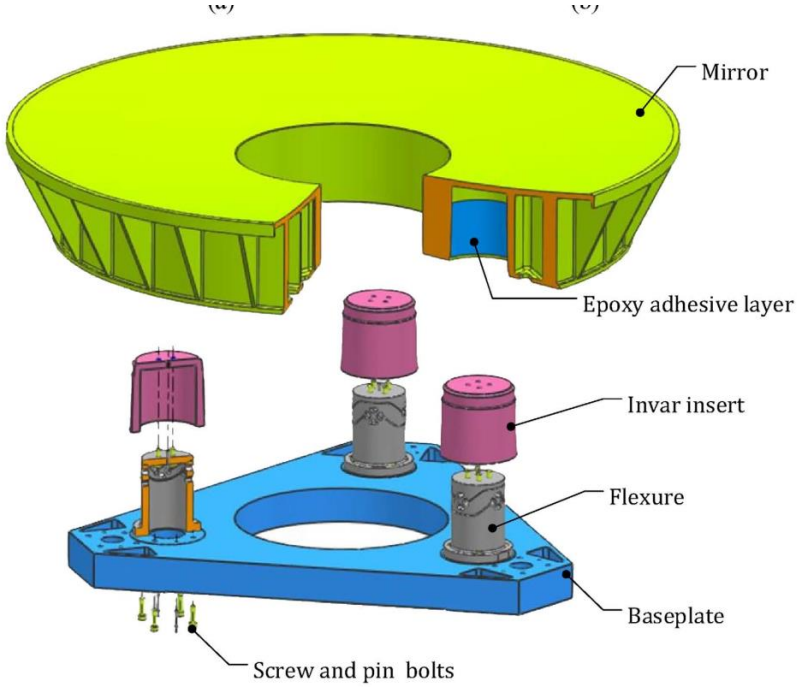

Figure 2.10: Design Concept of Primary Mirror Assembly.

It has been observed in literature review that most common materials for primary mirror design is Zerodur and Silicon Carbide. Hexagonal, triangular and circular pocketing were used for lightweight mirror designing, although some researchers design with a customized rib structure. Primary Mirrors were designing to optimize the optical surface distortion due to gravity and thermal load. Gravity can either be applied parallel to the optical axis or perpendicular to optical axis, depending on the Assembly, Integration and testing orientation of the mirror. Back support and side supported flexure mountings are the most commonly used mounting techniques for large mirrors.

3 DESIGN REQUIREMENTS AND CONSTRAINTS

3.1 Distortion Requirement

The optical surface of a primary mirror is very sensitive to distortion. Small surface error makes a huge impact on the optical performance of the system. Optical surface error is the most important consideration for primary mirror design. It has been observed from the literature review that a primary mirror has been designed for P-V of λ/10 and RMS of λ/40 for λ=633 nm, so for surface error design requirement RMS ≤ 15 nm.

The other important consideration is the loads that can induce surface error in the optical surface of primary mirror. Temperature change of the optical system is the only load that induces surface error during operation of telescope in space. The telescope is assembled, integrated and tested on the Earth in the presence of gravity but in space there is no gravity. It has to be designed in a way that the structure and mechanics of optical elements are enough stiff that it will not induce any surface error when gravitational force will be removed in space. Gravity induces optical surface error on the Earth during AIT of system that will create problem to achieve the optical performance of system on earth to ensure that system is correctly integrated. On other hand, the optical surface has been adjusted on the Earth during assembly and integration of system and system will give required performance on the Earth with gravity load. When gravity will be removed after launch of the system in space, a surface error could be induced as the result of removal of gravity. While designing the primary mirror, gravity is the one of the most critical design loads. Direction of the applied gravity depends on the AIT plan of the system. During AIT of the system and mirror, the optical

axis is usually either parallel to gravity or perpendicular to gravity. Horizontal gravity is defined as the gravity vector being perpendicular to the optical axis, while vertical gravity is defined as gravity vector being parallel to the optical axis.

The third important load case that can induce surface error is combination of vertical gravity and polishing pressure while the mirror is placed on a flat surface. This load is especially important for pocketed and sandwich mirror structures. It induces a permanent pattern of deformation that is polished into the mirror surface during the fabrication of the optical surface of the mirror. The deformation is caused in the face skin of mirror by the pocketed area. This problem is more severe for a sandwich mirror as compared to the open back pocketed mirror. Counter pressure can be applied from the open side of pocketing to balance the pressure on face skin. It can also be controlled by reducing the pressure on the polishing head but reducing the pressure will increase the polishing time, which will increase the polishing cost. The other loads that are induced the surface error are the mounting stress, adhesive curing but these are related to the mounting design of primary mirror.

Table 3.1 presents the loads that will be analyzed to validate that the design meets requirements of optical surface deformation as specified in Table 3.2. These loads will be used for designing the primary mirror. It is necessary to achieve the SE requirement under 1 g gravity in at least one direction, horizontal or vertical. Thermal temperature loads are assumed for each primary mirror design case. These loads are derived from the thermal design of the system, so it can be negotiable with thermal designer on a case by case bases, depending upon the material used for designing. Loads for polishing pressure are taken from literature review [6]. The design should meet the distortion requirements with optical bench having CTE value ≥ 3.9 µm/m-°K. This requirement has been set by system designer and has influence on the design of PM flexure.

Table 3.1: Load Requirement for Optical Surface Deformation Analysis.

S.NO	Load	Amplitude
1	Gravity	1 g Horizontal 1 g Vertical
2	Thermal	ΔT= ±5 °C
3	Polishing Pressure	5 KPa + 1 g vertical gravity
4	CTE of Optical Bench	≥ 3.9 µm/m-°K

Table 3.2: Passing Criteria for Optical Surface Deformation.

S.NO	Requirement	Passing Criteria
1	Optical Surface Distortion (SE)	RMS ≤ 15 nm
2	Optical Surface Tip/Tilt	±5 Arc sec
3	Optical Surface Decenter	±20 µm
4	Optical Surface Axial Displacement	±8 µm
5	Optical Surface Radial Distortion	±2 µm

3.2 Strength Requirement

The strength of the mirror is indirectly related to the stiffness of the material and we can correlate the stiffness to the distortion of the mirror. There are different types of load that the mirror has to bear from manufacturing until end of life. The extreme loads that have major impact on the mirror design are considered during designing of the mirror. These loads include the mirror surface polishing load with gravity, which is very important to get required surface finish. This load become very important for pocketed mirrors to avoid the pocketing impact on mirror optical surface.

The most extreme loads regarding strength of mirror design are the vibration load during launch activity that are static, sinusoidal load, random and shocks loads. Normally a mirror is designed on the equivalent static loads that are derived from design limit load (DLL).

Table 3.3 present the calculation of DLL with specified the values of different load factor used for calculation.

Design Limit load is a combination of Satellite and subsystem load factor. Design Limit Load (DLL) have been calculated for the LM2D launch vehicle [11] as per the ECSS standard for space engineering [12].The load factors used for calculation of DLL is defined as follow:

K_Q is defined as the load factor used for the qualification testing of satellite level and the value used is recommended by the Launch agency in the launch vehicle user manual [11].

Project factor (K_P) is applied for the satellite and subsystem level to account for the maturity of design. The value of design factor is initially defined for satellite and subassembly level at 1.5 and can be reduced with the maturity of design. As no information is available for the satellite so its value taken for satellite is 1.5 and 1.3 for the subsystem level as the design is new but enough literature is available for guiding design.

A Model factor (K_M) is applied to cover the margin of uncertainties in the analysis model. This factor can also be reduced up to 1 after building up confidence on the analysis model by correlating the analysis results with testing.

Local design factor (K_{LD}) addresses the difficulties faced due to specific uncertainties in analysis model of fittings, welding, riveting, bonding, inserts, and for composite layup, sandwich structure. Typical values of 1.2 are taken for all the above mention cases. This is not applicable for our design model, so the value taken is 1 for system and subsystem level.

Table 3.3: Design Limit load Calculation.

Environment	**Flight/Launch**		**Transportation**	
Direction	Long	Transverse	Long	Transverse
Satellite Payload Design Load (g)	8.70	3.00	3.00	3.00
K_Q	1.50	1.50	2.00	2.00
K_P	1.95	1.95	1.95	1.95
K_M	1.56	1.56	1.56	1.56
K_{LD}	1.00	1.00	1.00	1.00
K_{MP}	1.00	1.00	1.00	1.00
DLL (g)	39.68	13.68	18.24	18.24

All the various load factors used in calculation of design limit load comes from Table 3.4. These values have been taken as per recommendation of optomechanical design experts on the basis of previous experience.

FOSY is defined as the factor of safety for metallic parts with reference of yield strength. FOSU is defined as the factor of safety for composite and brittle material with reference of ultimate strength. Values of FOSY and FOSU are 1.25 and 2.0 as per ECSS standard [12]. These values have been used to validate the passing criteria for strength of materials. Passing criteria used for mirror glass material are the Weibull probability of failure (PoF) and its value should be < 0.3% as the passing limit.

Table 3.4: **Design Limit load Factors.**

Factor	Satellite level	Explanation	Subsystem level	Explanation
K_Q	1.5	From Launch Manual >= 1.5	1	Not applicable
K_P	1.5	No information on Satellite	1.3	New design but sufficient literature is available on design.
K_M	1.3	Assumes a non-correlated FE model	1.2	Fine Finite Element Model with some assumptions. Model is not correlated with testing.
K_{LD}	1	N/A	1	Not implemented
K_{MP}	1	N/A	1	N/A

The other important load for strength of the mirror is the thermal survival load This load defines that what are the extreme temperature ranges under which the primary mirror should survive without any damage. During these extreme temperatures, mirror surface deformations are not important because mirror will be non-operative at these temperatures. Table 3.5 presents the design loads for a strength analysis and passing criteria are presented in Table 3.6.

Table 3.5: Design Loads for Strength Analysis.

S.NO	Design Loads	Amplitude
1	Natural Frequency	>100 Hz
2	Equivalent Static Design load	40 g Longitudinal and 19 g Lateral Direction.
3	Thermal Survival Load	-20 °C for Cold and +70 °C for Hot case.

Table 3.6: Passing Criteria for Strength Analysis.

S.NO	Design Requirement	Passing Criteria
1	Passing Criteria (Glass Materials)	Weibull Probability of Failure > 0.3%
2	Passing Criteria for Metallic parts (Yield Strength)	FOS=1.25
3	Passing Criteria for Brittle materials (Ultimate Strength)	FOS=2

4 DESIGN METHODOLOGY

4.1 Designing Trade-offs

In this chapter, we will analyze the primary mirror optical surface error for different load conditions. Trade-offs will be performed for the mirror mounting concept, mirror pocketing design and materials used for the mirror. Table 4.1 shows the constant design variables used for the tradeoff analysis of mirror mounting and pocketing shape.

Table 4.1: Design parameter for Trade-offs

S No	Design Parameter	Value
1	Outer Diameter	620 mm
2	Inner Diameter	280 mm
3	Pocketing Inscribed Circle	40 mm
4	Pocketing Ribs thickness	3 mm
5	Rib Thickness at inner and outer diameters	10 mm
6	Minimum face skin thickness	5 mm
7	Mirror Thickness	60 mm
8	Mass	< 20 Kg

4.1.1 Mirror Mounting Trade off

The primary mirror can be mounted from the central hole, outer diameter (side supported) and back side of the mirror. In this section the effect of the mirror mounting location on the optical surface error will be analyzed. For this analysis a triangular pocketed mirror has been modelled with support at three points of diameter 50 mm for all three case. Fixed supports have been applied on all three mountings of the mirror in each case to analyze the effect of optical surface error due to gravity. Figure 4.1 shows the mirror pocketing design with three different mounting concepts for trade-off of optical surface error under gravity load.

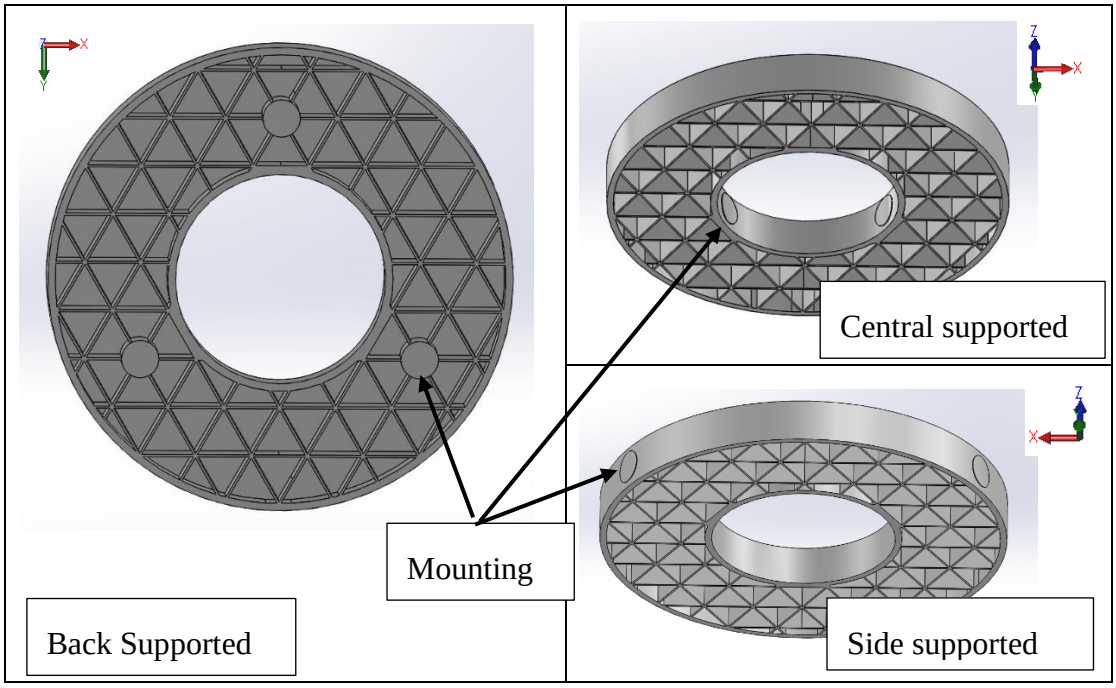

Figure 4.1: Primary Mirror Mounting Concept.

Figure 4.2 shows the RMS of surface error under vertical (Z direction) and horizontal (X and Y direction) gravity loads for central support, side support and back support of the primary mirror. It has been observed that back supported mirror works best for vertical gravity while for horizontal gravity the side support is the best option. It also has been observed that the amplitude of surface error for vertical gravity are much higher than the horizontal gravity.

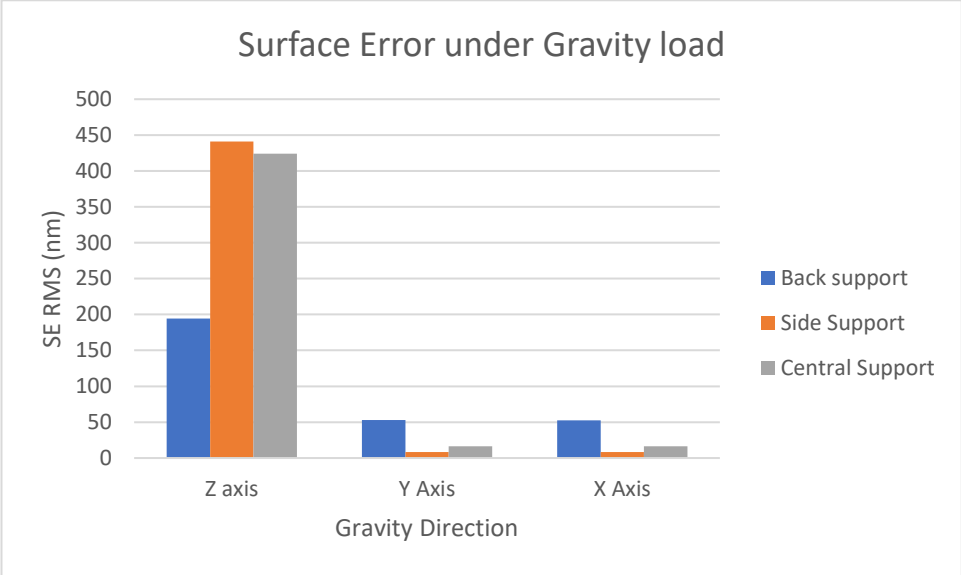

Figure 4.2: Optical Surface Error for Mounting Concepts.

To meet the surface error requirement only for horizontal gravity, the side support mounting option is good but for better performance in both horizontal and vertical direction then the back supported mounting is the better option for further design refining. These values are only for the mirror constraints. The values may increase when the mounting mechanics of the mirror will be integrated with the mirror for analysis.

The back-support mounting has been analyzed for the surface distortion error under a vertical gravity load. The triangular pocket mirror with back supported mount as shown in Figure 4.1was used for this analysis. Keeping all the parameters same just change the mounting distance. Figure 4.3 shows the effect of mounting distance from center of the mirror for the back supported mounting. The X-axis shows the mounting distance from the center of the mirror while the Y-axis represents the RMS of surface distortion error under a vertical gravity load. It has been observed that the surface distortion error is minimum for the range of 210 mm to 230 mm with the variation of about 0.95%. Even for the range of 200 mm to 240 mm the maximum variation is about 3.6%, which is not too large a value.

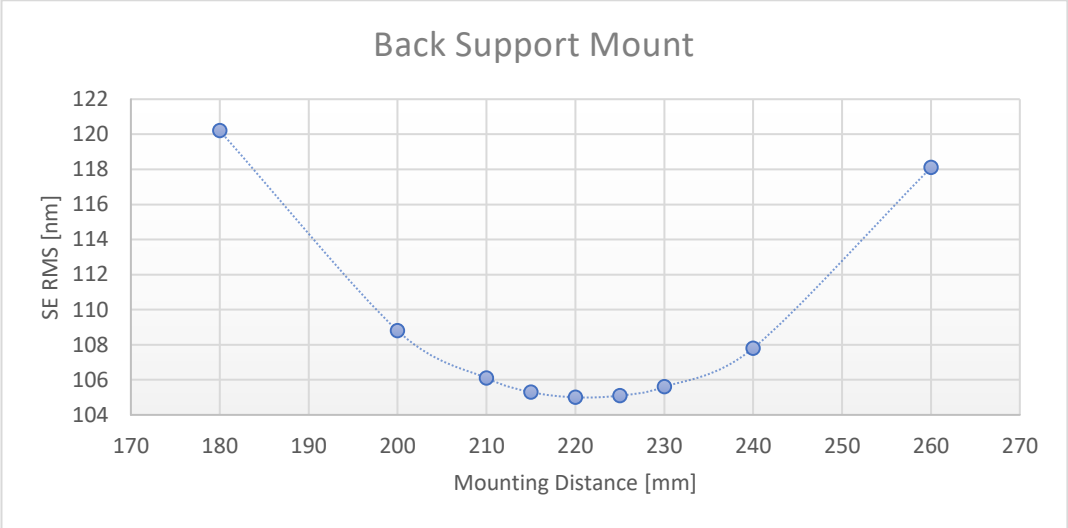

Figure 4.3: Surface Distortion Error for mounting distance from Centre.

4.1.2 Mirror Structure Concepts Trade Off

Hexagonal, triangular, square, circular pocketing and a circular rib structure mirror concepts were analyzed to check the effect of pocketing shape for optical surface error under 1g vertical gravity loads. The rest of the design parameters were used as specified in Table 4.1. Fixed constraints have been applied at the mounting of the mirror. All designs are based a on three-point back supported mounting. The hexagonal and triangular pocket structure concepts are shown in Figure 4.4.

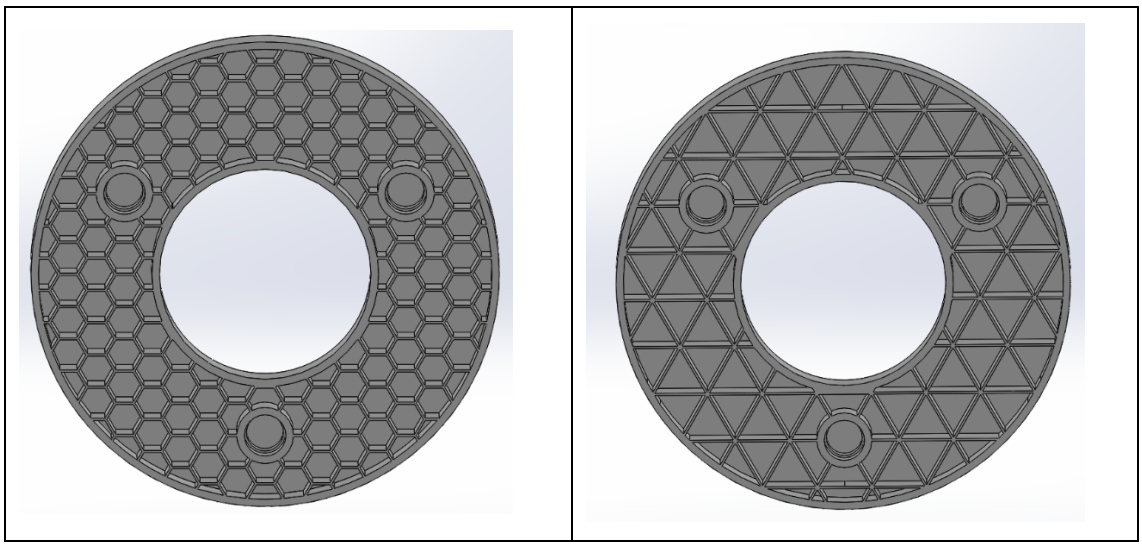

Figure 4.4: Hexagonal and Triangular Pocketed Structure Concept.

Figure 4.5 shows the concept of square and circular pocketed mirror structures.

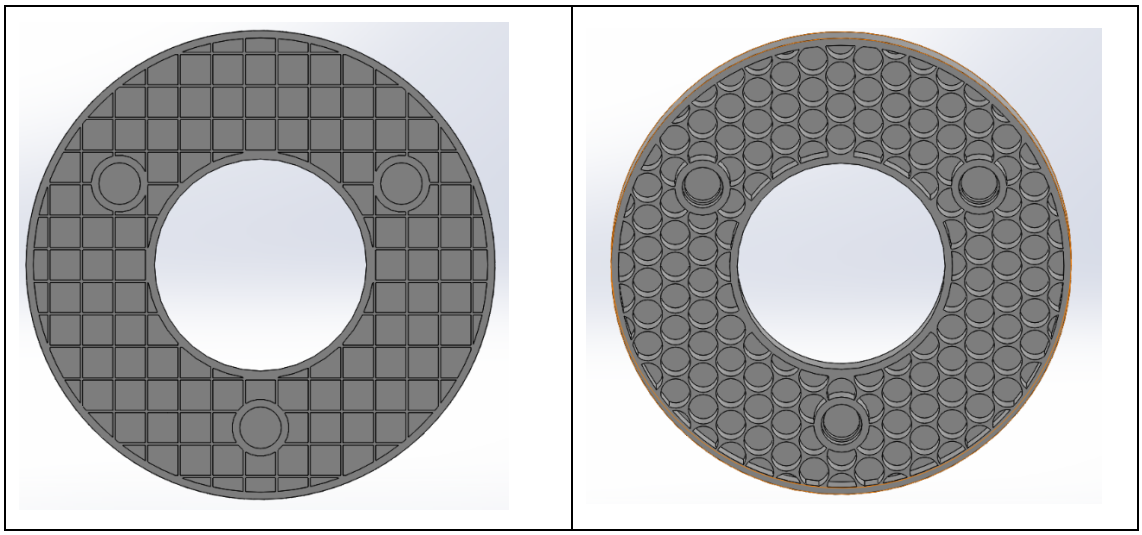

Figure 4.5: Square and Circular Pocketed Structure Concepts.

The circular ribs structure mirror design is presented in Figure 4.6. All five mentioned concepts have been analyzed for optical surface error generated by vertical 1 g gravity.

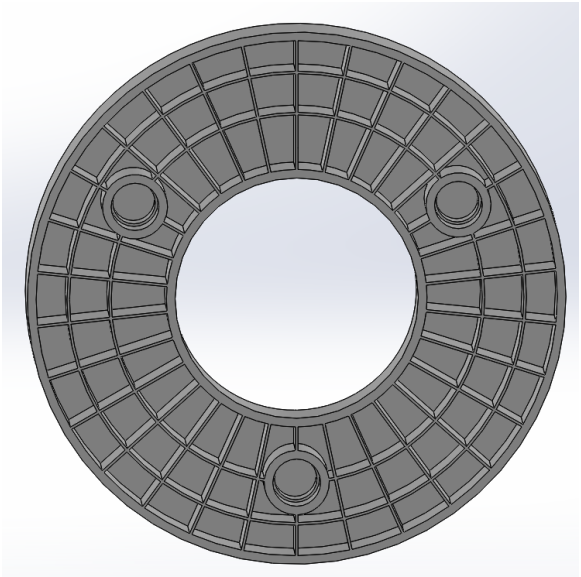

Figure 4.6: Circular Ribs Structure Concept.

All five pocketing concepts have been analyzed for vertical gravity load. Figure 4.7 shown the RMS surface error for the pocketing concept under a vertical 1 g gravity load. It has been observed that triangular pocketing has the least surface error while the hexagonal pocketing has the maximum optical surface error.

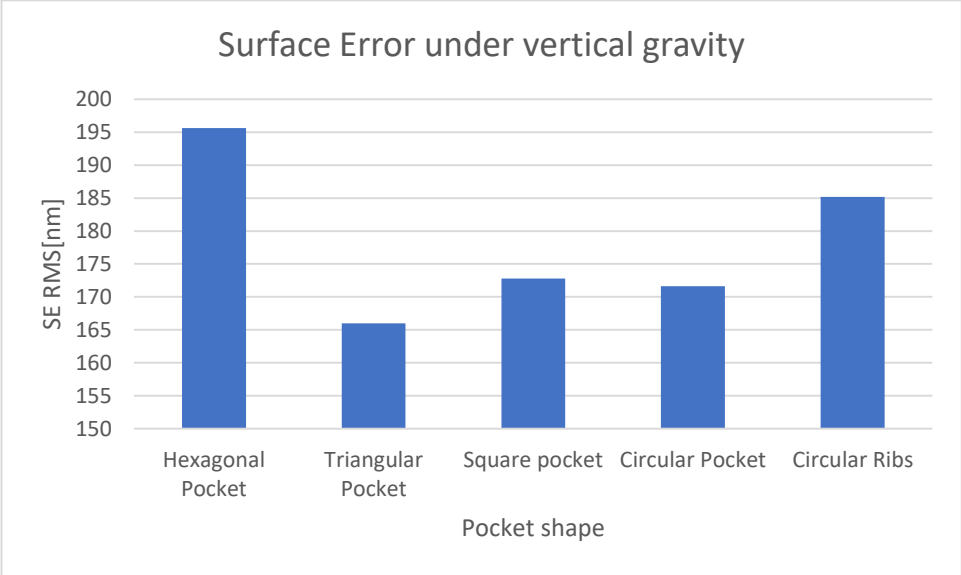

Figure 4.7: Surface Error for pocketing design.

The hexagonal, triangular and square pocketing designs were analyzed for 60 mm, 80 mm, 100 mm and 120 mm thickness of the mirror by keeping all other parameters constant. Results are presented in Figure 4.8. It has been observed that the mirror surface error decreases significantly with increasing thickness of the mirror. The performance of the triangular and square pocketing is significantly close to each other with little edge for triangular pocketing Mirror. The triangular pocketing mirror have another benefit over the square pocketing mirror that it will maintain the mirror symmetric while the square pocketing disturbs the circular symmetry of the mirror, which may create problems during thermal expansion of the mirror.

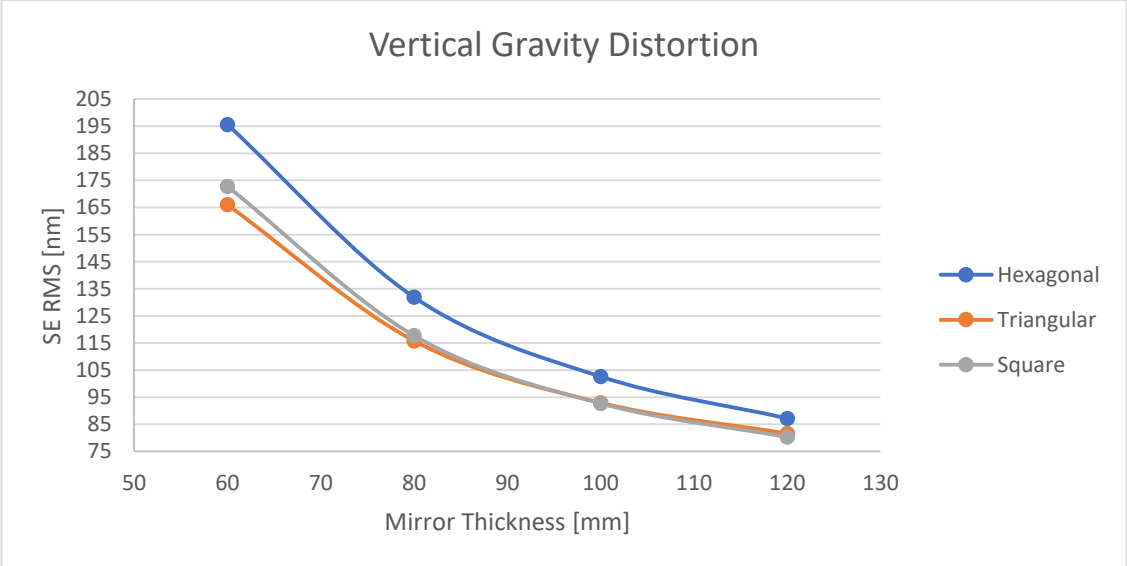

Figure 4.8: Mirror thickness vs SE of Mirror under Vertical Gravity.

Although mirror thickness positively contributes toward the stiffness of the mirror that helps to minimize the surface error of optical surface. But increase the thickness of the mirror also increase the mass of the mirror as shown in Figure 4.9. Each 20 mm of thickness increase approx. 20% of the mass of the mirror.

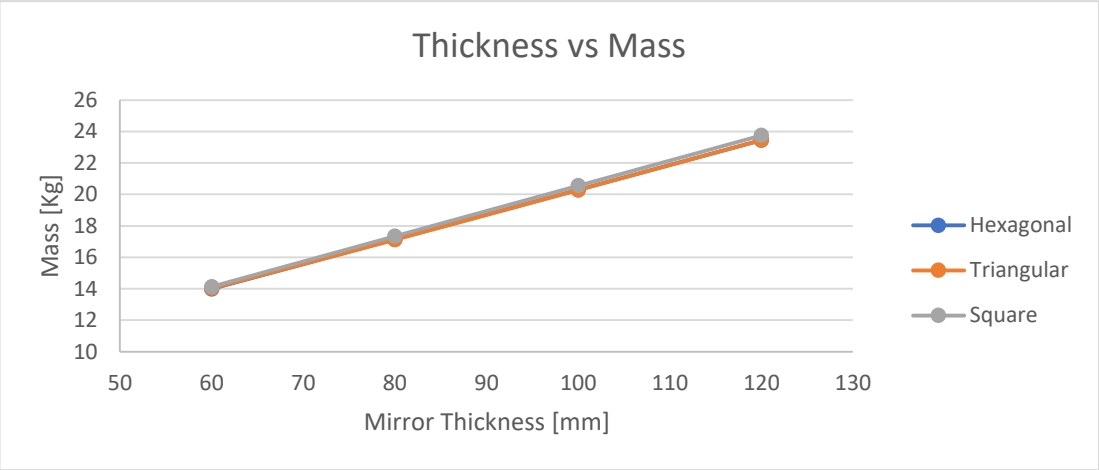

Figure 4.9: Mirror thickness vs Mass of Mirror.

4.2 Evaluation of Design Variables

The stiffness of Zerodur primary mirror has been optimized to reduce the surface distortion error due to vertical gravity loads. The triangular pocketed mirror with back support mounting has been used for the stiffness optimization. Selection of triangular pocketed mirror is based on the tradeoff study of mirror pocketing shape. The stiffness of the mirror structure has been optimized by defining the design variables of mirror structure. The effect of each design variable on the mirror surface error has been analyzed under a 1 g gravity load. A preliminary CAD design model with twelve design variables with initial values is presented in Figure 4.10. These design variables have been evaluated to analyze the effect of these design variables on the surface error when the mirror is subjected to gravity load in the vertical direction. Each of these design variables has been evaluated separately while keeping the others constant.

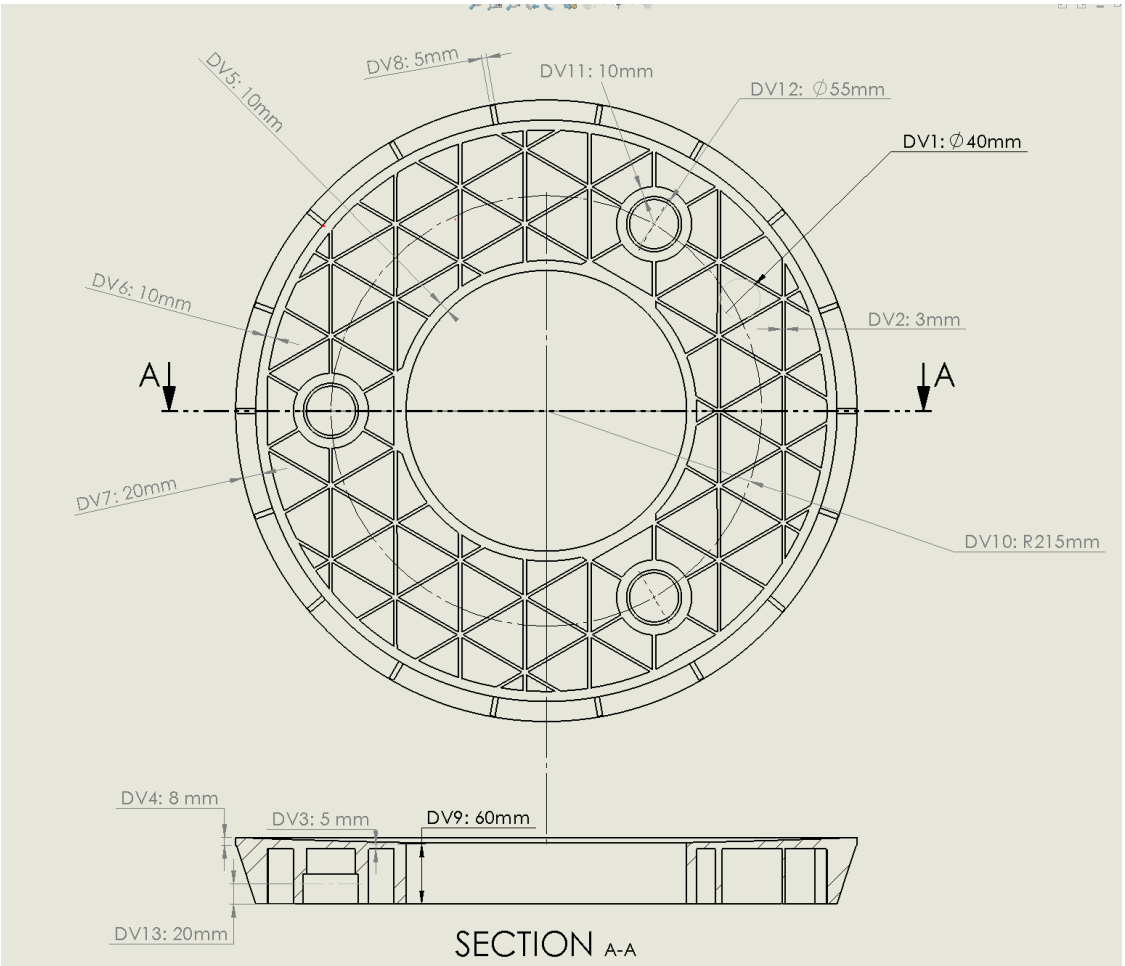

Figure 4.10: Mirror CAD model for evaluation of Design Variables.

Design Variable 1 (DV1) defines the inscribed circle diameter of the pocket. Physically it defines the size of the pocket. The analysis has been performed by changing the DV1 and keeping all the other design variables constant as specified in Figure 4.10. Effect of changing DV1 on the surface distortion error and mass of mirror is shown in Figure 4.11. It has been observed that as the surface error (SE) decreased with decrease in DV1 while mass increased. So DV1 has a linear relation with surface error and inverse relation with mass in the range of 35 to 45 mm. A change in SE of 26.1 nm per kg change in mass has been observed for 45 to 40 mm DV1, while for 40 to 35 mm the change in SE is 14.6 nm per kg.

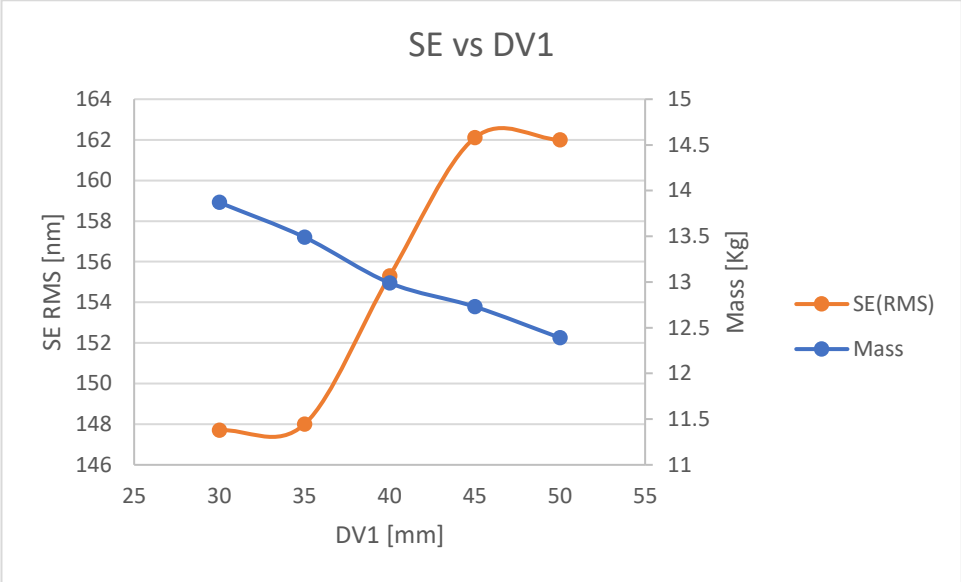

Figure 4.11: Surface distortion error of Design Variable 1.

Design Variable 2 (DV2) is defined as the rib thickness of the pockets. Figure 4.12 shows that by increasing DV2 the surface error will be decreased. The RMS SE is inversely proportional to DV2. A max change of 6.6 nm SE per kg has been observed.

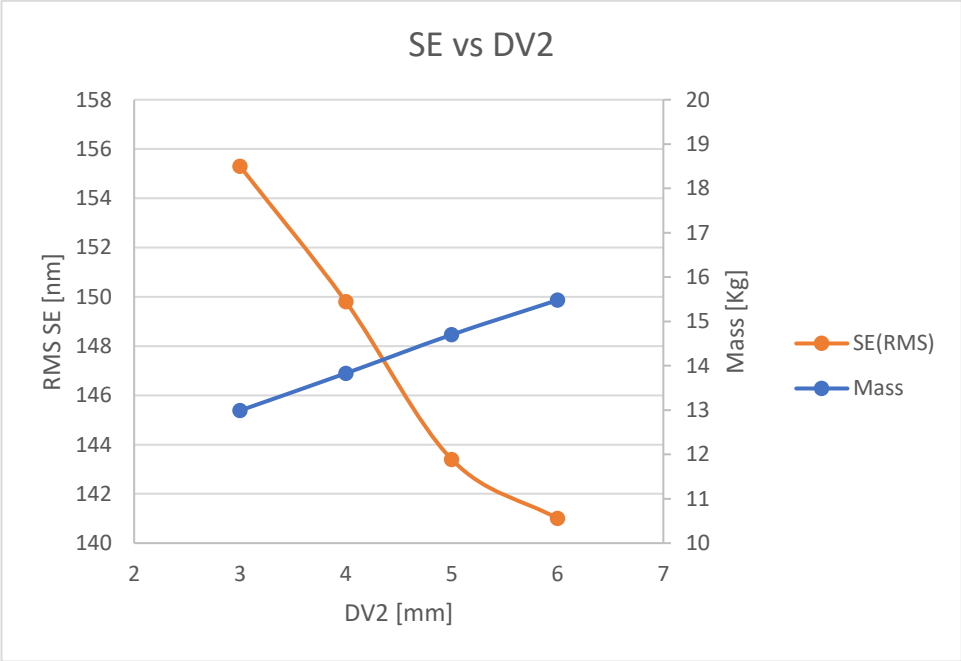

Figure 4.12: Surface Error for Design Variable 2.

Minimum face skin thickness of mirror is defined as DV3. Figure 4.13 shows that there is optimum value for DV3 for which lowest surface error has been observed. Improvement in SE for range of 3 to 5 mm of DV3 not very significant. So, it can be optimized in between range of 3 to 5 mm.

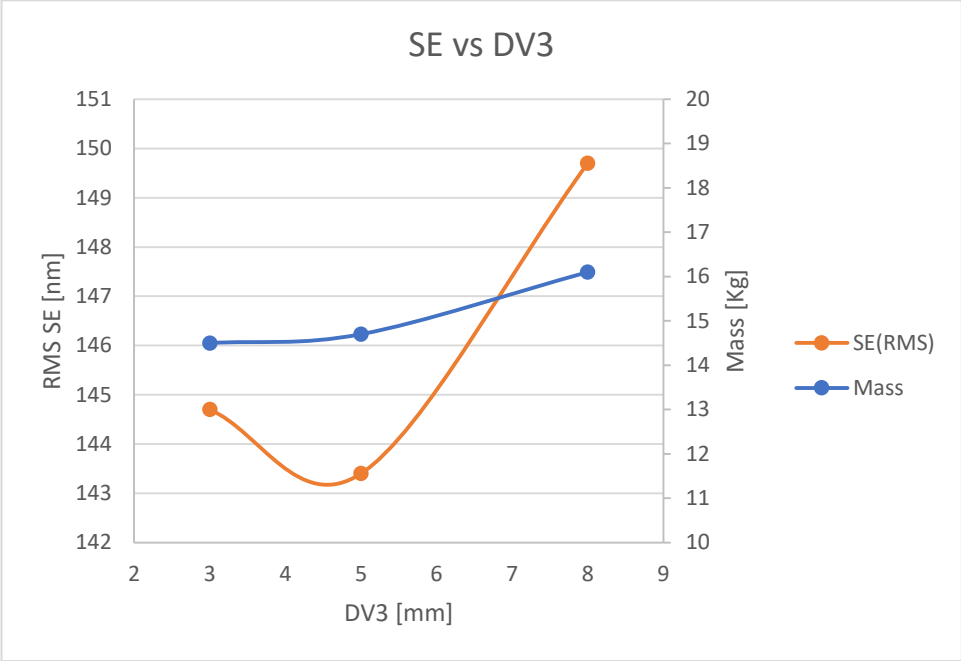

Figure 4.13: Surface Error for Design Variable 3.

The face skin thickness at the outer diameter of the mirror is defined as DV4. Figure 4.14 shows that DV4 has linear relation to the surface error of optical surface. It is good to have minimum DV4, but limitation has been imposed by manufacturing of minimum thickness.

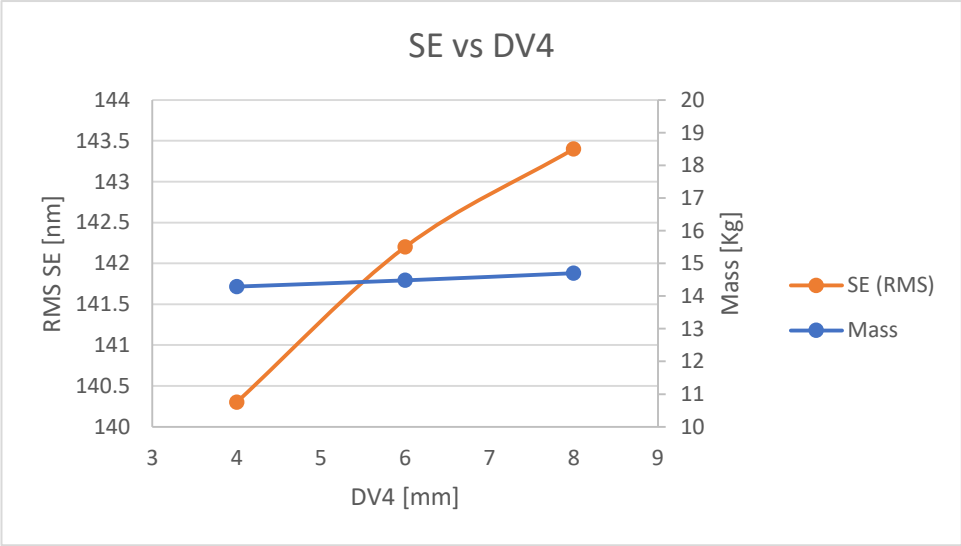

Figure 4.14: Surface Error for Design Variable 4.

The thickness of the inner circle rib is defined as the DV5. It has inverse relation with the SE and directly proportional to the mass as shown in Figure 4.15. 10 mm of DV5 is

observed as optimum value for SE. Higher than 10 mm of DV5 is not bring significant reduction in SE.

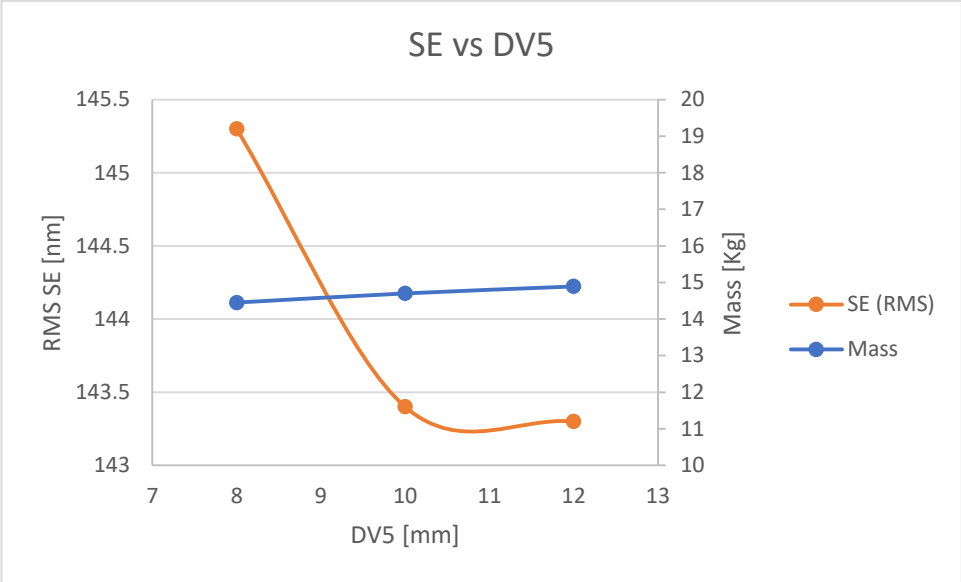

Figure 4.15: Surface Error for Design Variable 5.

The thickness of outer circular rib is defined as the DV6. Figure 4.16 shows that a DV6 of 10 mm is the optimum value for SE.

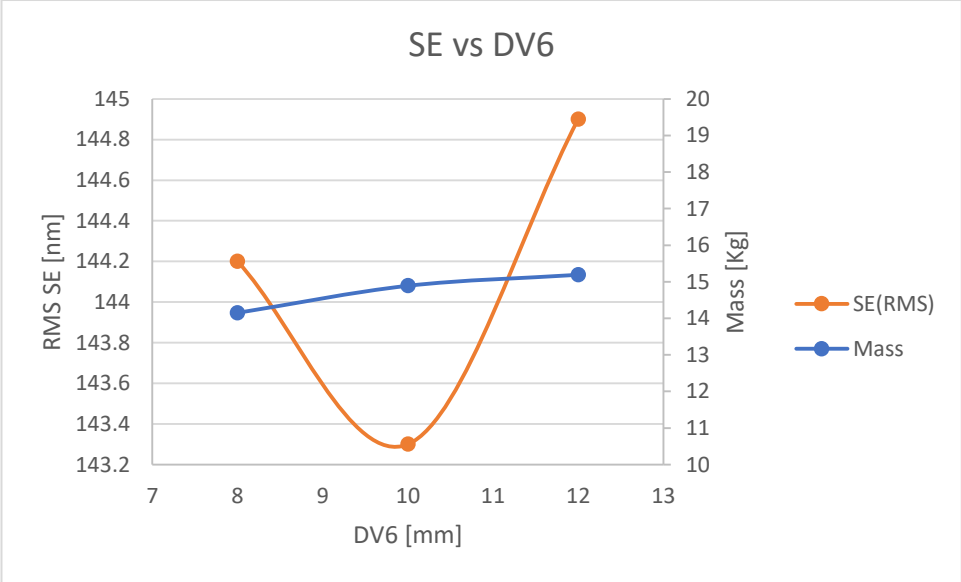

Figure 4.16: Surface Error for Design Variable 6.

The overhang face skin at the outer diameter is defined as the DV7. Analysis shows that DV7 has inverse relation with the surface error but after certain value the change is not much significant as shown in Figure 4.17.

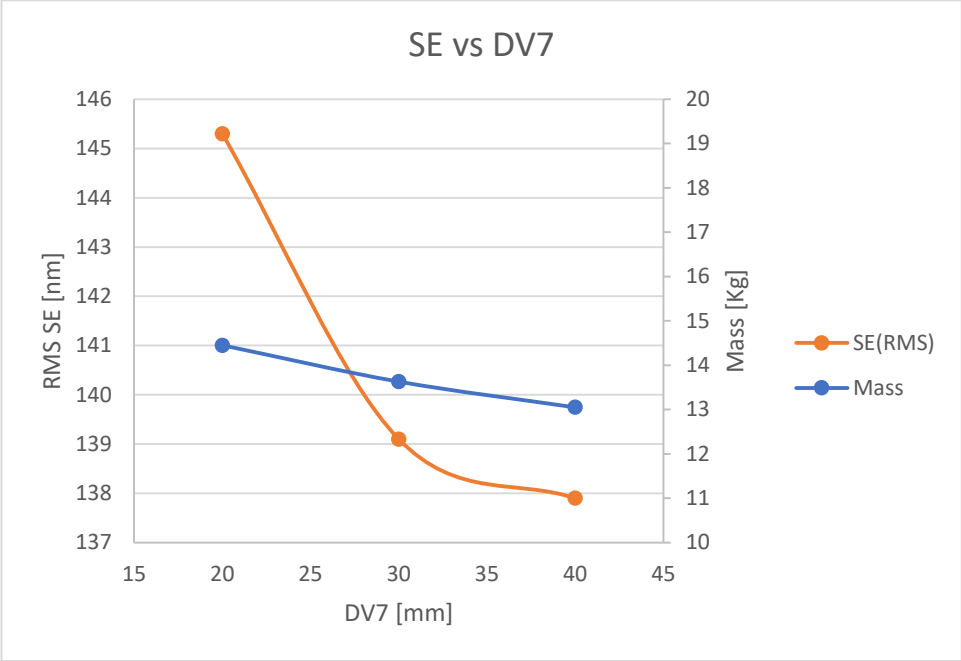

Figure 4.17: Surface Error for Design Variable 7.

The thickness of the radial ribs at the outer diameter is defined as the DV8. It has direct relation with the surface error as shown in Figure 4.18. The minimum manufacture-able thickness is the optimum value for DV8.

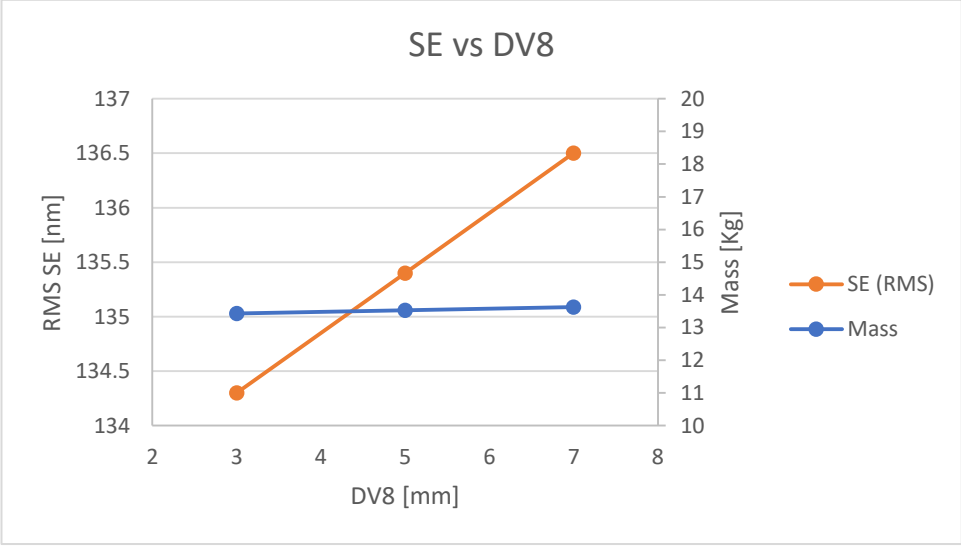

Figure 4.18: Surface Error for Design Variable 8.

Mirror thickness is defined as DV9. Analysis shows that DV9 has an inverse relation with surface error and a direct relation with the mass of the mirror as shown in Figure 4.19. Thickness of the mirror contribute a lot toward the stiffness but on the other hand it also increases the mass of the mirror. DV9 is highly sensitive to the optical surface

error for an initial 30 mm increase in thickness. Later on, the sensitivity of the DV9 reduced for higher values. The contribution of DV9 toward mass is linear at 1.58 kg per 10 mm increase of DV9.

.

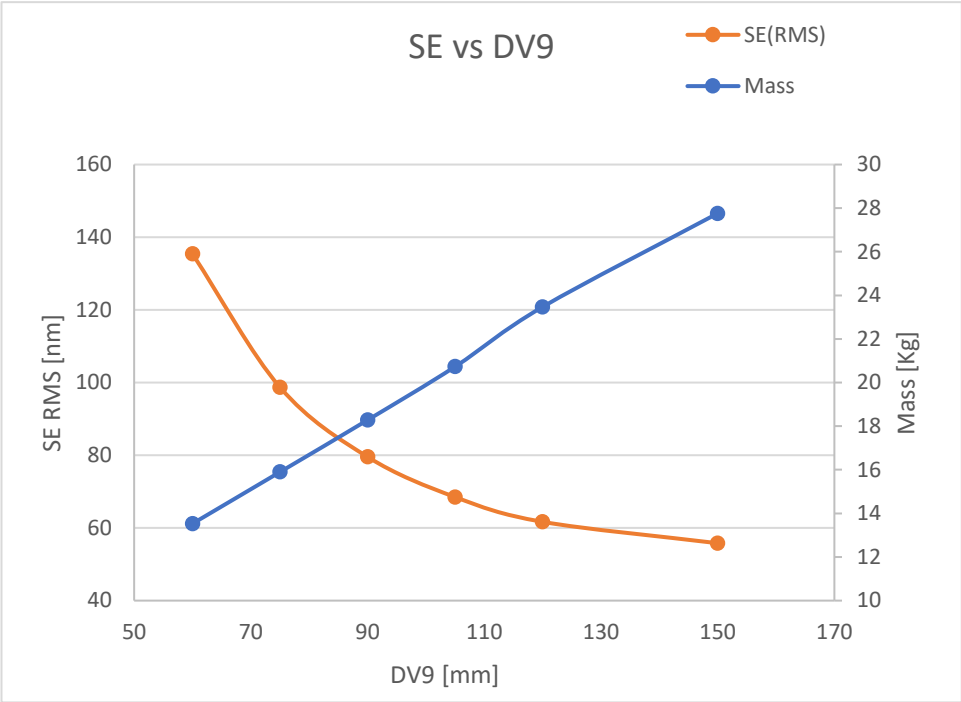

Figure 4.19: Surface Error for Design Variable 9.

The radial distance of mounting location is defined as DV10. Figure 4.20 shows that there is an optimum radial location for mirror mounting at distance between 205 to 215 mm. But if we look at the SE values it shows DV10 is not very sensitive to surface error.

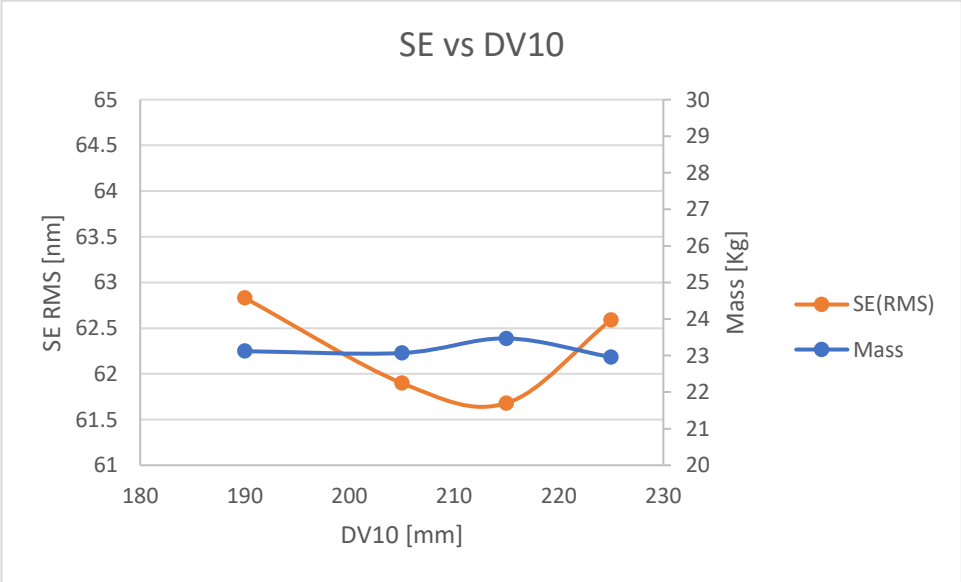

Figure 4.20: Surface Error for Design Variable 10 (Vertical gravity).

The thickness of mounting interface is defined as DV11. Figure 4.21 shows that DV11 has an inverse relation with optical surface error. Increasing the value DV11 will minimize the optical surface error.

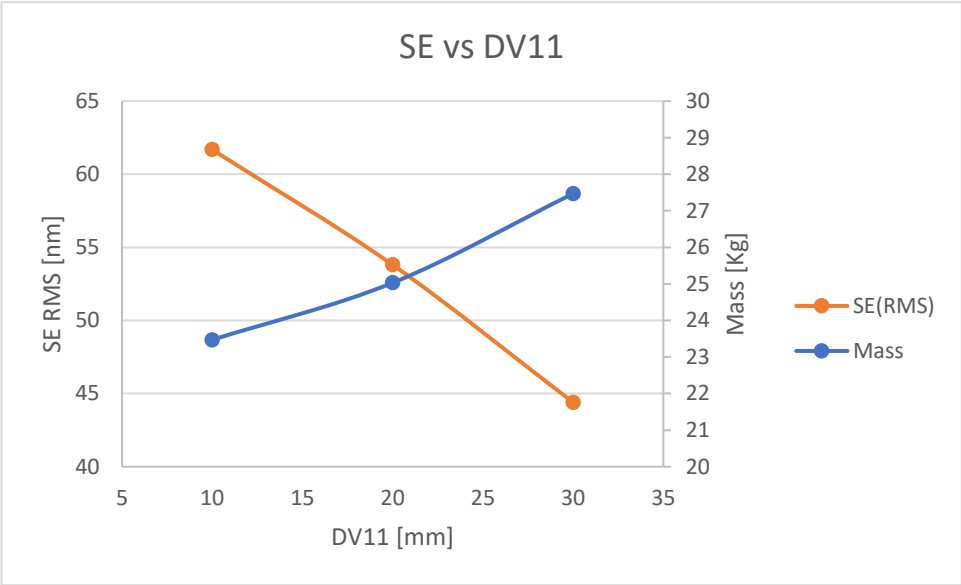

Figure 4.21: Surface Error for Design Variable 11.

The diameter of the mounting interface hole is defined as DV12. It has a direct relation with mass and an inverse relation with the SE.

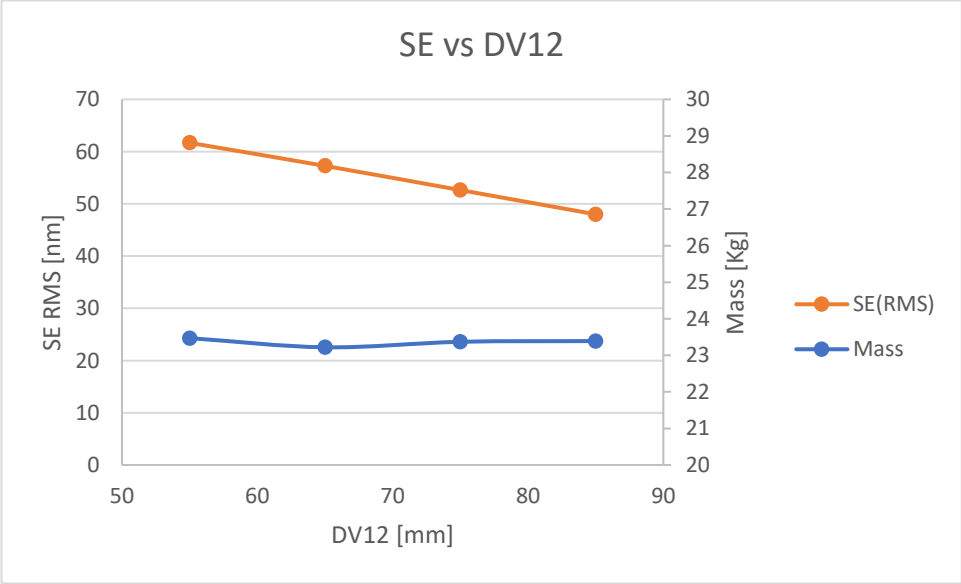

Figure 4.22: Surface Error for Design Variable 12.

Figure 4.23 presents the trend relation for surface error with mass of the mirror. This data has been compiled from the evaluation of different design variables for surface errors of the optical surface of the mirror when gravity is applied vertically (parallel to the optical axis). It shows that surface error decreases with addition of the mass during the analysis of the design variables. Surface error can be minimized at the cost of mirror mass.

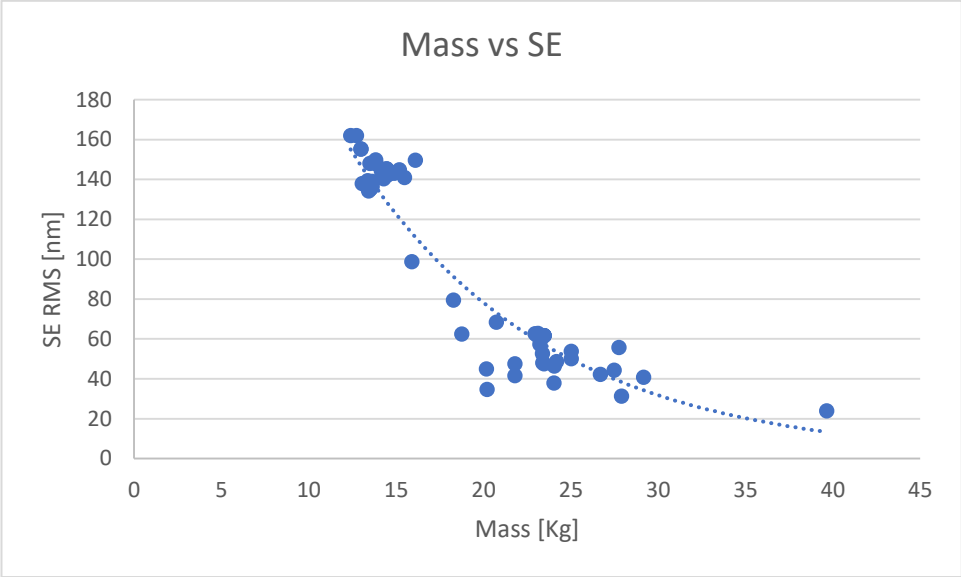

Figure 4.23: Trend for SE vs Mass of Mirror Trend.

4.3 Mirror Materials Trade off

Trade off analyses were performed for Zerodur and silicon carbide mirrors having the same structure design as shown in Figure 4.24. For this analysis we assumed a mirror with a thickness of 120 mm and applied fixed constraint at mounting spots of the mirror for gravity load analysis in lateral and longitudinal direction. Linear static thermal analysis was also performed for a high temperature load case of 27.5 ˚C with reference temperature of 22.5 ˚C. Properties of materials used are specified in Table 1.1.

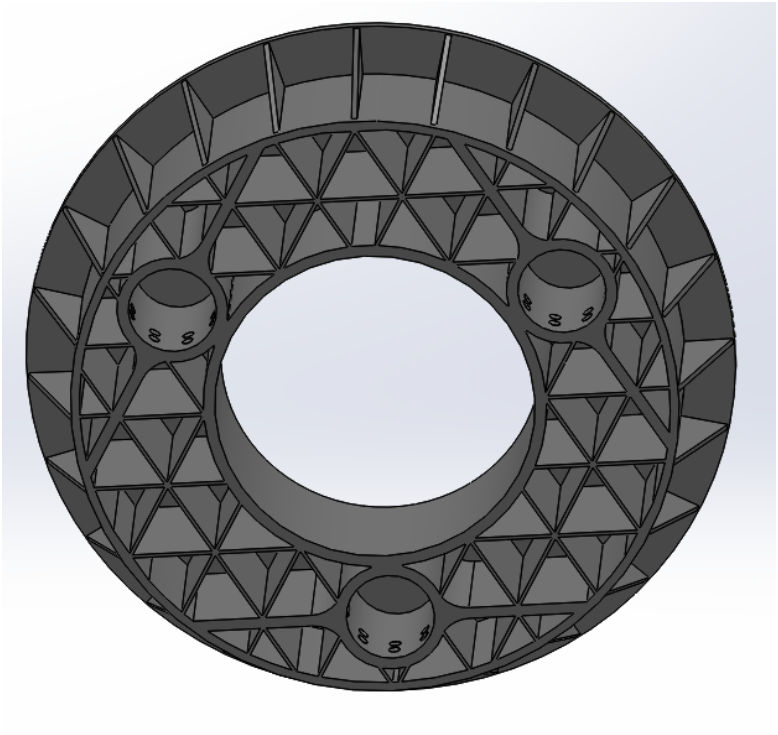

Figure 4.24: Mirror Structure design for Materials Trade off.

Zerodur and silicon carbide were analyzed for optical surface distortion errors under high temperature loads, and under vertical and horizontal gravity loads. Results are presented in Figure 4.25. These result show that silicon carbide has much lower surface error as compare to Zerodur for the gravity load case because of the high material stiffness. On the other hand, it has a very high surface error compare with Zerodur for thermal load case due to its high CTE value. If we specifically discuss this design, the Zerodur mirror meets the SE requirement for thermal load case while silicon carbide is meeting the requirement of SE for gravity load case. The silicon carbide mirror can be used by resolving the problem of surface error under thermal load.

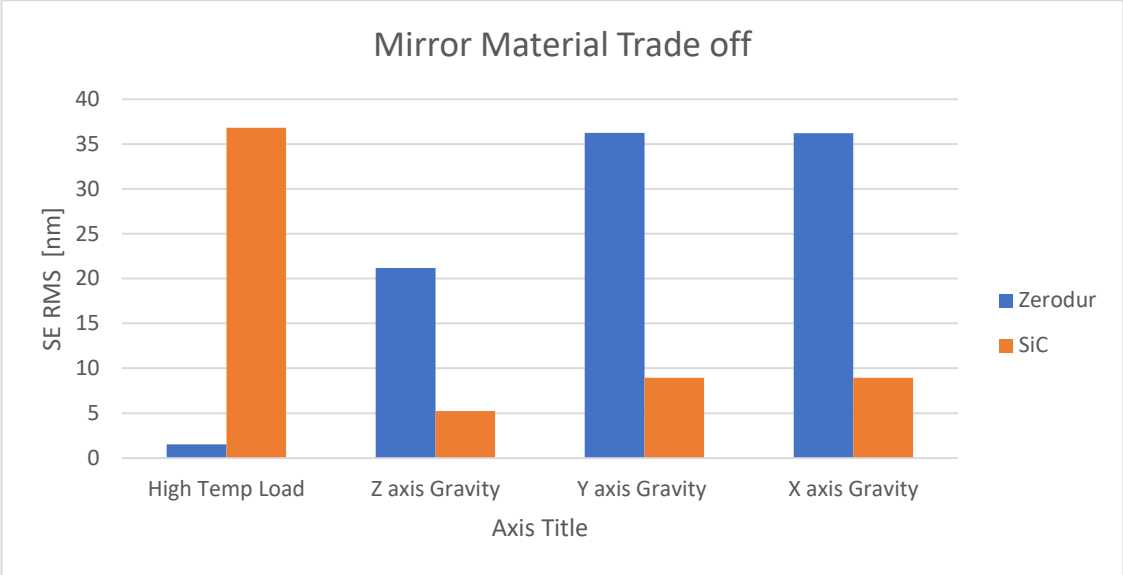

Figure 4.25: Surface Error vs Mirror Material.

Figure 4.26 shows the contours of optical surface error for the silicon carbide mirror under a high temperature load case. It is noted that the major portion of defocus is present in the surface error. Defocus of the primary mirror can be compensated by adjustment of the secondary mirror in system, but it requires specialized design to be able to adjust the position of the secondary mirror with change in temperature of the primary mirror.

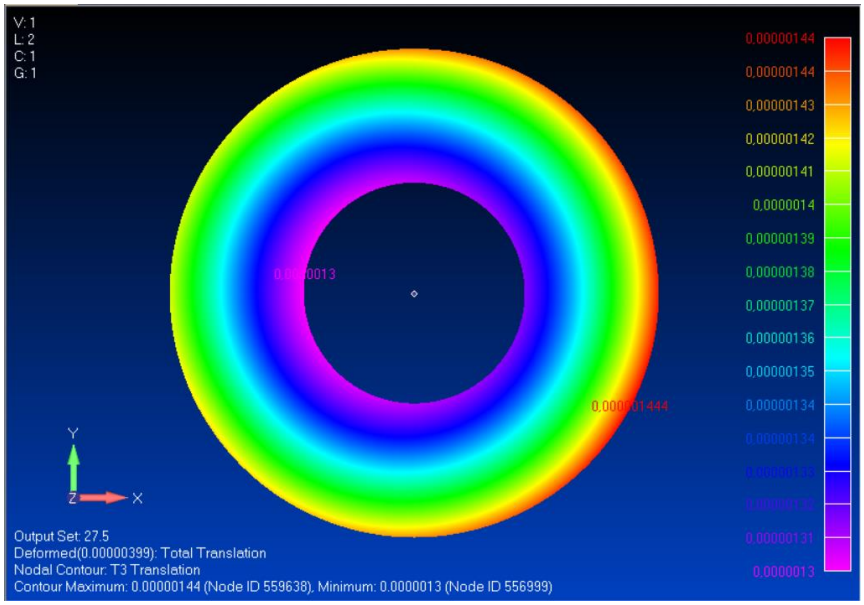

Figure 4.26: Optical surface distortion for SiC (Thermal Load) [m].

The other solution to reduce the surface error for the silicon carbide mirror is by modifying the operational temperature range of the primary mirror. It will put more effect toward the thermal design of the primary mirror. Figure 4.27 shows that the

thermal surface error is directly proportional to the temperature change. A SE of 15nm is noted at a temperature of 24.5 ˚C. So, this SiC mirror design is workable for a both gravity load of 1 g and a thermal load of 22.5 ± 2 ˚C.

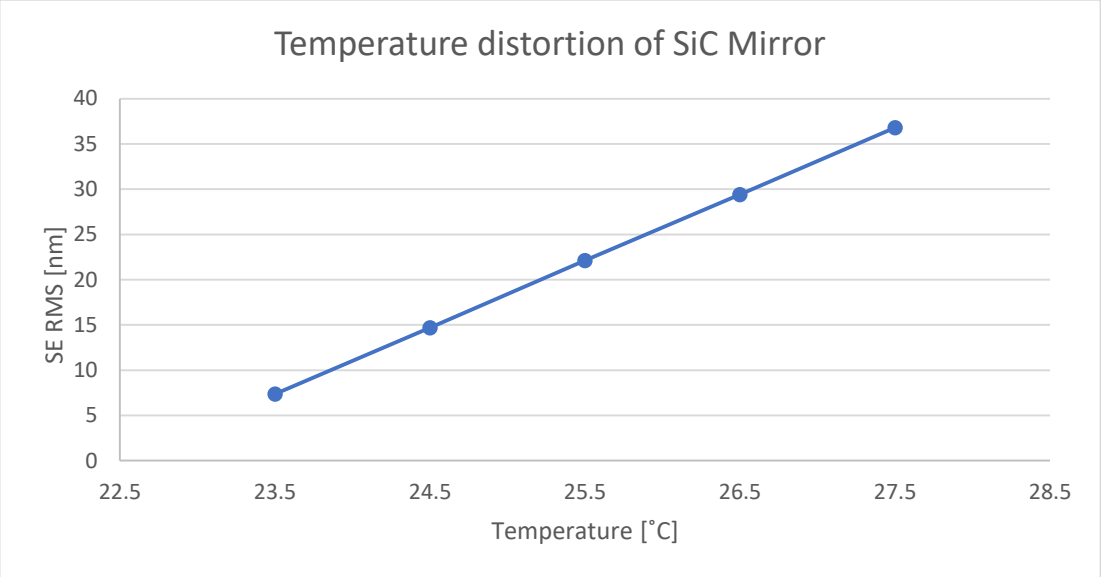

Figure 4.27: SE vs Temperature of SiC Mirror.

A primary mirror made of Zerodur is working well for a temperature load of 22.5 ± 5 ˚C but its surface error for gravity load is on higher side. The surface error of the mirror can be reduced by mounting the mirror near the shear centre of the mirror. Figure 4.28 shows the relationship of SE with mounting location (along the thickness of the mirror) to the vertical and horizontal gravity. Surface error for horizontal gravity is reduced when mounting distance from the base of the mirror is increased. It shows that mounting near the shear centre of the mirror will optimize the surface error in horizontal gravity while surface error under vertical gravity will be increased.

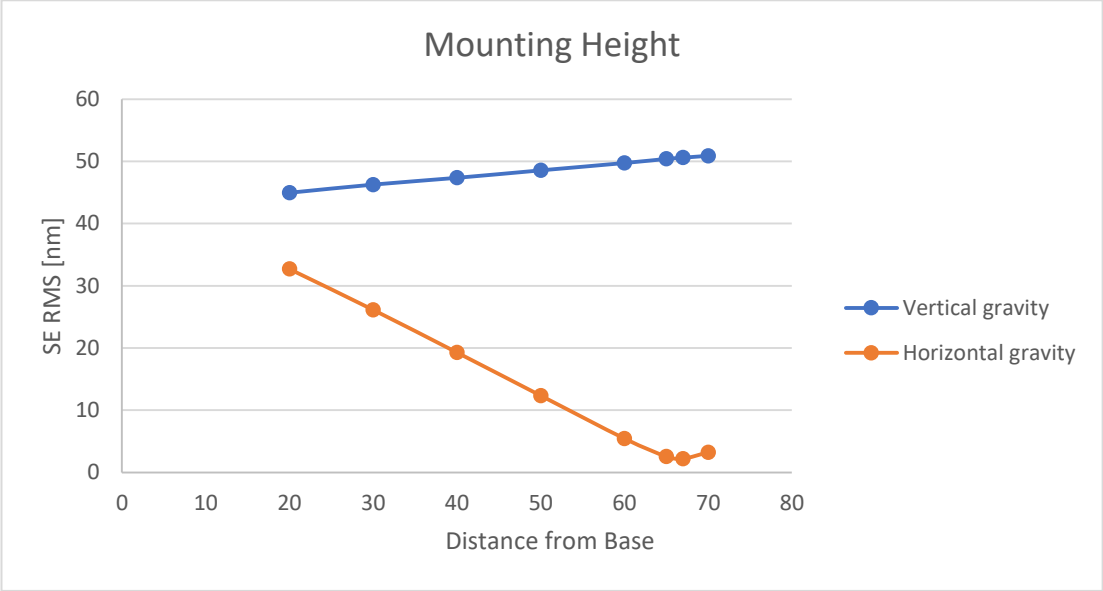

Figure 4.28: Surface Error for Vertical and Horizontal gravity.

It has been concluded from the trade-off analysis and evaluation of design variables that stiffness of the mirror material contributes a lot to meet the surface error requirement under vertical gravity, while the CTE of the mirror material contributes toward the surface error under the thermal expansion load. As per design requirement of the primary mirror it should meet the surface error requirement for the desired temperature range and 1 g gravity load in the horizontal or vertical direction. For this design problem the Zerodur primary mirror having low CTE property is better option.

5 OPTOMECHANICAL DESIGN DESCRIPTION

It was concluded in chapter 4 that there are two feasible design solutions with two different materials that can fulfil the design requirements. One with a silicon carbide mirror and the other one with a Zerodur mirror. Silicon carbide is the material with better stiffness but poor CTE as compared to Zerodur. A silicon carbide mirror can be used for a relatively narrow range of operating temperature or with some specialized focus adjustment mechanism that can compensate the surface error of defocus due to temperature variation. On the other hand, Zerodur has good CTE properties but relatively low stiffness properties. So, it will be quite difficult to use Zerodur in an AIT environment where gravity is acting perpendicular to the optical surface of mirror. Taking all this into consideration, a lightweight Zerodur mirror with low CTE value that can operate in a wide temperature range is a better option for designing of the large primary mirror. The only disadvantage of a Zerodur mirror is that the assembly, integration and testing of the mirror has to be performed when gravity is acting horizontally (i-e perpendicular to optical axis).

5.1 Primary Mirror Assembly Design Description

The primary mirror assembly (PMA) is mounted on the optical bench (OB) that is defined as a flat surface having an interface for the mounting of the primary mirror flexure. The optical bench (OB) is not the part of the PMA, but it is important to define the OB because the CTE of the OB has influence on the designing of the flexure. The CTE of OB is assumed to be 3.9 µm/m°C in the radial direction and it should be radially symmetrical. The axial CTE of the OB is not critical because it will only contribute to the axial displacement of optical surface and has no impact to the design of flexures.

The primary mirror assembly consists of following components:

- a Primary Mirror
- three Mounting Bosses

- three Bi-pod flexures.

The primary mirror has been designed with open back triangular pocketing to make it lightweight and stiff as shown in Figure 5.1. Zerodur has been used to design the mirror because of its low CTE value. The design has three flat surfaces at the outer diameter of the mirror separated 120˚ from each other to create the mounting interface of the mirror. Three additional 10 mm ribs have been added in the pocketing to provide additional stiffness to the mirror. The three mounting areas of the mirror are kept as solid, with no pocketing. The lightweight ratio of the mirror is 57%.

Origin of the PMA is defined at center of optical surface of the mirror and plus Z-axis is the optical axis of the mirror as shown in Figure 5.1.

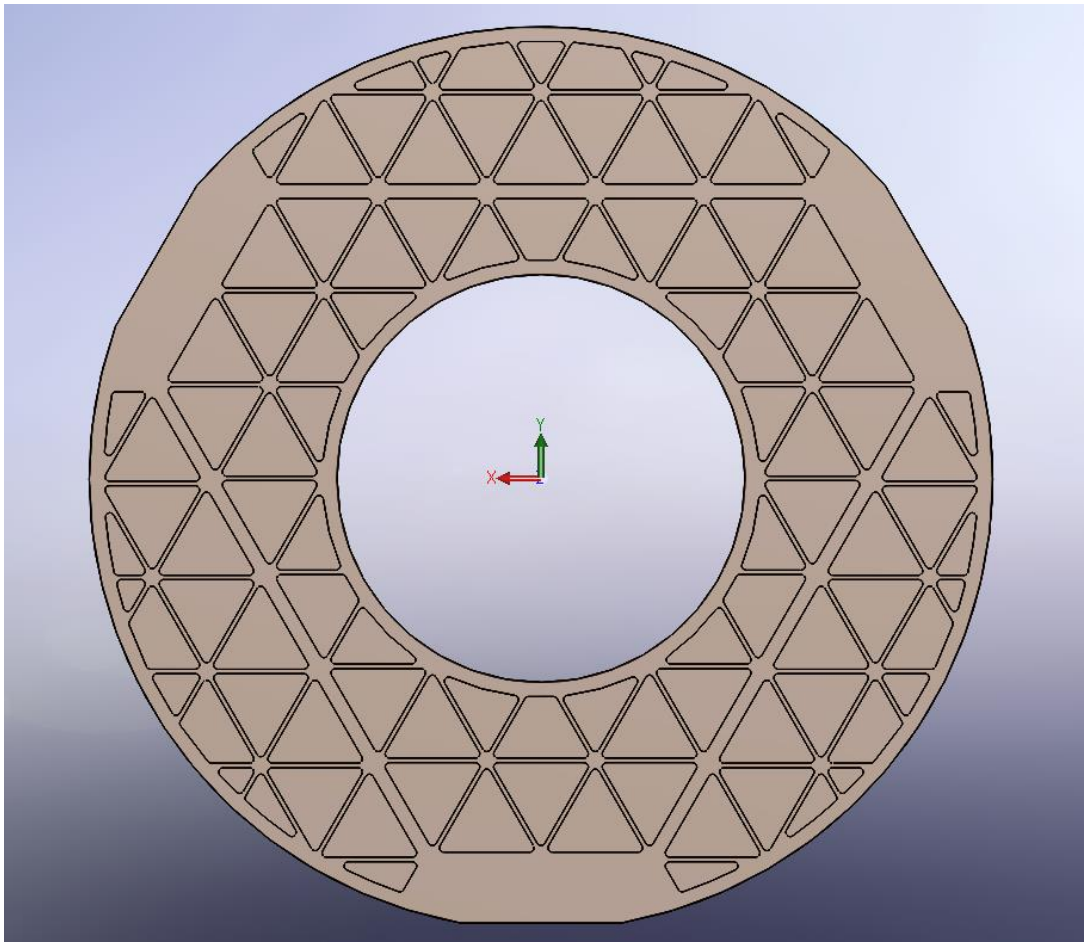

Figure 5.1: Primary Mirror Pocketing Design.

Figure 5.2 shows values of design variables and dimensions of the mirror design. A 3 mm fillet has been added to all the corners of the pockets and 1 mm chamfer to all the sharp edges at the inner and outer diameter.

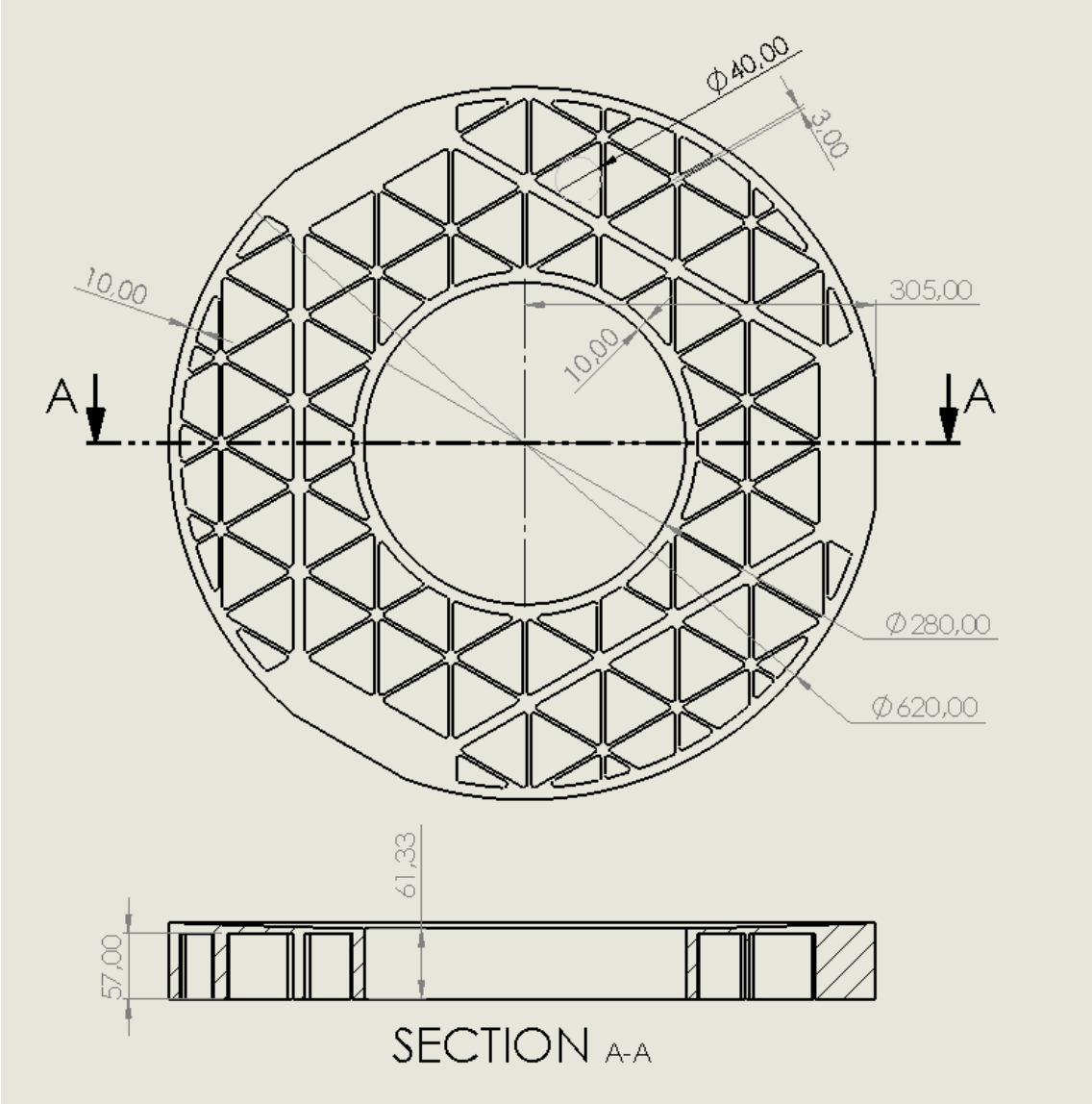

Figure 5.2: Primary Mirror design variables.

The three mounting bosses have been designed of Invar 36 material because of its low CTE properties so that the CTE of the mounting bosses can be as close as possible to the CTE of the mirror material. This will avoid the distortion in the optical surface of the mirror due to temperature fluctuation. Figure 5.3 presents the CAD design of the primary mirror mounting boss. Three bosses will be bonded on to the primary mirror to create mounting interfaces for the flexures.

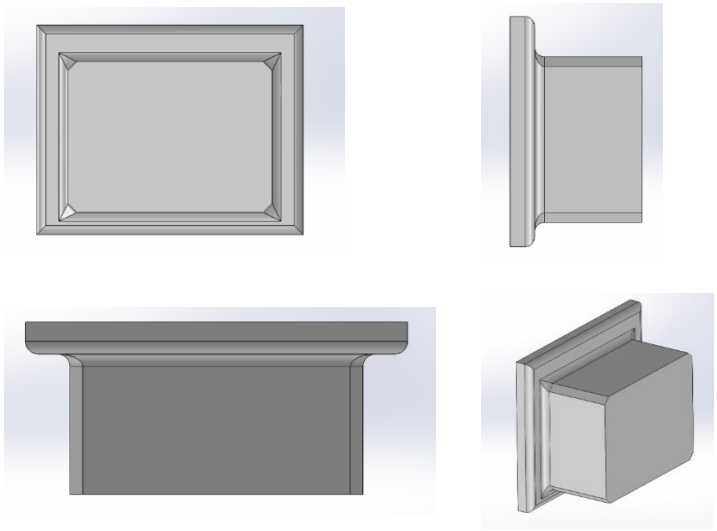

Figure 5.3: CAD design of mounting boss.

Figure 5.4 presents the CAD design of the primary mirror flexures. These are designed for Titanium material because of its high stiffness and strength. It should be stiff so that it can carry the load of the PMA and it must be flexible enough so that it will isolate the mirror from thermal expansion and contraction of the optical bench. Each flexure has four surfaces for bonding with the mounting boss and two mounting surfaces for the optical bench having three bolt connection at each.

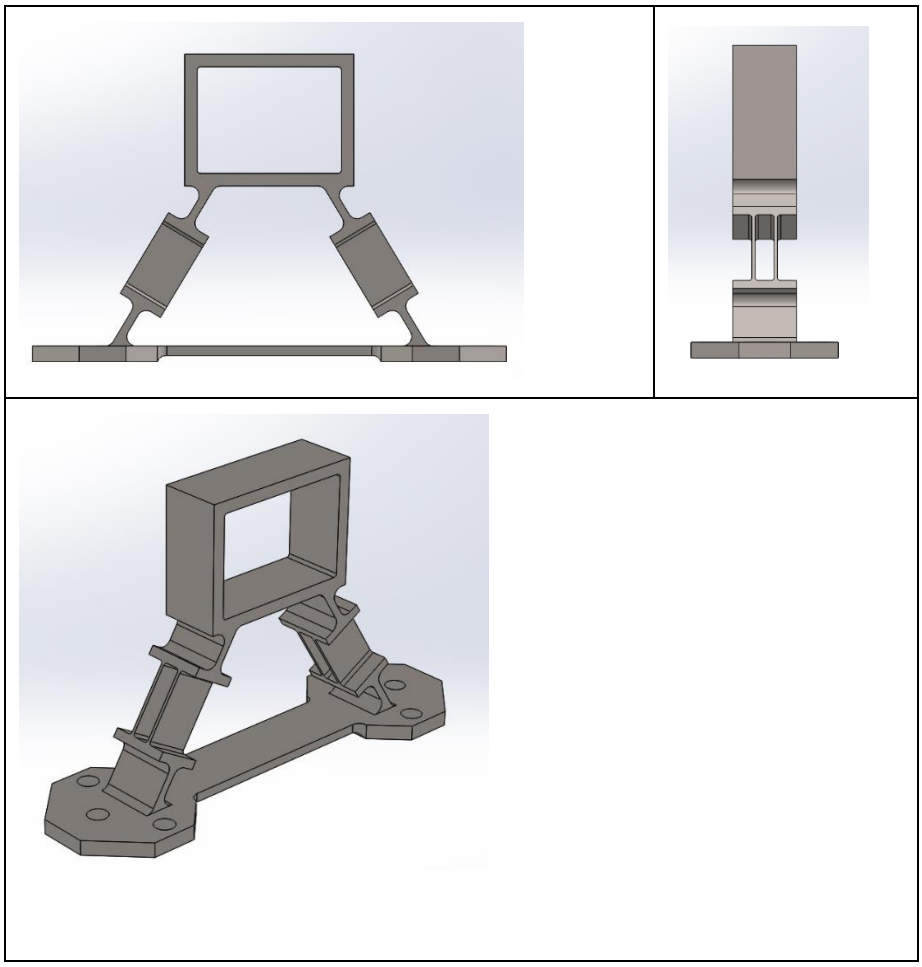

Figure 5.4: CAD Model of Primary Mirror Flexure.

The glass to metal bond is one of the critical design areas of the PMA. Normally the CTE of adhesive is much higher than that of bonding glass. 3M EC 2216-B/A is a commonly used adhesive for mounting optics. Recommended thickness of EC2216-B/A for a good bond strength is 75 – 125 µm. Bond thickness can be achieved by using shims of specified thickness or by mixing the glass beads into the adhesive bond before applying it. Curing of the bond develops shear stress in the glass. This can be control by limiting the size of the glue bond as a small size adhesive bond generate less shear stress in glass [13]. The adhesive bond area can be calculated by using following equation:

$$Q_{min} = \frac{W.a_g.f_s}{j}$$

where Q_{min} is minimum adhesive bond area, W is weight of glass (mirror), a_g is maximum expected acceleration load, f_s is factor of safety (at least 2 for adhesive bond) and J is the adhesive shear stress. On the basis of above equation, the adhesive bond

interface of 12 x bond spots has been designed as shown in Figure 5.5 for three mounting interfaces of the primary mirror.

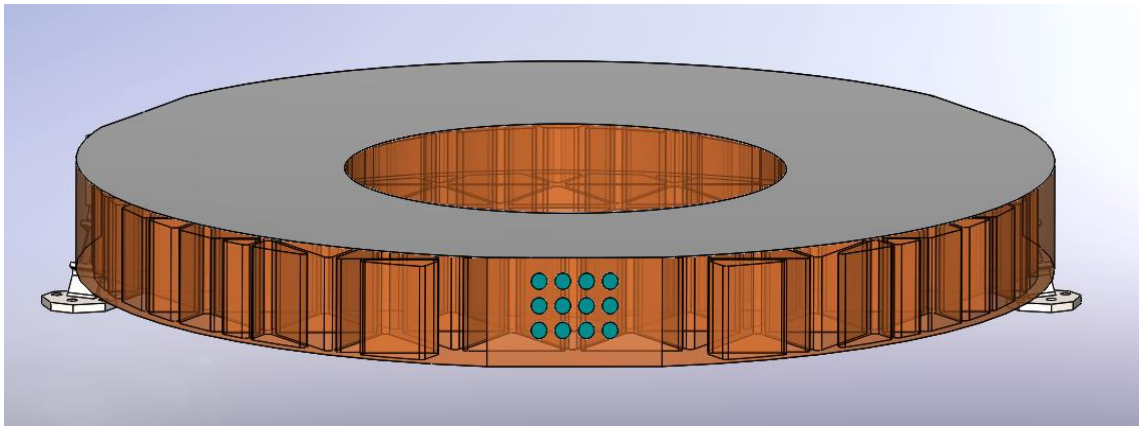

Figure 5.5: Primary Mirror Adhesive Bond design.

The primary mirror (PM) has three flat surfaces on outer diameter for interfacing with the mounting bosses. The bosses will be mounted on the primary mirror by mean of an adhesive bond joint. There will be 12 holes in mounting boss at the location of each adhesive spot. Adhesive will be injected from those holes using pneumatic adhesive injector. Mounting bosses will create interfaces for PM flexures as shown in Figure 5.6. There are bolted connection between the mounting boss and the flexure. .The PM flexures have mounting interface of PMA with the optical bench with six bolts connections at each flexure. Figure 5.7 shows the assembled view of the primary mirror, boss and flexure.

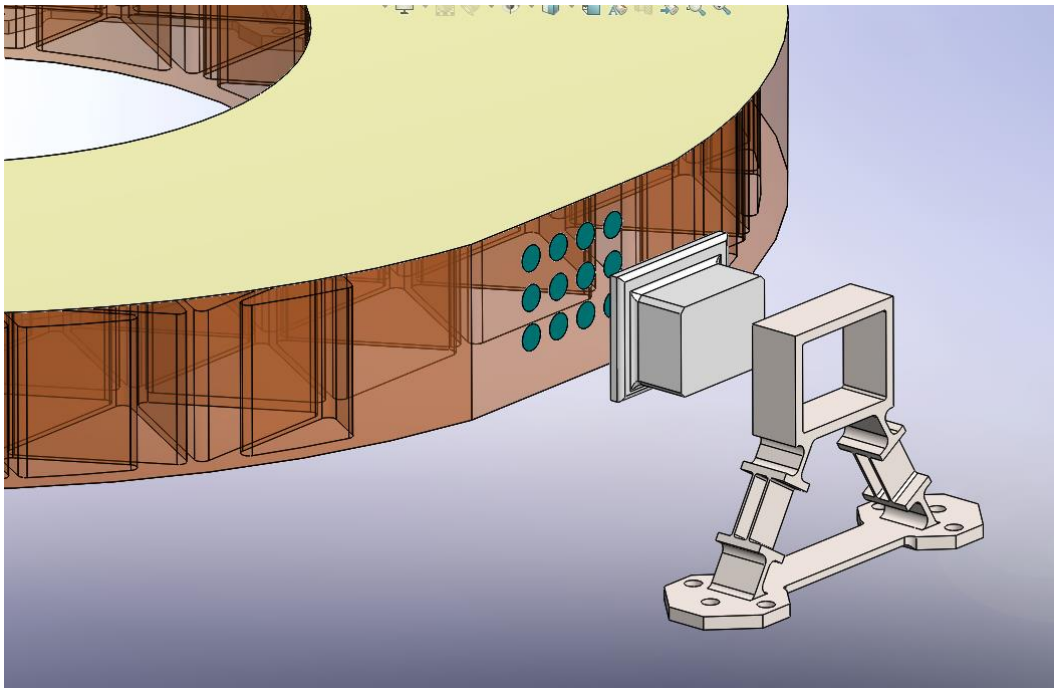

Figure 5.6: Exploded view of Primary Mirror Assembly Mounting.

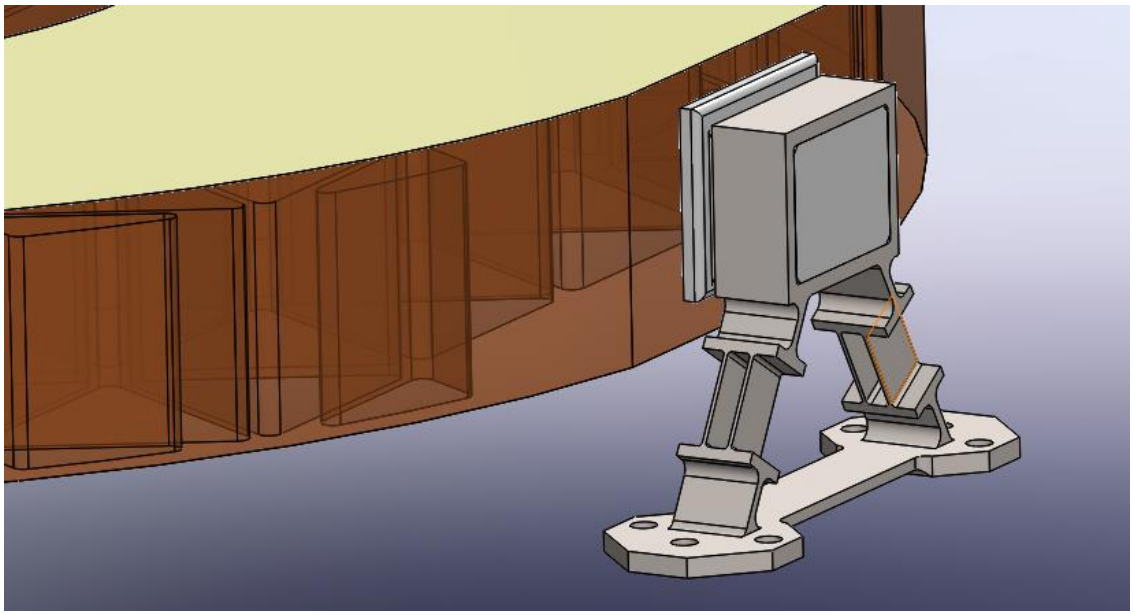

Figure 5.7: Assembly view of PM, Boss and Flexure.

Figure 5.8 shows the complete assembly design of the primary mirror assembly having a mirror, three mounting bosses and three flexures. All three bosses are separated by 120° from each other to maintain symmetry. This complete assembly will be mounted on the optical bench from two mounting foot pads on each flexure.

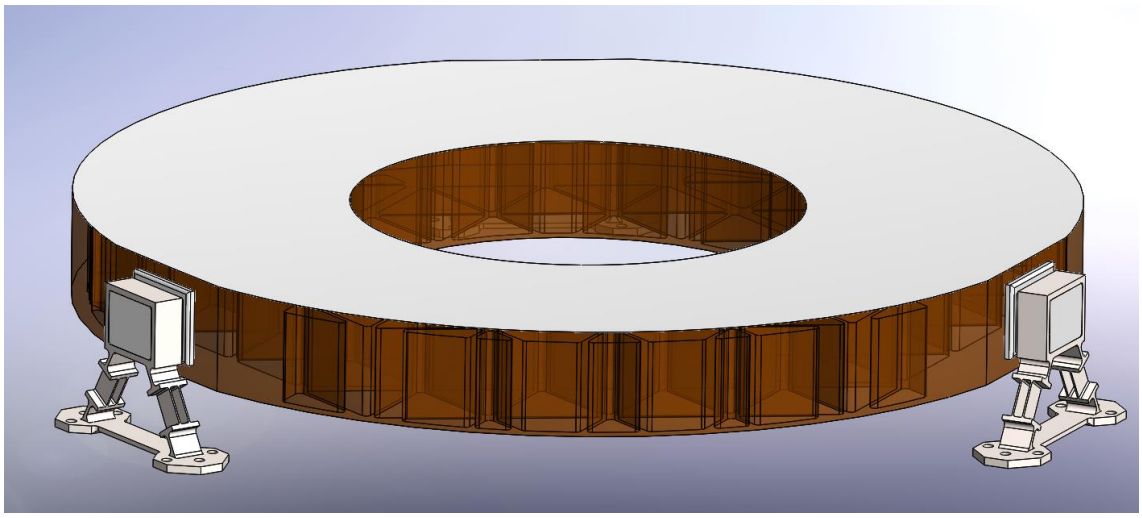

Figure 5.8: Primary Mirror Assembly Design.

5.2 Material Properties and Passing Criteria

Table 5.1 shows the material used for designing of the primary mirror assembly with their mass properties and allowable stress limits. Yield stress were used as the allowable stress for ductile materials with a factor of safety of 1.25. For glass materials, we defined an allowable stress level of 0.3% of the material's Weibull probability of failure.

Table 5.1: Material Selection and Mass Properties.

S/NO	Component	Material	Mass [Kg]	Allowable Stress [MPa]
1	Primary Mirror	Zerodur	17.02	37
2	PM Flexure	Titanium	0.551	662
3	PM Boss	Invar 36	1.16	544
4	Adhesive Bond	EC 2216 B/A	-	17.3

5.3 Finite Element Modeling.

Figure 5.9 shows the FE Model of the primary mirror, which has been modelled into three sections: Optical surface, mirror pocketing and bonding interface. All three sections have been combining together using FEMAP glue connection command. The optical surface has been created by using 2D Quad elements and maintaining the radial

symmetry of the mesh. The bonding interface has been created by using 3D Hex element in a way so that it has equivalence of nodes with glue mesh as shown in Figure 5.10.

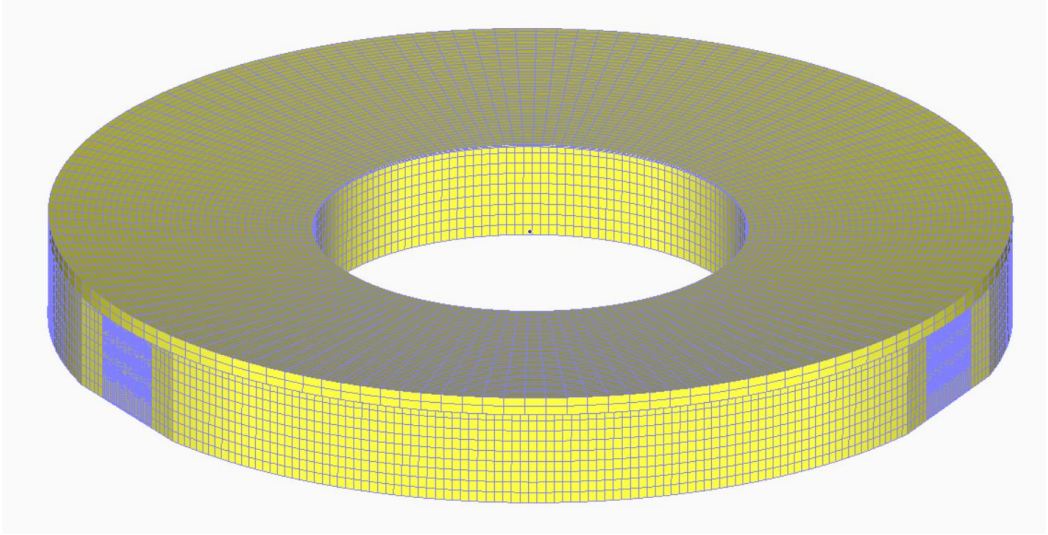

Figure 5.9: FE Model of Primary Mirror.

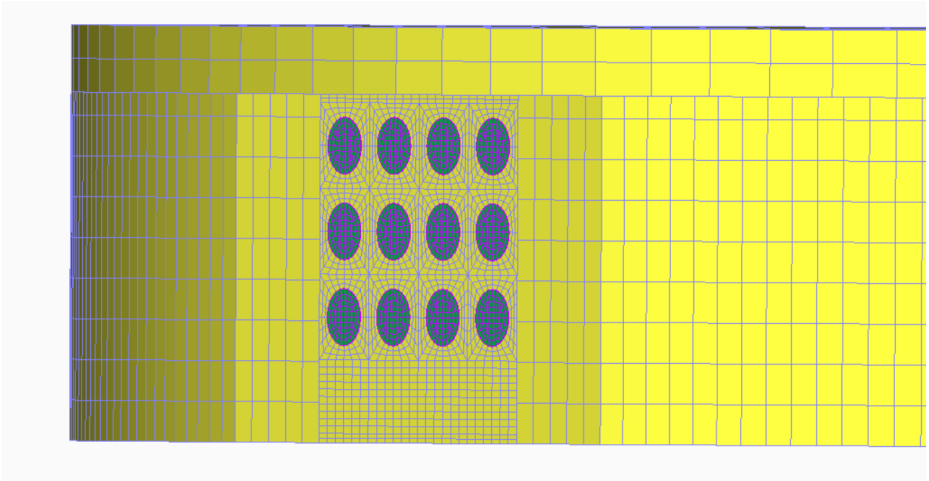

Figure 5.10: Primary Mirror Meshing Close-up View.

Third step is the modelling of the primary mirror pocketing as shown in Figure 5.11. Pockets have been meshed by using mostly hex elements and also maintaining the radial symmetry of the mesh so that it will not induce any error due to unsymmetrical meshing. Figure 5.12 shows the close-up view of the mesh used for pocketing. The no of elements used in the PM is 169194 and no of nodes are 207426. The FE model mass of the PM is 18.3 Kg.

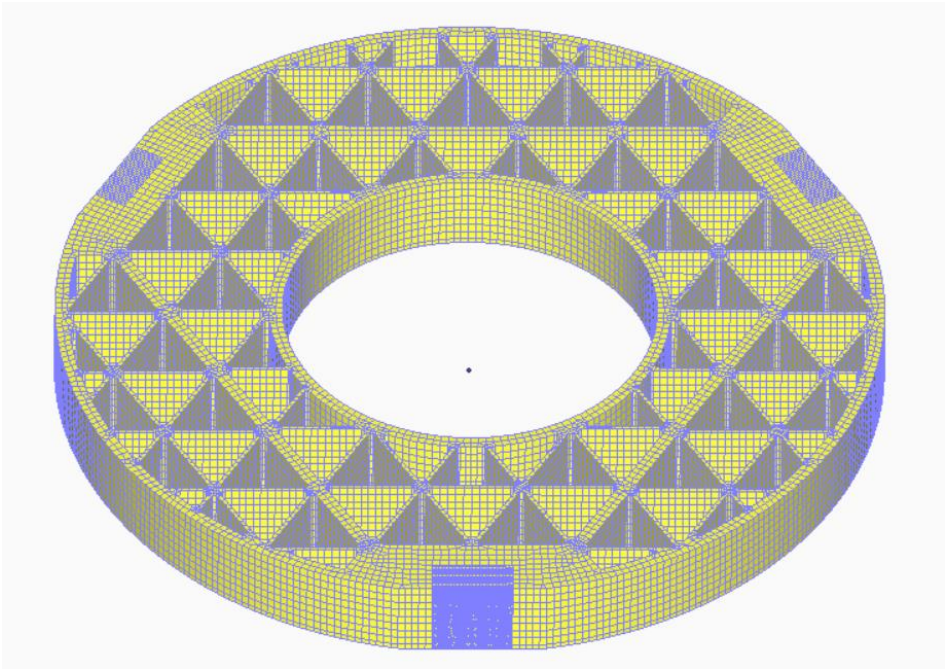

Figure 5.11: FE Modelling of PM pocketing.

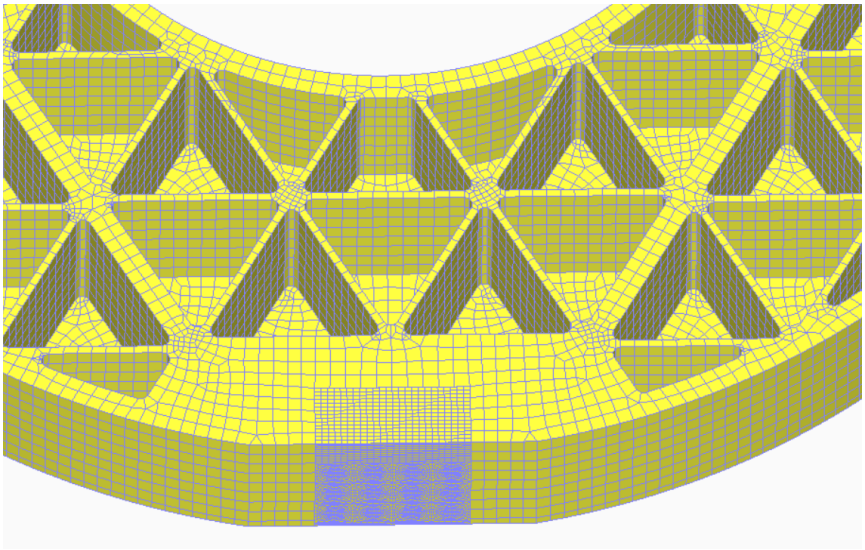

Figure 5.12: PM pocketing Mesh Close-up View.

Figure 5.13 presents the FE model of mounting boss and adhesive bonds. Adhesive bonds have been modelled with 3D hex elements and have node equivalence on both sides. The number of elements used for the FE model of adhesive bonds is 9072 and the number of nodes is 13968.

The PM boss has been modelled in two sections. The section on the adhesive bond side has a fine mesh to adhesive bond. While on flexure side a relatively coarse meshing has

been done. Both sections have been joined together by using the FEMAP glue connection command. The number of elements used in the FE model of the PM bosses is 21444 and the number of nodes is 28992. The FE model mass of PM bosses is 1.17 kg.

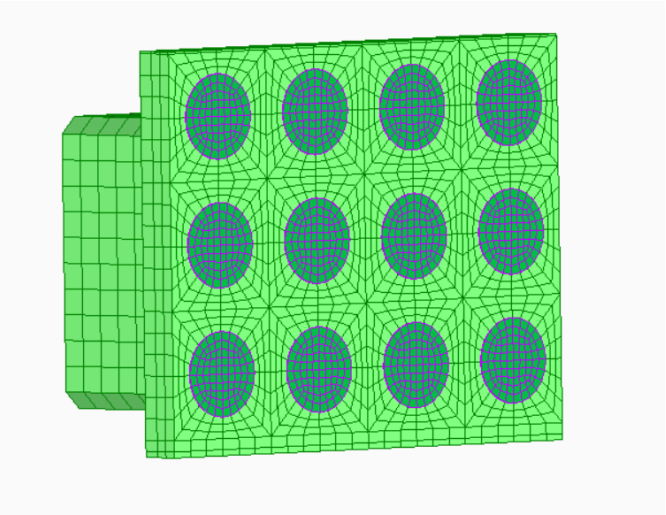

Figure 5.13: FE Model of PM mounting Boss.

The PM flexure has been modelled by using second-order tetrahedral element as shown in Figure 5.14. The geometry of the flexure is quite complex to model with hex elements. The connection between the PM boss and the PM flexure has been modelled as a FEMAP glue connection. The number of elements used in the FE model of the PM flexures is 130742 and the number of nodes is 224216. The FE model mass of the PM flexures is 0.55 kg.

Figure 5.14: FE Model of PM Flexure.

Figure 5.15 presents the FE model of the Primary Mirror Assembly. The total numbers of elements used in the FE model of the PMA is 330452 and the number of nodes is 467618. The FE model mass of the PMA is 20.04 kg. The PMA has been mounted on to the optical bench by three PM flexure. Each flexure has two connection with the OB. These connections have been modelled as FEMAP glue connection.

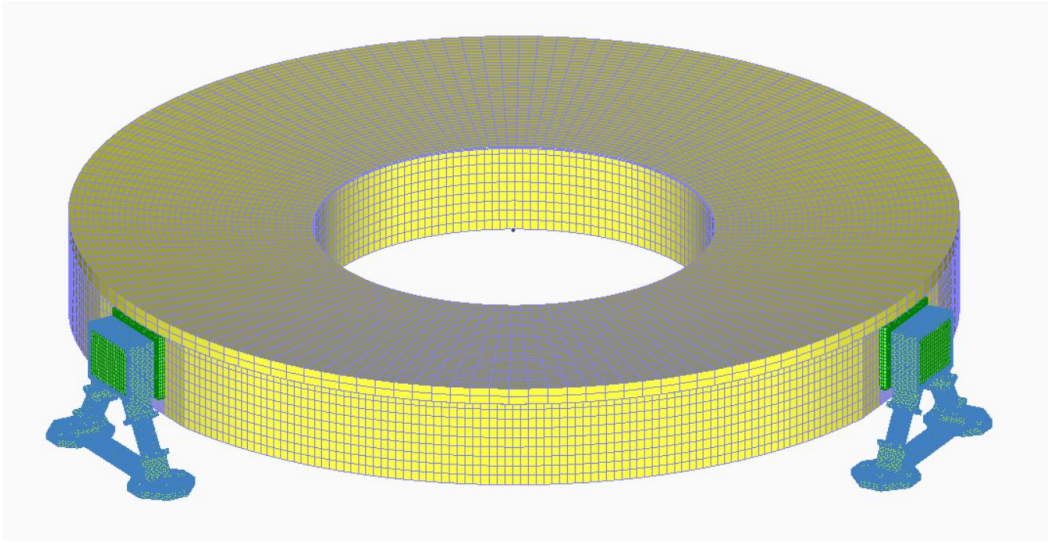

Figure 5.15: FE Model of the PMA.

5.4 Finite Element Distortion Analysis

5.4.1 Load cases

The Primary Mirror Assembly has been analyzed to validate the optical surface error of the Primary Mirror. The following load cases were applied:

1) Optical surface distortion and displacement analysis when the primary mirror is placed on a flat surface and 1 g gravity load in +Z direction and polishing pressure load of 5 KPa outward from optical surface is applied.
2) Three linear static load cases were analyzed for optical surface error when PMA is mounted on to the optical bench:
    a. 1 g gravitational acceleration applied in +X direction,
    b. 1 g gravitational acceleration applied in +Y direction, and
    c. 1 g gravitational acceleration applied in -Z direction.

3) Two linear static thermal load cases were analyzed (ref temperature of 22.5˚C) for optical surface error when the PMA is mounted on the optical bench:
    a. A high temperature load of 27.5 ˚C was applied to the PMA and Optical Bench, and
    b. A low temperature load of 17.5 ˚C was applied to the PMA and Optical Bench.

5.4.2 Analysis of load Case Results

5.4.2.1 Polishing Pressure Distortion

Figure 5.16 shows the contours of PM distortion under a polishing pressure load as specified in section 5.4.1. Peak to Valley surface distortion of 19.1 nm and RMS surface distortion of 4.59 nm has been observed. It meets the requirement of >15 nm surface RMS.

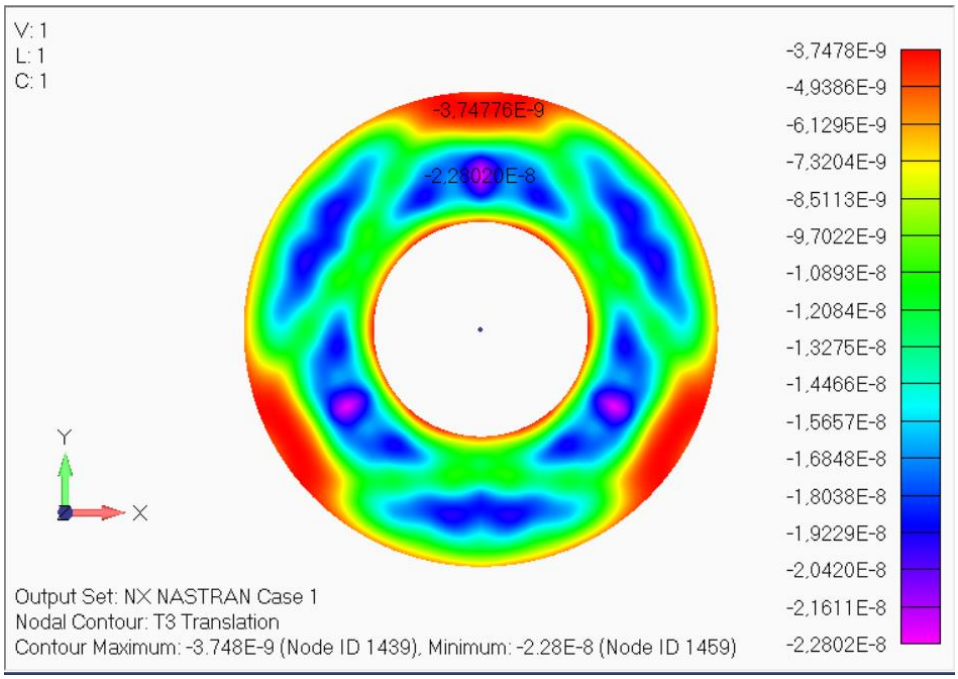

Figure 5.16: PM distortion under polishing load.

5.4.2.2 Gravity Distortion

The Primary Mirror Assembly has been analyzed for surface error under gravity load in the X, Y and Z direction as specified in section 5.4.1. Table 5.2 presents the displacement and distortions analysis results. Results shows that the design meets the requirements of all parameters of surface distortion and displacement. The RMS surface error in

horizontal gravity (X and Y direction) meet the requirement of <15 nm while the error is higher for vertical gravity as the mirror is not designed for vertical gravity.

Table 5.2: PM surface distortion due to gravity Load.

S No	Parameter	Gravity X	Gravity Y	Gravity Z
1	Decenter (X) [µm]	5.8	7.4E-4	5.2E-3
2	Decenter (Y) [µm]	9.7E-4	5.8	1.4E-2
3	Axial Translation (Z) [µm]	-1.9E-4	5.6E-4	-1.8
4	Tip/Tilt (X) [Arc Sec]	3.7E-4	3.7E-2	2.5E-3
5	Tip/Tilt (Y) [Arc Sec]	-3.8E-2	-4.5E-4	2.8E-3
6	Surface Error (RMS) [nm]	7.6	7.4	195.0
7	Surface Error (PV) [nm]	127	111	885

Figure 5.17 shows the axial surface distortion contours of the PM when a gravity load applied in the X-axis. It can be observed that the distortion has major component of tip/tilt in the Y axis. After removing rigid body motion (Tip/tilt and axial displacement) from surface distortion a surface error RMS is 7.6 nm is observed.

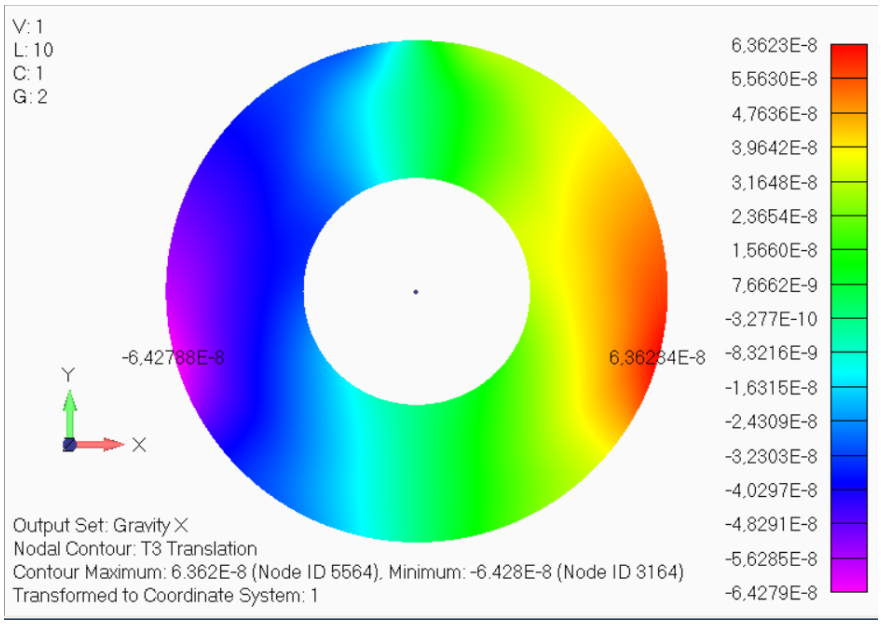

Figure 5.17: PM surface distortion in axial direction (X-axis gravity) [m].

Figure 5.18 shows the radial surface distortion contours of the PM when a gravity load is applied in the X axis. It shows that mirror surface has a 5.8 µm decenter in the +x direction.

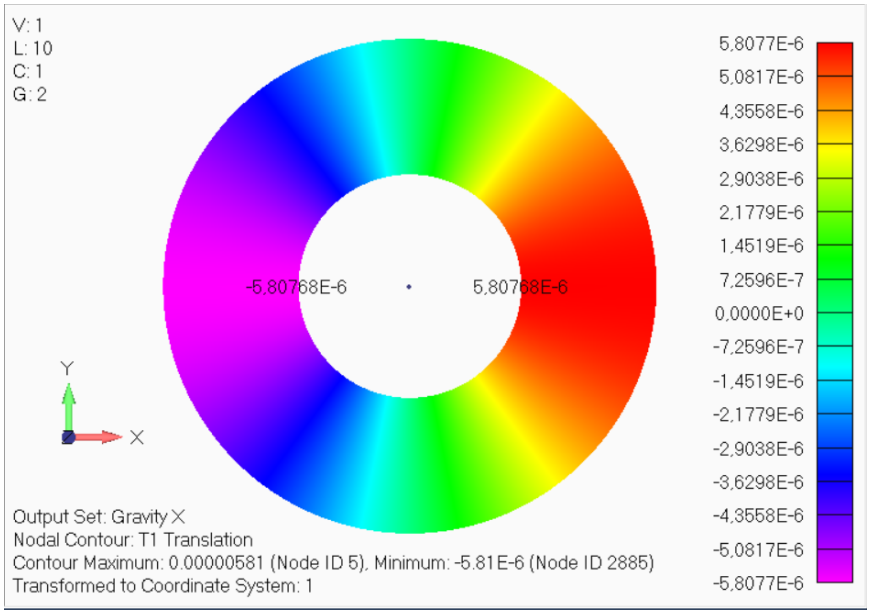

Figure 5.18: PM surface distortion in radial direction (X-axis gravity) [m].

Figure 5.19 shows the axial surface distortion contours of the PM when a gravity load is applied in the Y-axis. It can be observed that distortion has major component of tip/tilt at x axis. After removing rigid body motion (Tip/tilt and axial displacement) from surface distortion a surface error RMS is 7.4 nm is observed.

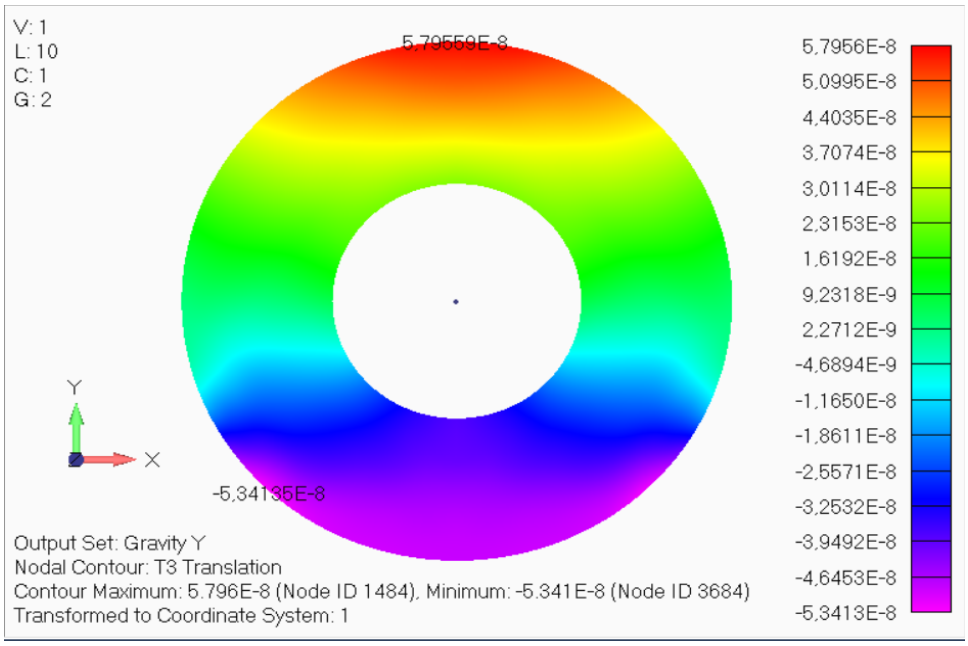

Figure 5.19: PM surface distortion in axial direction (Y-axis gravity) [m].

Figure 5.20 shows the radial surface distortion contours of the PM when a gravity load is applied in the X axis. It shows that mirror surface has 5.8 µm decenter in the x direction. In addition 0.047 µm of radial surface distortion has been noted.

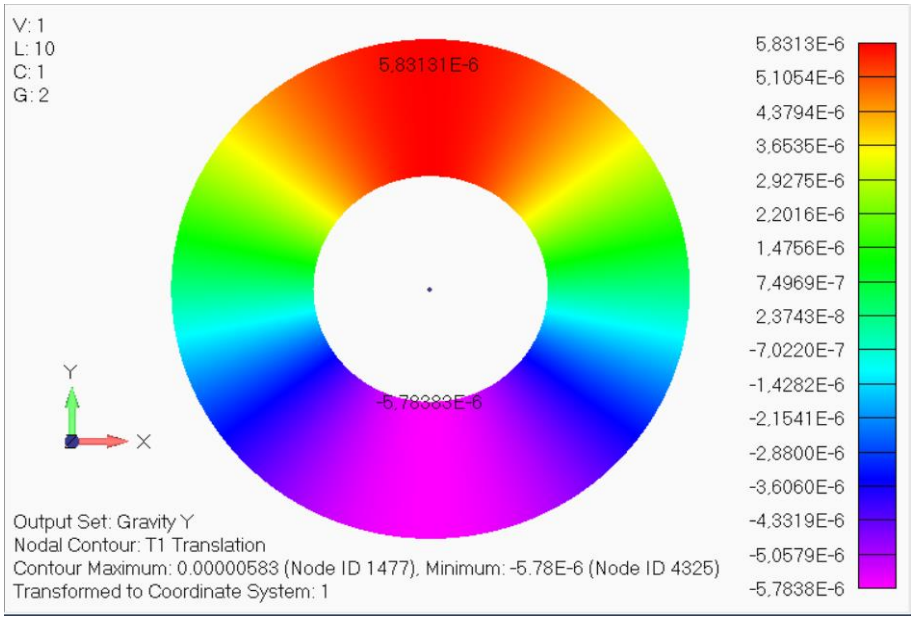

Figure 5.20: PM surface distortion in radial direction (Y-axis gravity) [m].

Figure 5.21 shows the axial surface distortion contours of the PM when a gravity load is applied in the Z axis. It shows that mirror surface has 1.18 µm axial displacement in the negative Z direction. Significant trefoil error has been observed in optical surface because of the three mounting points.

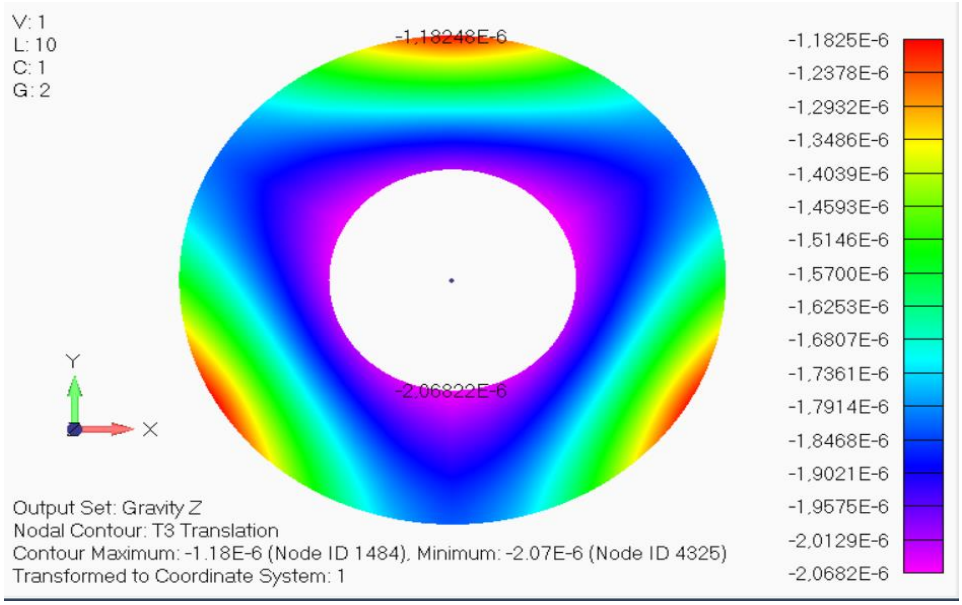

Figure 5.21: PM surface distortion in axial direction (Z-axis gravity) [m].

Figure 5.22 shows the radial surface distortion contours of the PM when a gravity load is applied in the Z axis. It shows that mirror surface has maximum of -0.167 µm radial surface distortion, which is less than the requirement ±2 µm, although we are not designing the PMA for vertical gravity.

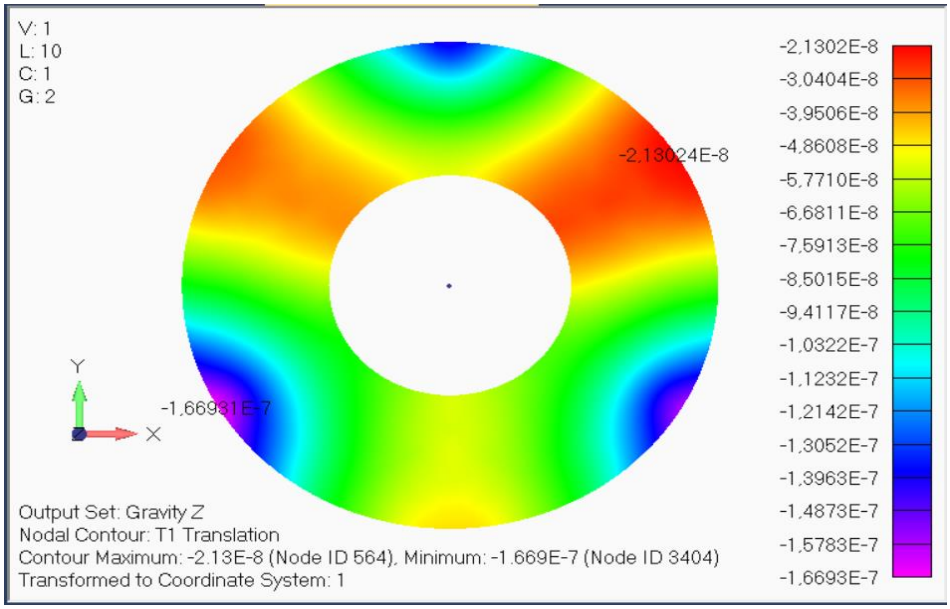

Figure 5.22: PM surface distortion in radial direction (Z-axis gravity) [m].

5.4.2.3 Thermal Distortion

The primary mirror assembly has been analyzed for surface error under thermal load as specified in section 5.4.1. Table 5.3 presents the displacement and distortions analysis

results. Results shows that design meets the requirement of all parameters of surface distortion and displacement. The RMS surface error in horizontal gravity (X and Y direction) meets the requirement of <15 nm, while for vertical gravity the surface error is on higher side as the mirror is not designed for vertical gravity.

Table 5.3: PM surface distortion due to Thermal Load.

S No	Parameter	Thermal Hot Case	Thermal Cold Case
1	**Decenter (X) [µm]**	**-0.052**	**0.052**
2	**Decenter (Y) [µm]**	**0.052**	**-0.052**
3	**Axial Translation (Z) [µm]**	**5.8**	**-5.8**
4	**Tip/Tilt (X) [Arc Sec]**	**1.0E-3**	**-1.0E-3**
5	**Tip/Tilt (Y) [Arc Sec]**	**-1.5E-3**	**1.5E-3**
6	**Radial Distortion [µm]**	**1.67**	**-1.67**
7	**Surface Error (RMS) [nm]**	**6.8**	**6.8**
8	**Surface Error (PV) [nm]**	**38**	**38**

Figure 5.23 shows the axial surface distortion contours of the PM surface when a high temperature of 27.5 ℃ is applied to the PMA (ref temperature of 22.5 ℃). It shows that the mirror surface has 5.9 µm axial displacement in the Z direction due to expansion of the PM flexure. A surface error of 6.8 nm has been observed after removal of rigid body

motion. Contours shows that the error is combination of defocus and trefoil, but the amplitude is with-in allowable limit of <15 nm.

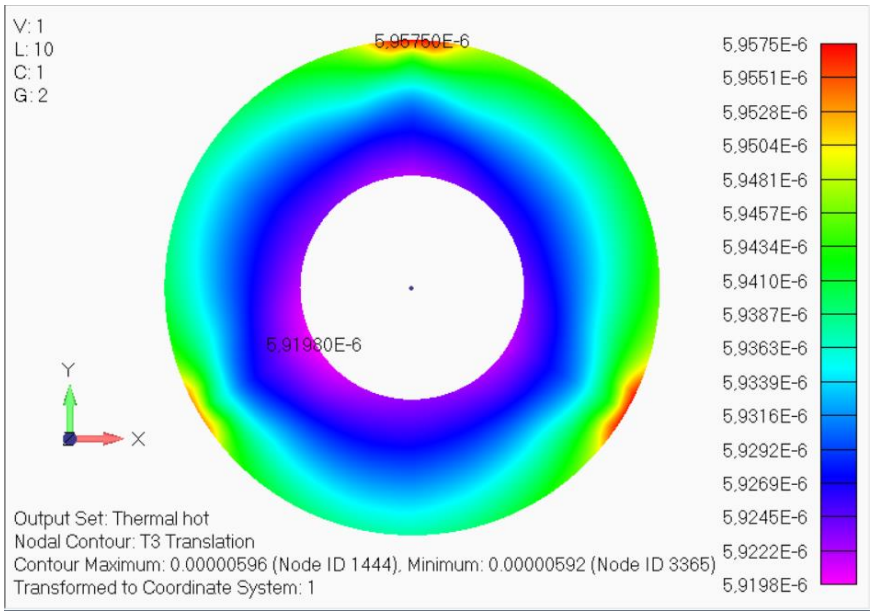

Figure 5.23: PM surface distortion axial direction (Thermal Hot) [m].

Figure 5.24 shows the radial surface distortion of the optical surface when a high temperature load is applied to the PMA. Contours show that maximum distortion of 1.67 µm is observed in the mirror, which is with-in allowable limit of ±2 µm.

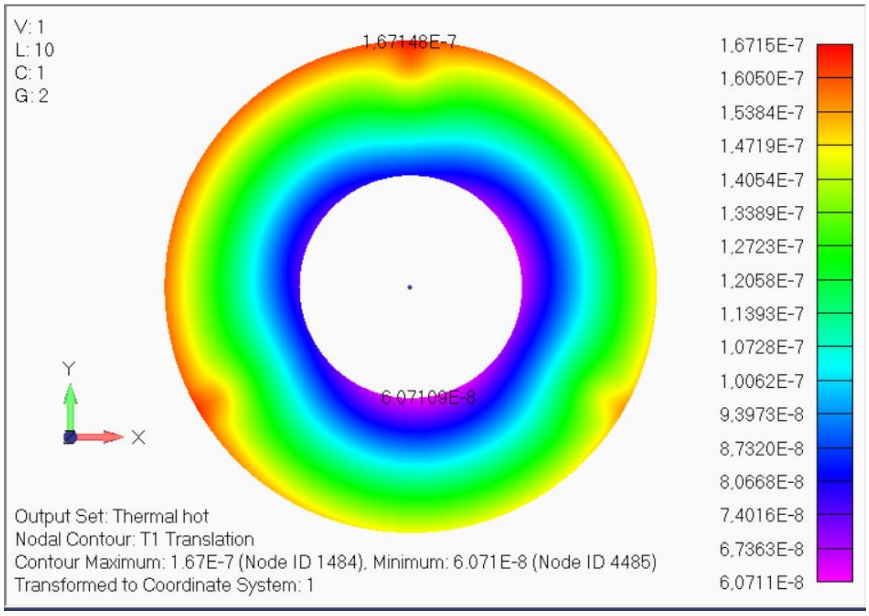

Figure 5.24: PM surface distortion in radial direction (Thermal Hot) [m].

Figure 5.25 shows the axial surface distortion contours of the PM surface when a high temperature of 17.5 °C is applied to the PMA (ref temperature of 22.5 °C). It shows that

mirror surface has 5.9 µm axial displacement in the negative Z direction due to contraction of the PM flexure. A surface error of 6.8 nm has been observed after removal of rigid body motion. The contours show that the error is combination of defocus and trefoil with-in allowable limit of <15 nm.

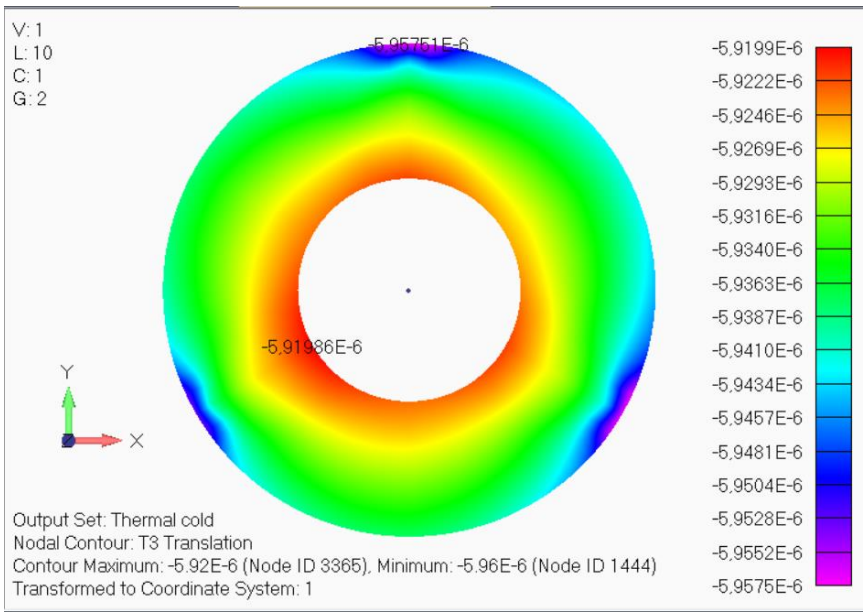

Figure 5.25: PM surface distortion in axial direction (Thermal Cold Case) [m].

Figure 5.26 shows the radial surface distortion of optical surface when a low temperature load of 17.5 °C is applied to the PMA. Contours shows that maximum distortion of -0.167 µm is observed in mirror that is with in allowable limit of ±2 µm.

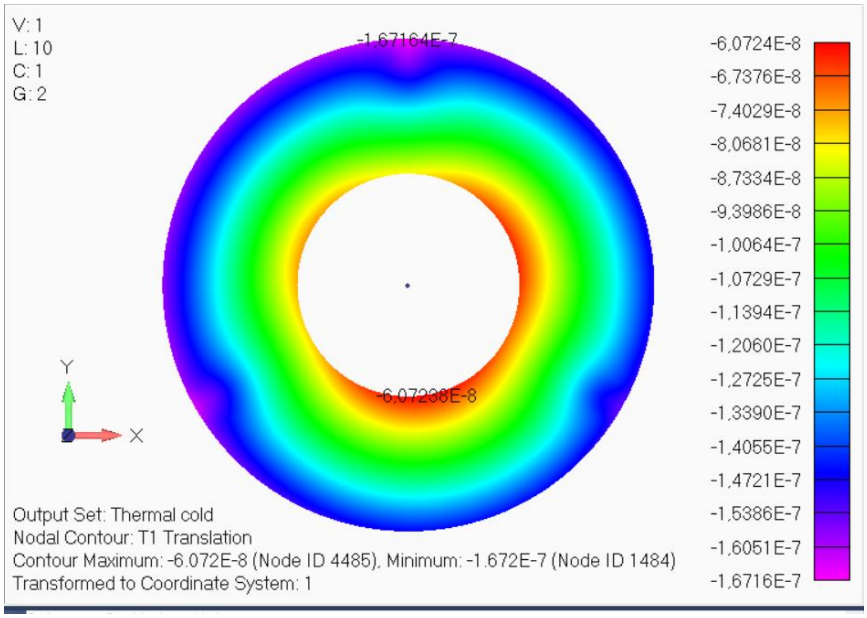

Figure 5.26: PM surface distortion in radial direction (Thermal Cold Case) [m].

7.1µm of radial thermal expansion has been observed at legs of the PM flexure as shown in Figure 5.27. The radial CTE of the optical bench has been calculated as 4.58 µm/m-°K which meets the CTE requirement of the optical bench.

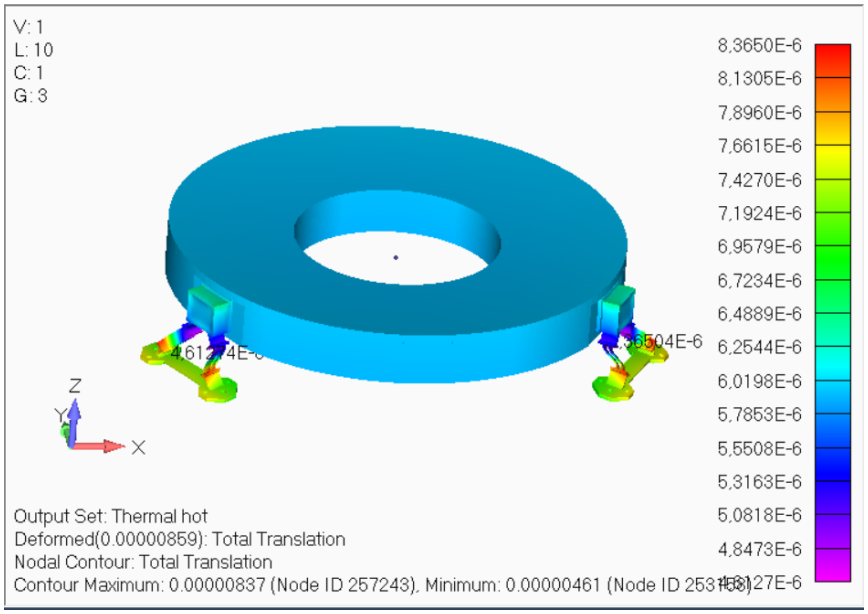

Figure 5.27: Thermal expansion of the PMA.

The PMA meets all the requirements of surface distortion and displacement requirement under gravity and thermal loads. The actual performance can be evaluated by calculating the Zernike polynomial and evaluating the optics performance on these values of rigid body motion and Zernike polynomials.

5.5 Finite Element Strength Analysis

5.5.1 Load case

The Primary Mirror Assembly has been analyzed to validate the strength requirement of all its components. The following load cases were applied:

1) Modal analysis has been performed to find the natural frequency modes of PMA.
2) Three Quasi-static load cases were analyzed to check the stresses in all the components of PMA at equivalent static launch load:
    a. 19 g gravitational acceleration applied in +X direction.
    b. 19 g gravitational acceleration applied in +Y direction, and
    c. 40 g gravitational acceleration applied in -Z direction.

3) Two linear static thermal load cases were analyzed (ref temperature of 22.5 ˚C) to check the strength of all the components of the PMA at extreme hot and cold temperatures as specified in the requirement.
    a. A high temperature of 70 ˚C was applied to PMA and optical bench.
    b. A low temperature of -20 ˚C was applied to PMA and optical bench.

5.5.2 Analysis Results

5.5.2.1 Modal Analysis

A modal analysis has been performed to find out the natural frequency modes of the PMA. A natural frequency of 213 Hz in the X, Y direction and 375 Hz in the Z direction has been noted for the PMA. Figure 5.28, Figure 5.29 and Figure 5.30 show the natural frequency modes in the X, Y and Z directions. It meets the requirement of >100 Hz.

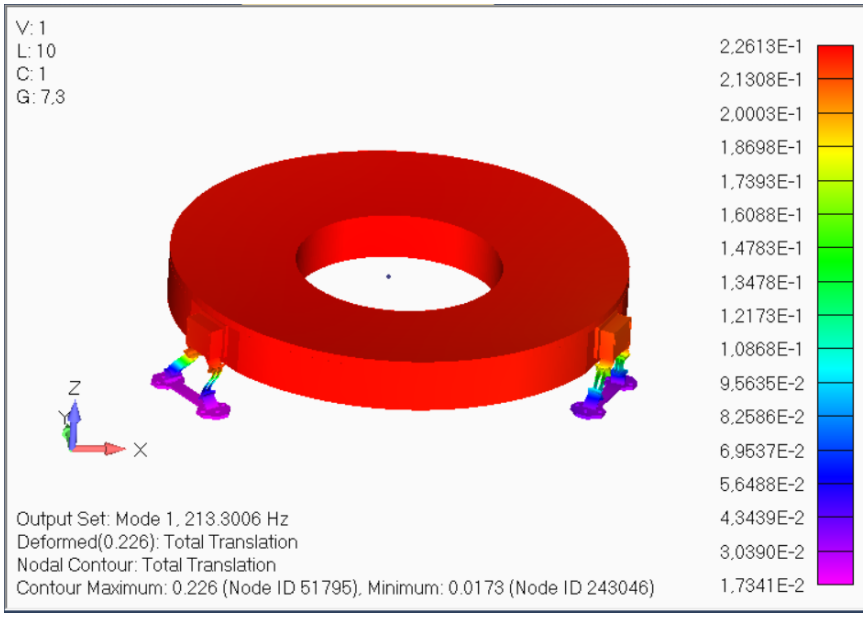

Figure 5.28: Natural Frequency Mode in the X Direction.

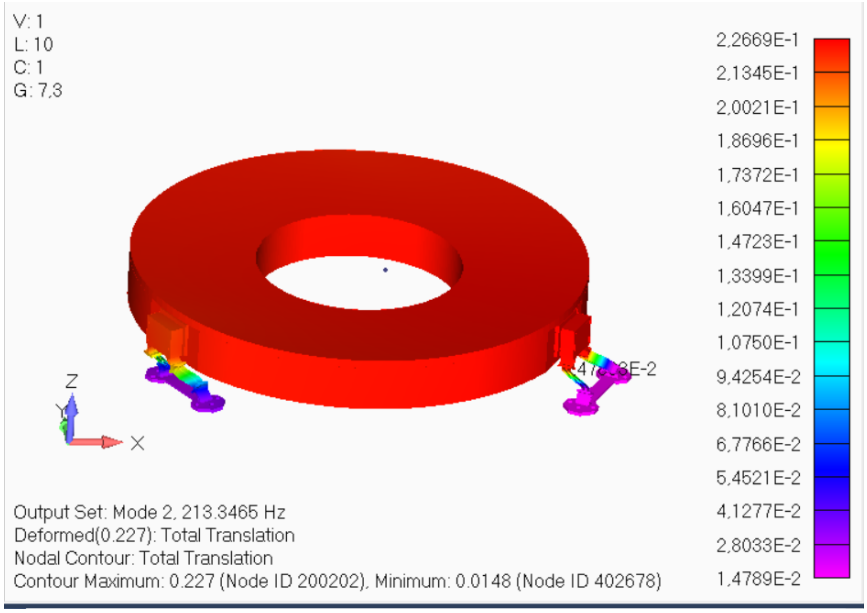

Figure 5.29: Natural Frequency Mode in Y Direction.

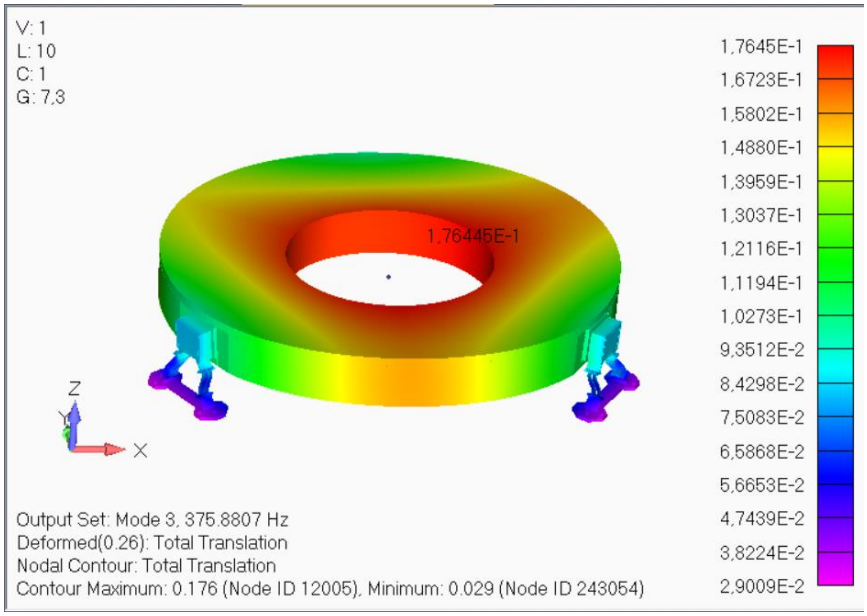

Figure 5.30: Natural Frequency Mode in the Z Direction.

5.5.2.2 Static Analyses

The primary mirror assembly has been analyzed to find the stresses due to equivalent static launch load and thermal survival load as specified in section 5.5.1. Table 5.4 presents the stress results when an equivalent static launch load is applied to the PMA in each axis separately. Results show that the PMA faces maximum stress when a static acceleration load is applied in the X direction. All the stresses are within allowable limits. Stress contours of the X direction are also presented.

Table 5.4: Stress in PMA due to Equivalent Static Load.

	Static X [MPa]	Static Y [MPa]	Static Z [MPa]
Primary Mirror (Max Principle Stress)	8.4	7.2	7.7
PM Boss (Solid Von Mises)	15.3	13.9	12.8
PM Flexure (Solid Von Mises)	113.3	121	92.3
Adhesive (Solid Normal Stress)	6.8	6.03	6.48

Figure 5.31 presents the stress contours for the primary mirror under a static load in the x direction. The mirror experiences a maximum stress of 8.4 MPa near the adhesive bond connection. This is why the adhesive bond surface of the mirror is kept as solid so that it will not break during extreme loads.

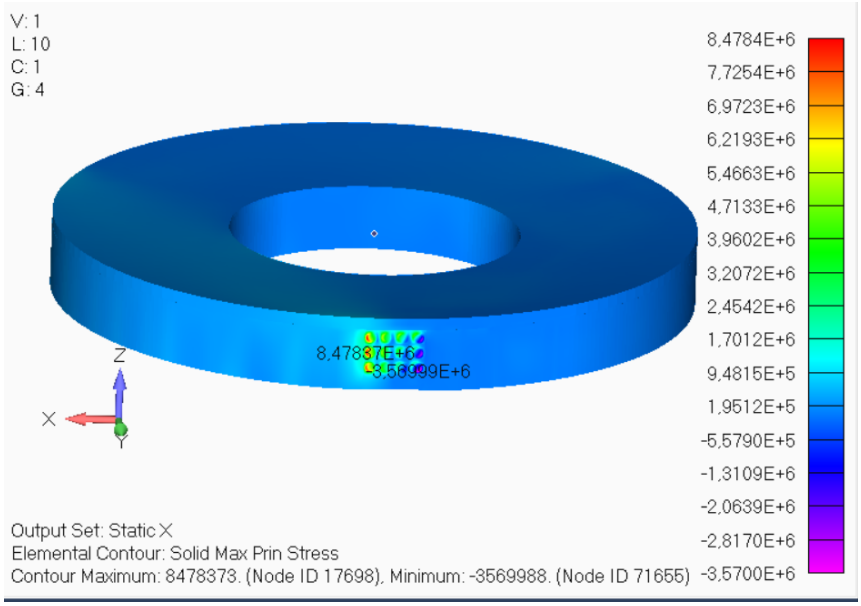

Figure 5.31: Max Stress in Primary Mirror under Equivalent Static load [Pa].

Figure 5.32 shows the stress contours of the PM boss under a static load in the x direction. Maximum stress of 15 MPa is noted near the edge of the PM boss. Although

there is some stress concentration observed near the edge of boss due to discontinuity it is still with-in allowable limit so it will not be further investigated.

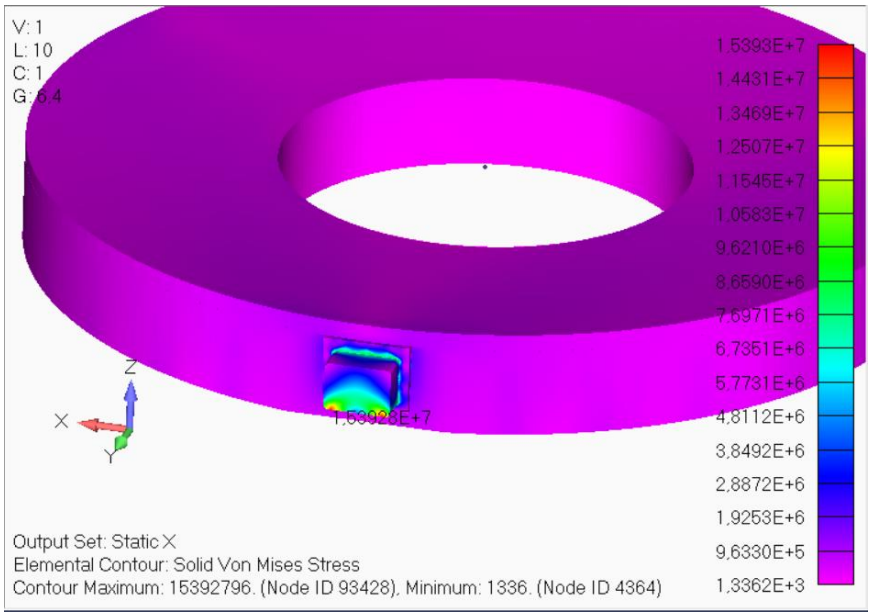

Figure 5.32: Max Stress in PM Boss under Equivalent Static load [Pa]

Figure 5.33 shows the stress contours for the PM flexure for a static load in the X direction. Maximum stress of 113 MPa is noted in the flexible part of flexure as it is the thinnest part of the flexure. This stress is within the allowable limit.

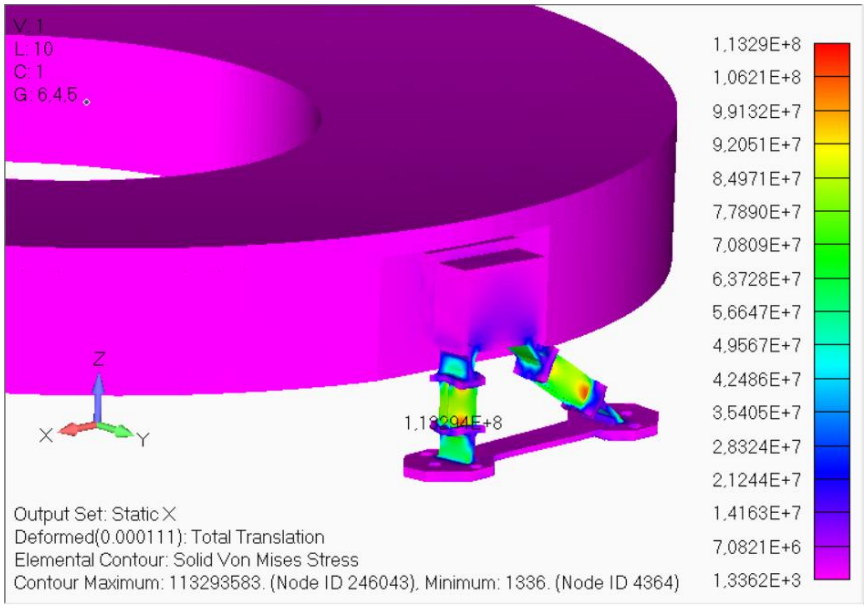

Figure 5.33: Max Stress in PM Flexure under Equivalent Static load [Pa].

Figure 5.34 shows the stress contours in the adhesive bonds under static load applied in the X direction. Adhesive bonds face tensile stress on one side and the compressive

stress on the other side because of relative rotational motion between the PM and PM boss. The stresses are with in allowable limits.

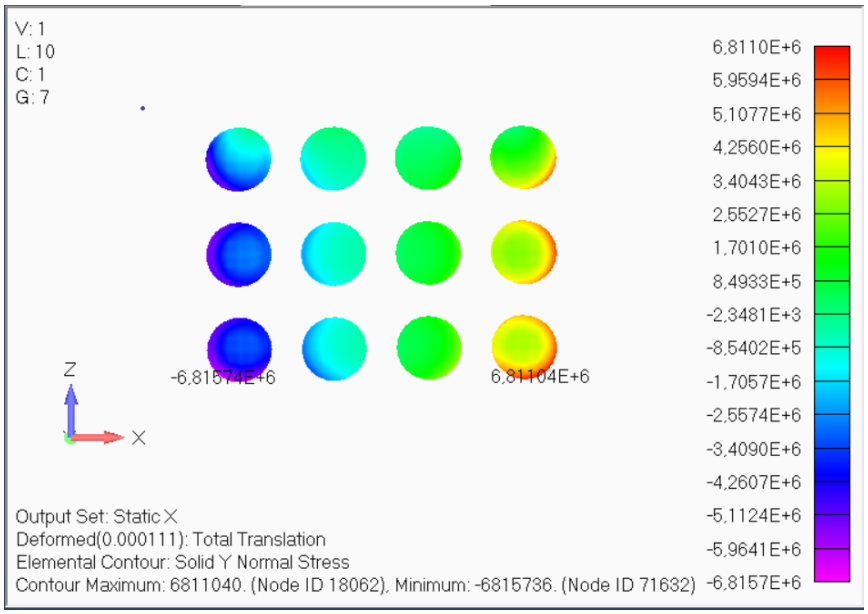

Figure 5.34: Max Stress in Adhesive bonds under Equivalent Static load [Pa].

5.5.2.3 Thermal Survival Analysis

The primary mirror assembly has been analyzed to find the stresses due to extreme thermal survival temperatures of +70 °C and -20 °C (ref temperature of 22.5 °C) to validate the design of the PMA to withstand these extreme temperatures without any permanent failure. Table 5.5 presents the stress results of all the components of PMA due to thermal survival loads. All the stresses are within allowable limits and there is no permanent deformation and damage of any component of PMA due to thermal survival loads. Contours of maximum stress are also presented.

Table 5.5: Stress in PMA due to Thermal Survival Load.

	Thermal Hot [MPa]	**Thermal Cold [MPa]**
Primary Mirror	5.07	6.4
PM Boss	48.7	43.6
PM Flexure	123	110
Adhesive	6.09	5.91

Figure 5.35 shows the stress contours of the primary mirror under extream low temperatures. Maximum stress of 6.4 MPa has been noted at the interface of the outer adhesive bond spots due to differences of CTE between the adhesive bond and mirror material. Adhesive has high a CTE property while the mirror material has a very low CTE. Adhesive try to shrink but mirror is resists shrinkage that develops stress on the edges, although these stresses are within allowable limits.

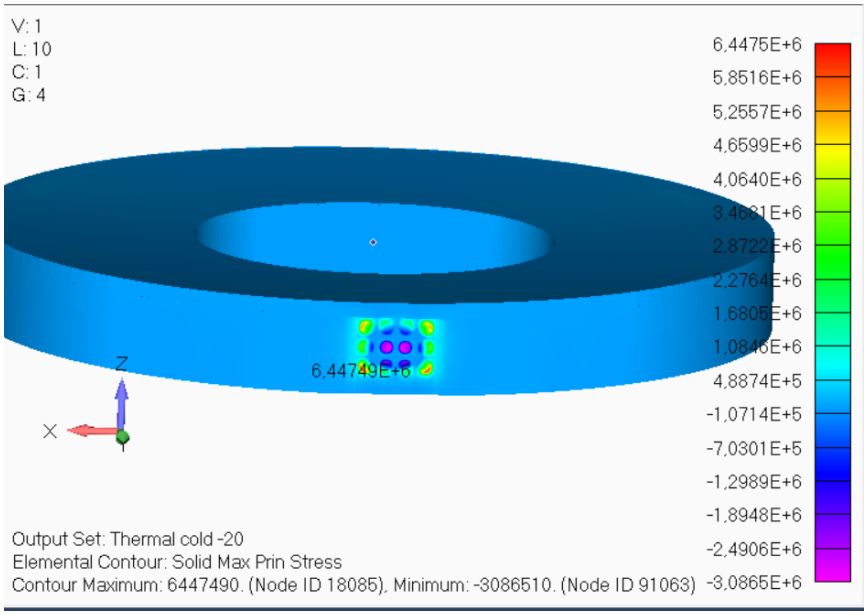

Figure 5.35: Max Stress in Primary Mirror under Thermal survival load [Pa].

Figure 5.36 shows the stress contours in the PM boss due to extreme high temperature load. Maximum stress of 48 MPa is noted at interface of the PM boss and the PM flexure because PM is designed from low CTE material while the CTE of the PM Flexure material is relatively high, resulting in high stresses near the interface of the PM boss and PM flexure. There are some stress concentrations also noted near the maximum stress point, but the maximum stress value is with-in allowable limits so no need to investigate further.

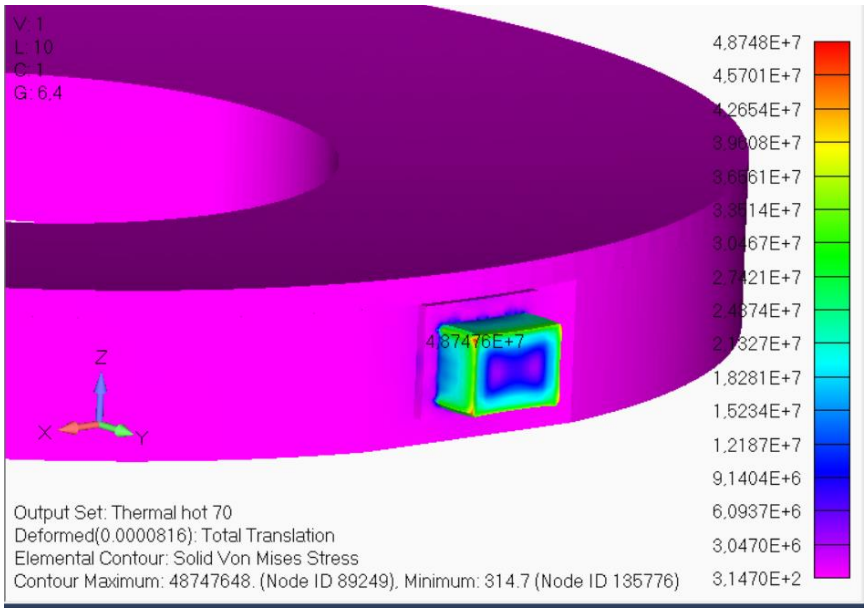

Figure 5.36: Max Stress in PM Boss under Thermal survival load [Pa].

Figure 5.37 shows the stress contours in the PM flexure under an extreme high temperature load. Maximum stress of 123 MPa is noted near the interface of the PM flexure and the PM boss.

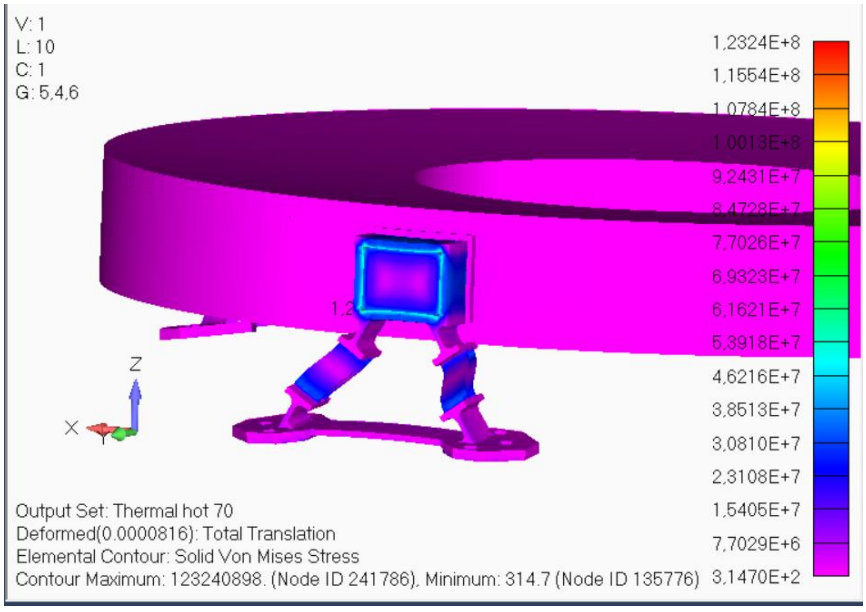

Figure 5.37: Max Stress in PM Flexure under Thermal survival load [Pa].

Strength analysis shows that all the components of PMA have enough strength to bear the equivalent static launch load and thermal survival load without any failure.

6 RESULTS AND CONCLUSION

The primary mirror assembly has been analyzed for optical surface distortion and displacement due to gravitational acceleration load and in-orbit temperature fluctuations during operation. It has also been analyzed for strength to withstand quasi-static launch loads and extreme in-orbit non-operational temperature load for survival. Analysis has been presented in Chapter five and the results extracted are summarized in the following section.

6.1 Surface Error Compliance

Optical surface displacement and distortion has been analyzed to find the surface error of the mirror under gravity load and thermal load. Table 6.1 presents the results of decenter, axial displacement, tip/tilt, radial and axial surface distortion of the primary mirror optical surface with the corresponding requirements. It shows that the proposed design meets all the parameters of surface error requirement for both gravity and thermal loads with sufficient margin so that it can achieve the desired optical performance. The design driver for the PMA is the optical performance of the system. It has been designed for horizontal gravity and a thermal load of ±5°C with reference a temperature of 22.5°C.

Table 6.1: PM Optical Surface Error Compliance.

S No	Parameter	Gravity	Thermal	Requirement
1	Decenter (X) [µm]	5.8	-0.052	±20
2	Decenter (Y) [µm]	5.8	0.052	±20
3	Axial Translation (Z) [µm]	5.6E-4	5.8	±8
4	Tip/Tilt (X) [Arc Sec]	3.7E-2	1.0E-3	±5
5	Tip/Tilt (Y) [Arc Sec]	-3.8E-2	-1.5E-3	±5
6	Axial Distortion (RMS) [nm]	4.02	7.04	≤ 15
7	Radial Distortion [µm]	0	1.67	±2

6.2 Strength Compliance

The strength of the PMA is important for its survival during extreme a lunch load and thermal survival loads. It has been designed for a quasi-static launch load of 19g lateral and 40g longitudinal acceleration and -20 ℃ to +70 ℃ survival temperature without any damage or permanent deformation. The maximum stress result for the quasi-static load and thermal survival loads is presented in Table 6.2. Results show that the maximum stress in all the components of the PMA are within the allowable limit with sufficient margin of safety (MoS) for all the mechanics and very low probability of failure (PoF) for mirror material.

Table 6.2: Stress Compliance of PMA elements.

	Component	Quasi-Static [MPa]	Thermal Survival [MPa]	MoS or PoF
1	Primary Mirror	8.4	6.4	3E-9 (PoF)
2	PM Boss	15.3	48.7	7.9 (MoS)
3	PM Flexure	113.3	123	3.3 (MoS)
4	Adhesive	6.8	6.09	0.3 (MoS)

The margin of safety has been calculated by using following equation:

$$\boldsymbol{MoS = \frac{\sigma_{all}}{\sigma_{max}.FoS} - 1}$$

where σ_{all} is the yield stress of the material, σ_{max} is maximum stress in a specific component and FoS is the factor of safety, which is set to 1.25 for metals and 2 for adhesive.

The horizontal stippled line shows the 0.3% mirror PoF design requirement in Figure 6.1 [14]. The PoF of the primary mirror is shown by lozenge point on the curve. The acceptable PoF should be less than 0.3% as specified in chapter 3. Figure 6.1 shows that the PoF for proposed design is 3E-9, which is very low as compared to the acceptable value. Strength analysis shows that the design PMA has enough strength for survival of launch load and thermal survival loads.

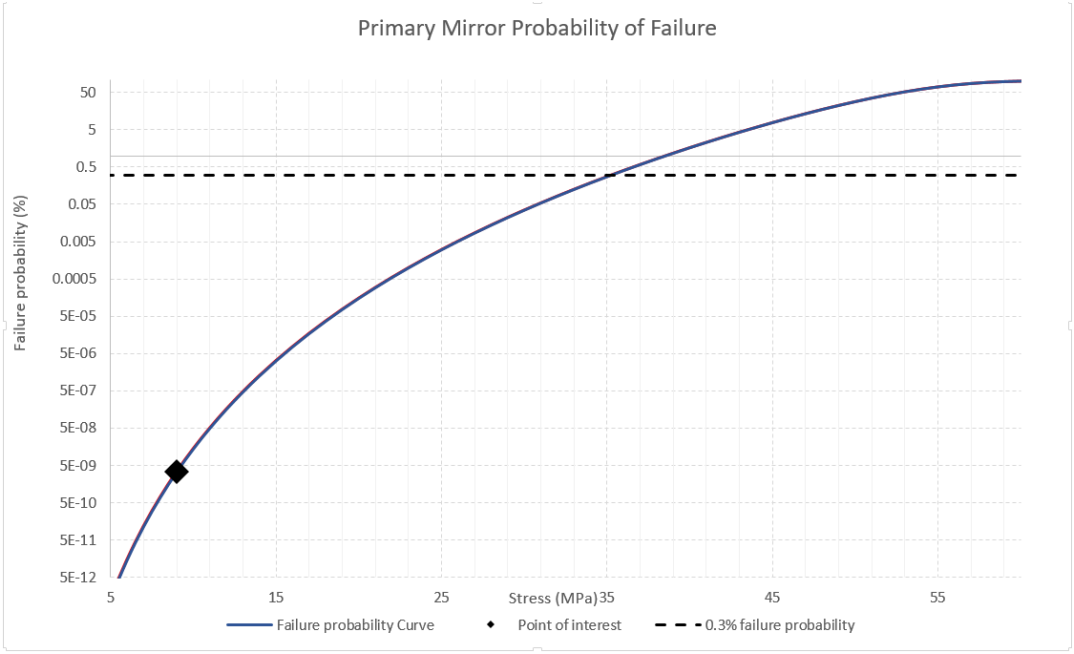

Figure 6.1: Probability of Failure for Zerodur Primary Mirror.

6.3 Optical Performance Analysis

The primary mirror assembly meets the design requirement for optical surface distortion and displacement as well as having enough strength to survive the launch loads. Two cases have been selected to evaluate the optical performance of the primary mirror by calculating the Zernike polynomials. These are the gravity load case in which gravity is applied in the Y axis of mirror, and the thermal load case of low temperature of 17.5 °C is applied to the PMA with a reference temperature of 22.5 °C.

6.3.1 Zernike polynomial calculation

The design of the PMA meets the requirement of surface error to achieve the desired optical performance of the system. Optical performance analysis of the system not the scope of this thesis but a brief overview of optical performance of the designed PMA is presented in this subsection. Zernike polynomials of the distorted surface have been calculated by using python coding. These Zernike Polynomials will be used to analyze the optical performance of the system for specific load cases. Table 6.3 presents some properties of Zernike polynomial fitting for the distorted surface due to thermal load and gravity loads.

Table 6.3: Properties of Zernike polynomials.

Number of Zernike Polynomial = 20		
	Thermal Cold Case	Gravity Y axis
RMS FEM [nm]	3.83362	3.4509
RMS Sag [nm]	5.56479	3.94863
P-V FEM [nm]	24.5857	25.1006
P-V [nm]	22.4721	25.0214
RMS Zernike fit [nm]	5.49226	3.44713
RMS Residual error [nm]	0.895525	3.69004
P-V Zernike fit [nm]	19.8385	16.5691
P-V Residual error [nm]	8.08821	23.1415

Table 6.4 presents the values of twenty Zernike polynomials of the distorted surfaces.

Table 6.4: Zernike polynomials fitting for distorted Optical Surface.

Zernike	**Thermal [nm]**	**Gravity [nm]**	**Zernike**	**Thermal [nm]**	**Gravity [nm]**
Z0	-4.87622	-1.58108	Z10	0.100277	-0.01437
Z1	-0.000629942	0.000673	Z11	-0.124096	-1.39341
Z2	-0.0228564	-0.22995	Z12	0.000554288	0.000104
Z3	1.58061	-0.72751	Z13	0.264375	1.54281
Z4	-0.0036236	-0.00317	Z14	-0.00158474	0.000267
Z5	2.02383	0.973733	Z15	-0.000363891	0.000936
Z6	0.0371309	1.34051	Z16	0.0114374	-0.39304
Z7	0.0039401	0.000248	Z17	0.00199499	0.000659
Z8	-1.01157	-0.78048	Z18	-1.08776	0.015784
Z9	0.00794653	0.001806	Z19	0.000512008	0.000838

6.3.2 Optical performance analysis

The wave front of the primary mirror has been analyzed with the help of calculated Zernike polynomials by using Zemax optical studio. Figure 6.2 shows the wave front error diagram of the thermal cold case with the RMS value of 0.077λ waves and peak to valley of 0.387λ waves which means that the for the thermal cold case, the PMA design is close to diffraction limited. Figure 6.3shows the wave front error diagram of the y-axis gravity load case with RMS of 0.025λ waves and peak to valley of 0.127λ waves. Its means that PMA design is diffraction limited for the Y-axis gravity load case.

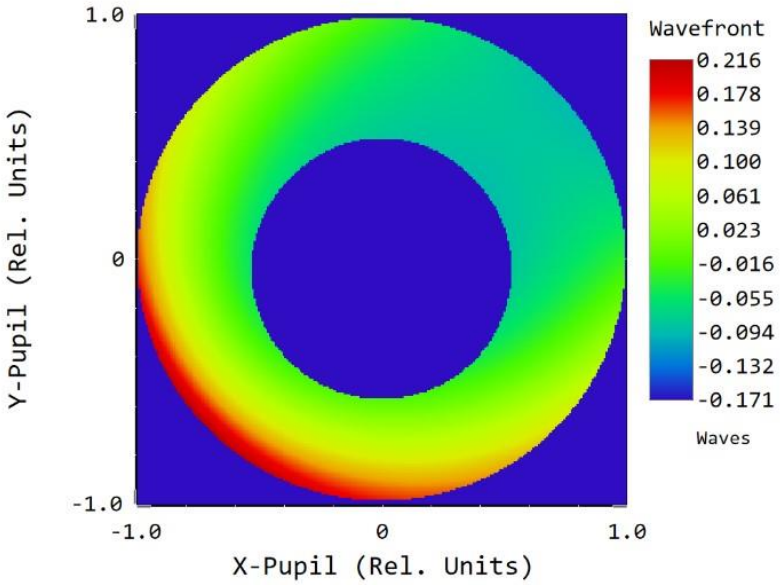

Wavefront Function	
RC CASSEGRAIN_Asim 2019/10/07 0.6250 µm at 0.0000, -0.6100 (deg) Peak to valley = 0.3874 waves, RMS = 0.0776 waves. Surface: Image Exit Pupil Diameter: 1.1652E+02 Millimeters	Zemax Zemax OpticStudio 16.5 SP5 Saaed Thesis.ZMX Configuration 1 of 1

Figure 6.2: Wave Front Error of Thermal Cold Case.

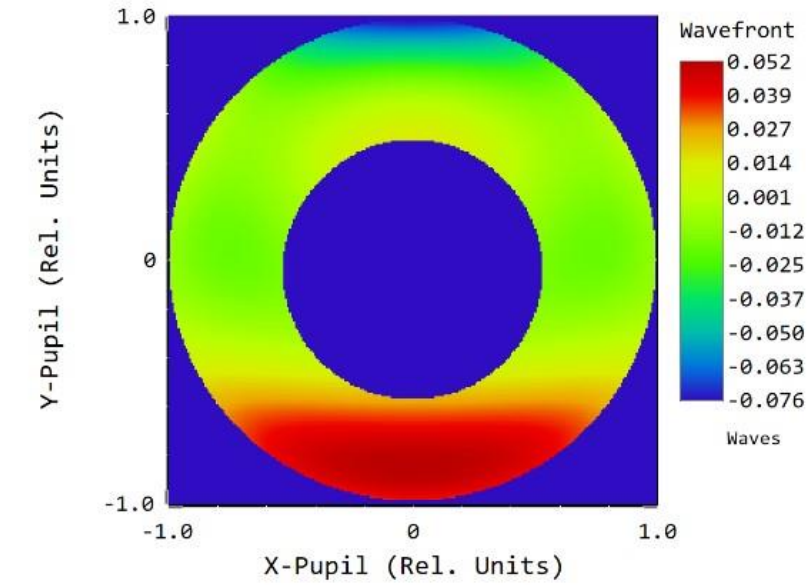

Wavefront Function	
RC CASSEGRAIN_Asim 2019/10/08 0.6250 µm at 0.0000, -0.6100 (deg) Peak to valley = 0.1278 waves, RMS = 0.0251 waves. Surface: Image Exit Pupil Diameter: 1.1652E+02 Millimeters	Zemax Zemax OpticStudio 16.5 SP5 Saaed Thesis_Y.ZMX Configuration 1 of 1

Figure 6.3: Wave Front Error of Y-axis gravity Case

6.3.3 Conclusion

It has been concluded from the analyses and results that the design of the primary mirror assembly meets all the design requirements related to optical performance as well the mechanical strength of the system. To get more confidence on the design of the PMA the Zernike polynomials have been calculated for the optical distorted surface and the optical performance has been analyzed for these Zernike polynomials by using Zemax optical studio. Results of wave front error analysis show that the optical performance of the primary mirror assembly is diffraction limited and meets the design requirements.

In next phase the PMA design will be verified by interferometry testing for optical performance. Strength verification will be performed by thermal cycling and vibration on an electromagnetic shaker. Detail design of mounting bosses and flexure having all the details of interfaces, manufacturing tolerances and AIT plan are the scope of future work.

REFERENCES

[1] D. Vukobratovich, "Lightweight Mirror Design," in *Optomechanical Engineering Handbook by Anees Ahmed*, Boca Raton, CRC Press LLC, 1999, p. Chapter 5.

[2] Y. Yong, J. Guang and Y. Hong-bo, "Design and analysis of large spaceborne light-weighted primary mirror and its support system," in *3rd Internation Symposium on Advanced Optical Manufacturing and Testing Technologies: Large Mirrors and Telescopes*, 2007.

[3] P. R. J. Yoder, "Design and Analysis of Opto-Mechanical Assemblies," in *Opto-Mechanical Systems Design*, vol. 1, Boca Raton, CRC Press, 2015.

[4] H. Kihm and H.-S. Yang, "Design optimization of a 1-m lightweight mirror for a space telescope," *Optical Engineering*, vol. 52(9), September 2013.

[5] H. Kihm, H.-S. Yang, I. K. Moon, J.-H. Yeon, S.-H. Lee and Y.-W. Lee, "Adjustable bipod flexure for mounting mirrors in a space telescope," *Applied Optics*, vol. 51, no. 32, pp. 7776-7783, 10 November 2012.

[6] Y.-C. Chen, B.-K. Huang, Z.-T. You, C.-Y. Chan and T.-M. Huang, "Optimization of lightweight structure and supporting bipod flexure for a space mirror.," *Applied Optics*, vol. 55, no. 36, pp. 10382-10391, December 2016.

[7] P.-H. Huang, Y.-K. Huang and J. Ling, "Mirror design, analysis and manufacturing of 550mm Korsch Telescope Experimental Model," in *Optomechanical Engineering*, California, United State, 2017.

[8] C. Wang, P. Ruan and Q. Liu, "Improved design of support for large aperture space lightweight mirror," in *International Symposium on Photoelectronics Detection and Imaging*, 2013.

[9] K.-S. Park, J. H. Lee and S.-K. Youn, "Lightweight mirror design method using topology optimization," *Optical Engineering*, vol. 44(5), May 2005.

[10] Z. Li, X. Chen, S. Wang and G. Jin, "Optimal design of a 760mm lightweight SiC mirror and the flexural mount for a space telescope," *Review of Scientific Instrumentss*, vol. 88, no. 125107, 2017.

[11] "LM-2D Launch Vehicle User's Manual," Beijing, China, 2015.

[12] "Space Engineering, Structural factors of safety for spaceflight hardware," ESA Requirments and Standards Division, Noordwijk, The Netherlands, 6 March 2009.

[13] J. Paul R. Yoder, Mounting Optics in Optical Instruments, Second ed., Washington UA: SPIE.

[14] "TIE-33 Bending strength of optical glass and ZERODUR," Technical Information Advanced Optics, December 2015.